Thesis for the degree of Doctorate of Philosophy

Gas and dust in early galaxy evolution

Jean-Baptiste Jolly

CHALMERS
UNIVERSITY OF TECHNOLOGY

Department of Space, Earth, and Environment
Division of Astronomy and Plasma Physics
Chalmers University of Technology
Gothenburg, Sweden 2021

Gas and dust in early galaxy evolution

Jean-Baptiste Jolly

© Jean-Baptiste Jolly, 2021.

ISBN 978-91-7905-571-4

Doktorsavhandlingar vid Chalmers tekniska högskola.
Ny serie Nr 5038
ISSN 0346-718X

Division of Astronomy and Plasma Physics
Department of Space, Earth, and Environment
Chalmers University of Technology
SE-412 96 Gothenburg
Telephone +46 31 772 1000

Contact information:
Jean-Baptiste Jolly
Onsala Space Observatory
Chalmers University of Technology
SE–439 92 Onsala, Sweden

Phone: +46 (0)31 772 55 44
Email: jean.jolly@chalmers.se

Cover image: *This image contains 9 galaxy clusters pictures all taken by the ©Hubble Space Telescope, surrounding a picture of the Atacama Large Millimeter Array, ©European Southern Observatory. From left to right and top to bottom the galaxy clusters are: Abell 370, Abell S1063, MACS J1149, MACS J0717, MACS J0416, Abell 1703, MACS J0138 and Abell 2218.*
Credit: NASA, ESA, *HST* and ESO.

Printed by Chalmers Reproservice
Chalmers University of Technology
Gothenburg, Sweden 2021

Gas and dust in early galaxy evolution

Jean-Baptiste Jolly
Department of Space, Earth, and Environment
Chalmers University of Technology

Abstract

In order to study the content of distant galaxies without focusing solely on the brightest objects – the tip of the iceberg – I developed a tool: LineStacker. As its name indicates this tool was designed to perform spectral stacking analyses. Stacking allows to shed light on otherwise invisible features, by averaging together observations of many sources from a common galaxy population.
Spectral lines emitted or absorbed by galaxies and the intergalactic medium carry information on the content of galaxies as well as their dynamics. The luminosity of certain atomic and molecular spectral lines is known to correlate with fundamental physical properties of galaxies, such as star formation rate. In addition, the shape of the lines can trace global dynamics of galaxies or peculiar events such as outflows. In this context, I used LineStacker to study distant galaxies by observing the average spectral lines, or continuum emission, emitted by a particular galaxy population. In this thesis I present the tool LineStacker in detail and with a specific emphasis on the statistical tools included with it.
In addition, I showcase three different analyses where we used LineStacker to study galaxy evolution. In the two first we studied ionized carbon, [C II] , in galaxies at redshift $z \sim 6$. One project focused on the faint outflow signatures below the main [C II] line, while the other project focused on the overall [C II] emission from faint, gravitationally lensed galaxies. Finally, in the last analysis, we studied the overall dust mass as well as the comoving dust mass density and their evolution with redshift. The results from all the analyses highlight the power and efficiency of stacking as a method, and the necessity to go beyond studying the brightest objects.

Keywords: Galaxies: evolution – Galaxies: high-redshift – methods: stacking – methods: data analysis – techniques: interferometric

Research Contributions

This thesis is based on the work contained in the following papers:

I **Jolly J. B.**, Knudsen K. K., Stanley F.:
LINE-STACKER: A spectral line stacking tool for interferometric data
Monthly Notices of the Royal Astronomical Society, Volume 499, Issue 3 (2020)

II Stanley F., **Jolly J. B.**, König S., Knudsen K. K.:
Outflows in $z \sim 6$ quasars
Astronomy & Astrophysics, Volume 631, A78 (2019)

III **Jolly J. B.**, Knudsen K. K., Laporte N.,Richard J., Fujimoto S., Kohno K., Ao Y., Bauer F. E., Egami E., Espada D., Dessauges-Zavadsky M., Magdis G., Schaerer D., Sun F., Valentino F., Wang W. H., Zitrin A.:
ALMA Lensing Cluster Survey: A spectral stacking analysis of [CII] in lensed $z \sim 6$ galaxies
Astronomy & Astrophysics, Volume 652, A128 (2021)

IV **Jolly, J. B.**, Knudsen K. K., Laporte N., Guerrero A., Kohno K., Fujimoto S., Koekemoer A. M., Richard J., et al.:
ALMA Lensing Cluster Survey: Dust mass and comoving dust mass density evolution with redshift, from $z = 1$ to $z \sim 6$
Manuscript intended for Astronomy & Astrophysics

I also participated in the following papers not included in this thesis:

I Sun, F., Egami, E., Pérez-González P. G., Smail I., Caputi K. I., Bauer F. E., Rawle T. D., Fujimoto S., Kohno K., Dudzevičiūtė U., Atek H., Bianconi M., Chapman S. C., Combes F., Jauzac M., **Jolly J. B.**, Koekemoer A. M., Magdis G. E., Rodighiero G., Rujopakarn W., Schaerer D., Steinhardt C. L., Van der Werf P., Walth G. L.; Weaver, J. R.:
Extensive Lensing Survey of Optical and Near-Infrared Dark Objects (El Sonido): HST H-Faint Galaxies behind 101 Lensing Clusters
Accepted for publication in the Astrophysical Journal.

II Guerrero A., Nagar N., Kohno K., Fujimoto S., Kokorev V., Brammer G., **Jolly J. B.**, Knudsen K. K., Bauer F. E., Gonzalez-Lopez J., Laporte N., Smail I., Caminha G., Caputi K. I.:
ALMA Lensing Cluster Survey (ALCS): median dust, gas, and star formation properties of cluster and field galaxies from stacking analysis
Manuscript intended for Monthly Notices of the Royal Astronomical Society.

Acknowledgements

First and foremost, I want to genuinely thank my supervisor, Kirsten. I truly believe she allowed me to thrive throughout my PhD, and I am very grateful for the trust she put in me and the opportunity she gave me. Under her guidance, I was able to grow both as a person and as a scientist. Looking back, I realize everything I have learned and achieved thank to her, and must say I am very proud to have been her student. I also want to thank Lucía, my girlfriend, for her support all the way through my PhD. She made the hard times easier and the easy times wonderful. By her side I could find serenity, comfort and kindness when confronted to obstacles. I want to thank my parents, of course, as they have always taught me to think for myself and make my own choices, and for raising me to be curious about everything –and what is more everything than the Universe. My sister, for her success and thirst for knowledge that motivated me to be better. Everyone in the AOP division for making my time in Chalmers and Onsala pleasant. More specifically, I want to thank Flora, whose help and guidance in the first half of my PhD were invaluable and Kiana, whose corrections made my thesis actually readable. Finally, Federica, Francesco C., Francesco G., Julia, Simon, Michael and Sandra for the sweet time, distracting me from my work. Thank you!

Jean-Baptiste Jolly, Larnagol, October 2021.

This too shall pass.

CONTENTS

CHAPTER 1

INTRODUCTION

1.1 From the Big Bang to the dark ages

The Universe as we see it today is mostly empty, and most of its energy content is invisible. The total baryonic matter accounts for only 4.5% of the total energy, from which less than 10% (0.3% of the total energy) lies in the visible matter, such as stars in galaxies[1], hot gas in clusters, and groups of galaxies. Aside from baryonic matter, the Universe is thought to consist of dark matter (24%) and dark energy (71.5%), about which little is known (Persic and Salucci, 1992). But the observable universe used to look very differently.

Modern cosmology describes the Universe as starting from the Big Bang[2], marking the beginning of time. The observable Universe has changed dramatically in appearance from the Big Bang to now. At that moment the Universe was extremely dense but started expanding rapidly, becoming sparser[3]. Because it is very complicated, still largely debated, and definitely not the scope of this work, we are going to skip the first seconds after the Big Bang, to start our story just around the first minute (see for example Tanabashi et al., 2018, for an extensive description of the very early universe).

At this time the Universe was still very dense and composed mainly of high energy photons created primarily through matter/antimatter annihilation. As the Universe continued expanding, the energy density diminished and the mean free path of photons got longer. After two minutes, the energy density was sufficiently low for the first nuclei to be stable. However, the energy density was still sufficiently high for the high energy photons to break apart the newly formed nuclei. Consequently only a handful of nuclide species were allowed to form (mainly protium, deuterium

[1]Galaxies are gravitational bound systems, composed of stars, gas, dust, and dark matter. They are typically composed of a few hundred billion stars, and have usually sizes of order 10^5 light years. We estimated that there are roughly 200 billion galaxies in our observable Universe (see Lauer et al. (2021) and Chapter 2).

[2]See Figure 1.1 for a graphical guide to the following description.

[3]It is worth noting that, unlike the common appreciation, if the Universe is infinite now (and that we cannot say for sure) it was infinite already "when" the Big Bang happened.

and helium-3 and 4). As the energy density decreased and the mean free path of particles increased, recombination became possible: electrons were captured by nuclei, thus forming the first neutral atoms. Due to the fact that recombination directly to the ground state is very inefficient, electrons are typically captured in higher states. They later drop to the lower states, releasing photons in the process. This phenomenon is know as photon decoupling (see e.g. Coc and Vangioni, 2017; Tanabashi et al., 2018).

All these photons start travelling freely for the first time since the Big Bang. They are "the first light of the Universe" and constitute the Cosmic Microwave Background (CMB). The CMB was first detected by Arno Allan Penzias and Robert Woodrow Wilson in 1964, and most recently studied by the *Planck* satellite, launched in 2009 (see Planck Collaboration, 2016). *Planck*'s very sensitive observations demonstrated the existence of a preferred correlation scale printed on the CMB fluctuations. This correlation translates, on large scale structures, to distances of 100-150 Mpc. SDSS observations showed that this distance matched the observed correlation scale for galaxies in the local Universe (Okumura et al., 2008). This effectively showcases the relationship between inhomogeneities in the particle soup of the early Universe and large scale structures thousands of light years large in the present Universe; hence connecting small scales to large scales, past to present, the Big Bang to galaxies.

After decoupling there are almost no new sources of photons in the Universe for over 100 million years. Since this epoch of the Universe is without sources of light (e.g., stars), it is commonly termed the "cosmic dark ages". Due to lack of photons, there is almost no information about this period and it is today one of the hardest tasks in astronomy to try and find objects (e.g., stars, galaxies), first of their kind, in the dark ages. During the dark ages, on large scales, dark matter gathered forming filaments and assembling in a dark matter network (see Figure 1.3). Normal matter, which was mostly in the form of gas at that point, is located in higher densities at the nodes of the dark matter network. In these dense matter cores, where the temperature is still too high to allow structured formation of normal matter, cold dark matter gravitationally collapsed starting from small inhomogeneities and grew linearly through accretion. Eventually these dark matter clumps reached critical density and collapsed, creating the first dark matter halos. These halos grew either through accretion or mergers. Ultimately, they will act as attractors for the normal matter, allowing it to become bound into structures earlier than otherwise possible.

1.2 The epoch of reionization

General reference: Zaroubi (2013); Wise (2019)

As the first stars form, and with them the first galaxies, high energy photons start roaming the Universe freely, the universe becomes bright, it is the end of the dark ages. As light propagates in the still dense Universe, neutral hydrogen, which is the main component of the interstellar medium, starts to ionize. This process is known as reionization. Reionization is the last phase transition of the gas in the Universe and many aspects of this transition are still heavily researched today; mainly the sources responsible for reionization and their relative contribution to it,

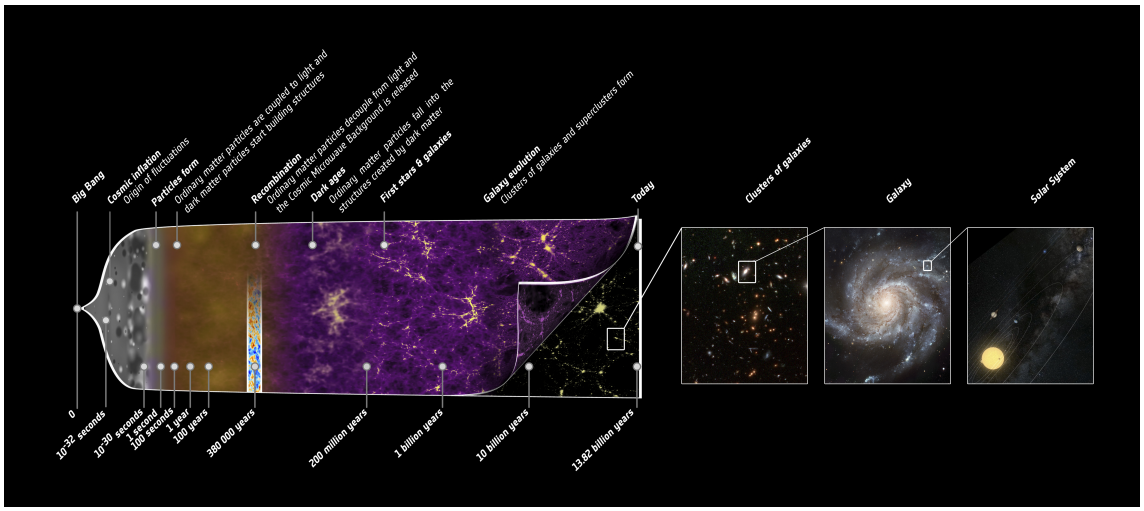

Figure 1.1: History of the Universe ©ESA – C. Carreau

the overall timing of the reionization process (i.e., its start, speed, and end), the exact topology of the first reionization regions and their evolution, and the relationship and impact of the global reionization process on galaxy formation. This section will summarize the current knowledge about reionization and present some of the main observational probes used for its study.

The global ionized state of the present Universe was first highlighted by the study and discovery of the absence of absorption features in the spectra of quasars (also known as quasi-stellar objects, or QSO). Gunn and Peterson (1965) studied the spectrum of a QSO at $z \sim 2$ and realized that its spectrum presented overall no absorption feature blueward of the Lyα line, indicating the intergalactic medium (IGM) in the path of the light emitted by the QSO was highly ionized. This was the first experimental evidence of the ionization of the IGM, hinting at a global reionization of the Universe at very high redshift.

With the drastic improvement in telescope sensitivity, a large number of spectra of QSO at $z > 6$ have been observed (e.g. Fan et al., 2006). By looking at these spectra one can identify Gunn-Peterson troughs from $z \sim 6$. Gunn-Peterson troughs are strong absorption regions in the spectra, indicating that the light traveled through a region of the IGM that is mostly neutral at the corresponding redshift. These troughs indicate that the IGM must have been almost fully ionised until redshift $z \sim 6$, indicating the probable end of reionization around this redshift.

The study of CMB radiation can provide hints about the start of the reionization epoch. While CMB photons travel through an ionized medium they may scatter off the free electrons present in that medium. This process is known as Thomson scattering. By measuring CMB polarization it is possible to probe the effect of Thomson scattering and learn about the overall ionization properties of the Universe. However, due to the integral nature of this measurement it can only be used to get an approximate estimate on the start of reionization. The most recent *Planck* measurement (Planck Collaboration et al., 2020) indicate that at $z \sim 7.82$ the Universe was half ionized. Dijkstra (2014) suggests that reionization may have started as early as $z \sim 16$ with the formation of the first galaxies.

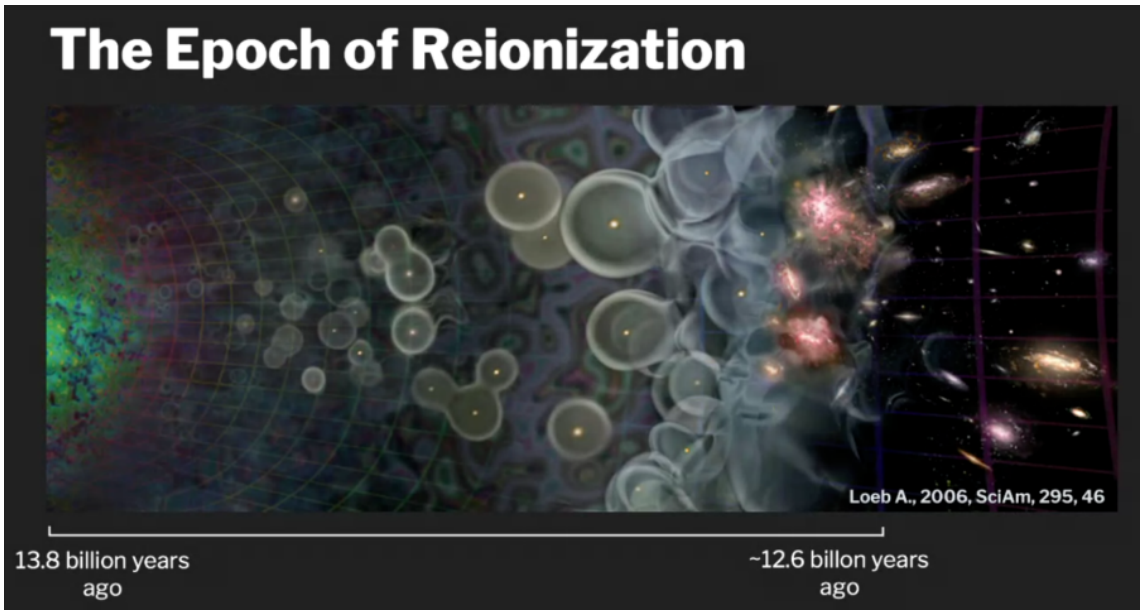

Figure 1.2: As stars and galaxies form they ionize the neutral medium around them. This ionization process is thought to be shaped like bubbles. As bubbles grow, and more start forming, they eventually merge to fill the entire Universe. Nowadays, the only remaining neutral Hydrogen lies inside galaxies (figure extracted from the Scientific American, Vol. 295, p. part no 5, 46-53, 2006)

An interesting source of reionization, existing solely in the very early Universe, is the primordial population of stars, referred to as the population III stars. These stars are composed only of hydrogen and helium atoms because they are born in an environment where no heavier elements are present. This makes them unique in the Universe as later stars, born from more complex environments enriched by primordial supernovae, contain metals and are hence intrinsically richer than population III stars. Simulations have hinted that population III stars formed almost constantly until the end of reionization (e.g. Wise et al., 2012). These stars are thought to be very massive, rather short lived (with typical lifetime of $3-10$ Myr), and produce a large number of high-energy ionizing photons with high escape fraction (Alvarez et al., 2006). These photons are thought to amount to as much as 70 % (Gnedin and Ostriker, 1997; Lu et al., 1998) of the total radiation responsible for reionization. As these photons propagate outward spherically around the stars, the surrounding neutral medium is thought to become ionised as "bubbles". With time, these bubbles overlap, giving rise to a fully ionised Universe(see Figure 1.2).

When population III stars die, most are thought to give rise to a black hole remnant because of their high initial mass. These black holes are among the first in the Universe and could be the seeds of the supermassive black holes we observe in the later Universe. The UV photons emitted from their accretion disks are most likely negligible compared to the UV radiation emitted from other sources (e.g., by population III stars); however, these primordial black hole accretion disks also emit high energy X-ray photons. These photons can typically travel to longer distances than their UV counterparts, and may hence be responsible for at least

partial reionization on a larger scale. Such emission may have an impact on the overall topology of reionization.

In addition, the first galaxies, specifically dwarf galaxies (e.g. Bouwens et al., 2012), also played a crucial role in the reionization process. These galaxies are typically metal poor, as they form from the pristine gas that gathered in the center of dark matter halos. Since dwarf galaxies are more compact, they have been shown to present higher escape fractions. This makes them better at hydrogen ionization than their larger counterparts (e.g. Wise et al., 2014), and around half of the total number of ionizing photons may come from galaxies with masses less than 10^9 $M_\odot$.

Further, the 21 cm line (see Chapter 2.4) can be used as a probe of the very first ionization patterns in the very early Universe. By measuring the overall 21 cm signal at very low frequency (i.e. emitted at very high redshift) and averaging over the whole sky, it is possible to observe a trough in the redshifted neutral hydrogen emission corresponding to the presence of a primordial ionized region. Bowman et al. (2018) observed the sky-averaged radio waves in the 50 to 200 MHz range and observed a trough centered at a frequency corresponding to a redshift of $z \sim 17$ and spanning approximately $15 < z < 20$. These results indicate that reionization occured as early as these redshifts, and Kaurov et al. (2018) argue that a few massive galaxies may be responsible for this signal. One of the most surprising finding from Bowman et al. (2018) is that the depth of the absorption feature they observe was possibly two times deeper than indicated by theoretical works, meaning that the IGM was effectively two times colder than expected. Such low temperature would imply additional cooling mechanisms of the IGM. The authors suggest that new physics, such as cooling interactions between baryons and dark matter, could explain their observations. Multiple experiments are currently trying to reproduce the same detection –LOFAR (van Haarlem et al., 2013), PAPER (Parsons et al., 2010), MWA (Bowman et al., 2013), HERA (Neben et al., 2016) and SKA (Dewdney et al., 2009) – as it is essential to independently confirm this groundbreaking detection.

Overall the reionization of the Universe was a fairly long process that started around 180 million years after the Big Bang and was complete when the Universe was around one billion years old. It involved multiple sources and can be probed through different signatures involving a few different messengers. The study of reionization is tightly linked to galaxy formation and evolution, and to the content of the IGM as it was triggered by primordial stars and galaxies and their relation to their surrounding gas.

1.3 From the first galaxies to the local Universe

At the end of the reionization, bigger galaxies started forming by accreting matter and/or through merging, and the Universe looked essentially the same as it does now. However, galaxy growth is not homogeneous; the most massive galaxies formed very fast while smaller clumps took a long time to evolve, leading to the wide range of galaxy classes we observe today. Galaxies come in all sizes and shapes. Some display strong, ongoing, star formation while others appear to have been passive for quite some time. Similarly, some galaxies are gas rich, displaying many different chemical

species, while others seem mainly metal poor. The evolutionary path leading to such differences is still unclear, and the complete picture of galaxy evolution has yet to be drawn.

1.4 This thesis

The present thesis is on the topic of galaxy formation and evolution. The number of galaxies in the observable Universe is estimated to be above two hundred billion (Lauer et al., 2021). With the growing number of sensitive telescopes, our knowledge of galaxy evolution is gradually increasing. Even with new and better telescopes, many scientific questions remain. While better instruments allow us to see further, these observations remain biased toward the brightest objects, preventing us from drawing a complete picture of galaxy evolution taking into account even the faintest galaxies. The scope of this thesis is two fold; (i) Present a summary of the research I conducted through my PhD: studying gas and dust evolution in galaxies, putting it in context, and discussing the main results as well as their implications in the wider field of galaxy evolution. (ii) Present the newly developed tool LineStacker which enables broader investigations of distant galaxies, more specifically by studying their gas and dust content. Through stacking a large number of sources, the signal to noise ratio (SNR) can be drastically improved, enabling the study of faint emission, thus highlighting otherwise invisible galaxy properties. In the following chapters I broadly introduce the current state of knowledge in the field of galaxy evolution before presenting the developed tool, LineStacker, itself. I then describe the aim, content and my own contribution to the four embedded papers, followed by a conclusion and potential outlooks.

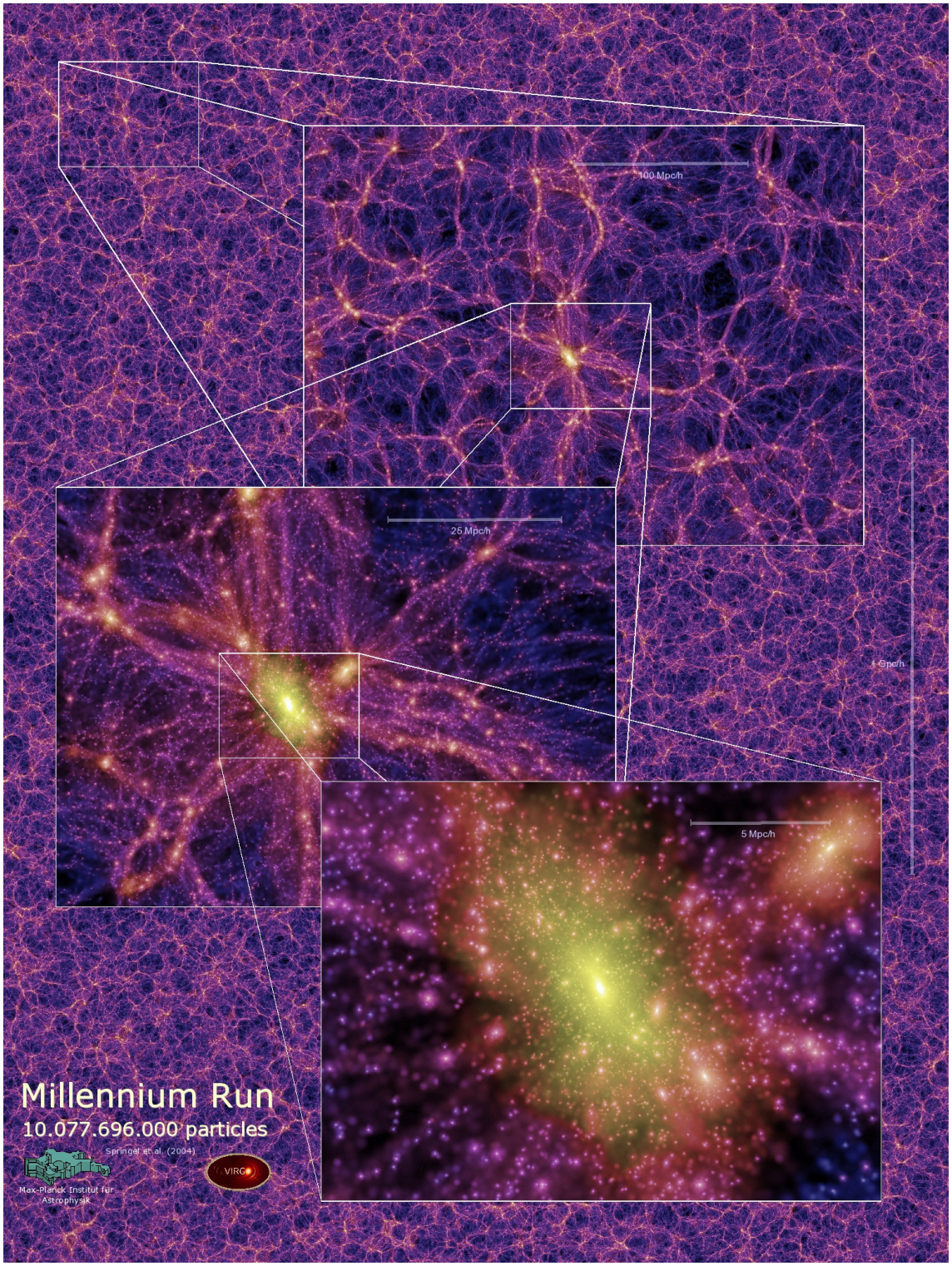

Figure 1.3: ©Millenium simulation: *Slices of the dark matter distribution. The following poster shows a projected density field for a 15 Mpc/h thick slice of the redshift z=0 output. The overlaid panels zoom in by factors of 4 in each case, enlarging the regions indicated by the white squares.*

CHAPTER 2

GALAXY EVOLUTION

2.1 Growth process

About a hundred years ago, the 'Great Debate' focused on whether the Milky Way represented the whole Universe, or if it was one galaxy among many others. It was resolved through distance measurements to the Andromeda galaxy, showing that it was too far away to be part of the Milky Way. From this time it was known that we lived in one galaxy among others, leading to new studies of external galaxies, and to the birth of extragalactic research. Galaxies are large systems of gas, dust and dark-matter, typically containing few hundred billion stars. Among the first important steps of extragalactic research was the classification of galaxies. The most common classification is the Hubble classification scheme which separates galaxies into four categories: elliptical, lenticular, spiral, and irregular (see Figure 2.1). Elliptical and lenticular galaxies are usually referred to as "early type galaxies" while spiral and irregular galaxies are referred to as "late type galaxies"[1].

Galaxies exhibit a wide variety of characteristics such as size, mass, and color. For example, galaxy stellar masses span a wide range over more than seven order of magnitude. The least massive (dwarf) galaxy detected has a (stellar) mass of $\sim 10^5\,M_\odot$ (Kirby et al., 2013), while one of the most massive galaxies detected to date has a (total) mass of $\sim 10^{13}\,M_\odot$ (Carrasco et al., 2010, ten times more massive than the Milky Way). The first large structures to form were likely star clusters, groups of stars, gravitationally bound (White and Rees, 1978). Thus the question: how did galaxies grow from the earliest phases to the structures we see today, in such a wide variety as described by the Hubble sequence? There are two major processes for galaxy growth: accretion of matter and merger processes.

[1]It should be noted that the terms "early" and "late" do not refer to temporal evolution. It is sometimes thought that Hubble intended this temporal relation, and that it was later disproved. But, as explained in Baldry (2008), Hubble borrowed this vocabulary from star classification and, as he wrote in his 1926 paper: *"Early and late, in spite of their temporal connotations, appear to be the most convenient adjectives for describing relative positions in the sequence... They can be assumed to express a progression from simple to complex forms."*.

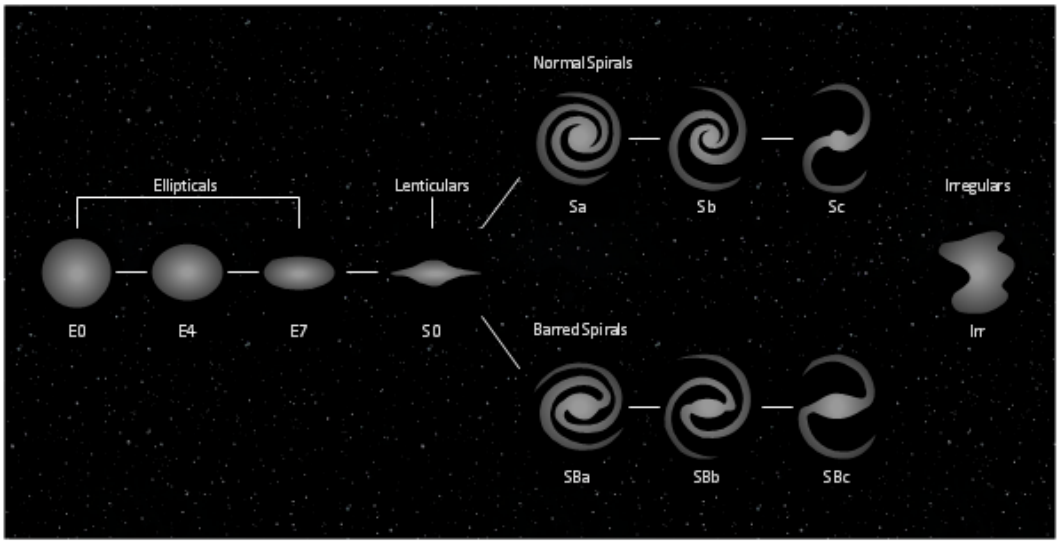

Figure 2.1: Hubble sequence: galaxy classification.

2.1.1 Accretion

Accretion of matter is facilitated by the dark matter network (as illustrated by Figure 1.3). Gas flows through the dark matter web and is accumulated at the nodes. Galaxies are usually formed along the filaments, with the most massive at their intersections (e.g. Springel et al., 2005; Vogelsberger et al., 2014). The gas flowing through the web is accreted by the galaxies, thus increasing their mass. There are two main modes of accretion: the hot and cold modes (e.g. Katz et al., 2003; Kereš et al., 2005). One of the main issues with accretion is that the accreted gas must be at sufficiently low temperature to be captured by the galaxy. Hot mode accretion implies that the infalling gas is hot (meaning $T_{\text{gas}} > T_{\text{virial}}$), due to shock heating and must cool, mainly through radiation, before it can be integrated into the galaxy. The hot mode is quasi-spherical and dominates at lower redshifts ($z < 1$) in high density environments. In the cold mode, the accreted gas is channeled along the filaments, allowing galaxies to draw gas from large distances. The gas is still heated from shocks and adiabatic compression, but it radiates its heat quickly, so that its temperature never reaches T_{virial}. Cold mode accretion is dominant at high redshifts and in low density environments at $z \sim 0$ (e.g. Kereš et al., 2005; Dekel et al., 2009).

2.1.2 Galaxy mergers

Galaxy mergers consist in combining two (or more) galaxies together to form a bigger one (see Figure 2.2). When it comes to growing galaxies we distinguish between three modes depending on the mass ratio of the two galaxies merging (M_r): "major" if $M_r > 1/3$, "intermediate" if $1/3 > M_r > 1/10$ and "minor" if $M_r < 1/10$.

When two galaxies of similar masses merge, the forces involved are such that their dynamic structure is lost after merging (Barnes and Hernquist, 1996). For this reason it is thought that elliptical galaxies are the product of major merger

events. As an example, our galaxy, the Milky Way, and the Andromeda galaxy are gravitationally bound and modelling suggests that they will eventually merge in roughly 4 billion years (van der Marel et al., 2012). Being of similar mass (ratio 1/1.5) this will be a major merging event and their global dynamic structure will hence most probably be lost. Minor and intermediate mergers should leave the structure of the most massive galaxies intact, hence being one of the possible process behind the growth of massive spiral galaxies (Naab et al., 2009). It is thought that our own galaxy grew, and is still growing today, through the absorption of the Canis Major Dwarf Galaxy and several other smaller systems (Martin et al., 2004).

Additionally, merger events can also be classified depending on the gas richness of the galaxies involved. If the galaxies are gas-rich the merger event is classified as a "wet merger". Conversely, if both galaxies are gas poor the event is classified as a "dry merger". The term "mixed merger" designates an intermediate mode, when one galaxy is gas rich and the other gas poor. Wet mergers seem to dominate at higher redshift, but the higher number of dry mergers at lower redshift may simply correlate with the increasing number of gas poor galaxies with reducing redshift (Lin et al., 2008). Gas-rich major mergers trigger starbursts in the early phase, followed by rapid black hole growth through gas inflow to the center (e.g. review by Sanders and Mirabel, 1996). It is thought that such events may be, at least in part, responsible for the observed quasar population; >75% of the red quasars population show evidence of recent/ongoing merging, decaying ultimately into a passive elliptical state (Hopkins et al., 2006, 2007). However, the frequency evolution of mergers with redshift is still debated (e.g. Bertone and Conselice, 2009; Le Fèvre et al., 2013; Rodriguez-Gomez et al., 2015).

2.2 Observing high-redshift galaxies

In 1995 extensive observations with the *Hubble Space Telescope* (*HST*) resulted in the release of the *Hubble Deep Field* (see Figure 2.4). The first of its kind, this extremely deep image showed a high number of galaxies. New galaxy classifications arose based on observed physical properties instead of solely on morphology. Around the year 2000 identification of distant galaxies were typically made through observations of extremes objects, mostly quasars, rest frame UV-bright Lyman-break galaxies (Steidel et al., 1996), or extremely red objects (Daddi et al., 2000). Later, new methods would be developed to identify weaker galaxies, like dust-obscured galaxies (Dey et al., 2008), distant red galaxies (Franx et al., 2003) or BzK galaxies (Daddi et al., 2004).

As the timescale of galaxy evolution is much longer than our life time, it is not possible to follow the evolution of an individual galaxy. The methods mentioned above allow for identification of galaxies holding specific characteristics, but since these methods are intrinsically very different and operate in different frequency ranges it is challenging to link galaxy types together. One of the biggest challenges is hence to tell if these classes represent different stages of galaxy evolution or if they are intrinsically different populations that have evolved separately.

Since distinct wavelength are linked to different physical processes or sources –e.g. dust, gas, and the different stellar populations are each associated

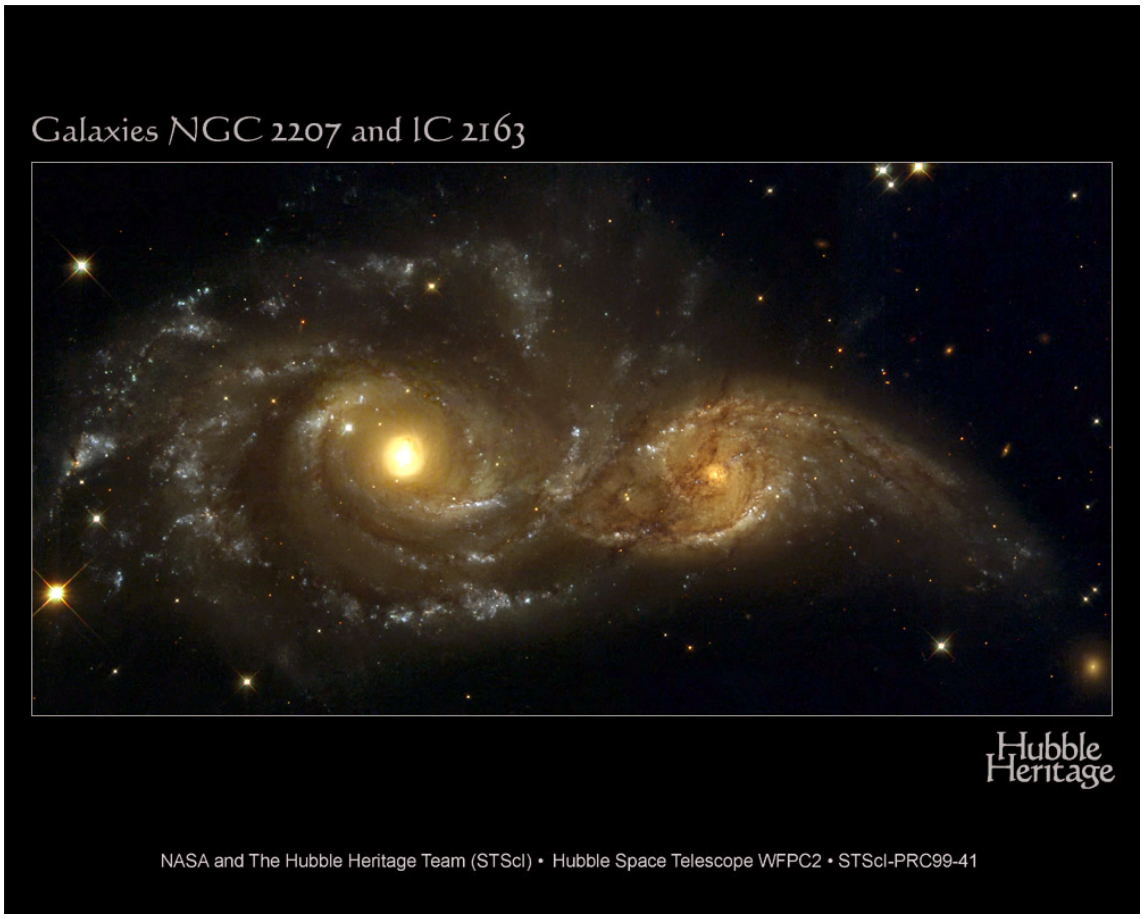

Figure 2.2: The merging of two spiral galaxies, NGC2207 and IC2163. ©NASA and The Hubble Heritage Team.

with specific emission and absorption patterns, see Section 2.4.3 and Figure 2.3– the spectral flux distribution of galaxies can drastically vary. A comprehensive understanding of galaxies and galaxy populations can hence only be reached through complete observations across the whole electromagnetic spectrum. Furthermore, because the observed frequency of a given spectral signature changes with the redshift of the galaxy, a multiwavelength approach is also necessary to study the evolution of a given phenomenon with redshift.

Observed flux goes down as the square root of the distance to the emitting object, and thus observed distant galaxies often have very high intrinsic luminosity. High luminosity objects at high redshift represent only the tip of the iceberg. They are a small, extreme part of the overall galaxy population. Making an extensive description of high-redshift galaxy populations even harder. Linked to this is the Malmquist bias, which leads to an overestimate of the average brightness of distant galaxies, inducing a miss-interpretation of the brightness level of the studied sample compared to the average population.

Figure 2.3: Multiwavelength Whirlpool Galaxy: Each image shows a narrow band of wavelengths of light across the electromagnetic spectrum. From: *Education and outreach collections from the University of Chicago, Multiwavelength astronomy.*

2.3 Gravitational lensing

Among the many predictions resulting from Einstein's theory of general relativity, there is one that is of specific interest for the work described in this thesis: gravitational lensing. In general relativity, massive objects bend space-time around them and light travels along space-time's curvature. Hence, when massive objects –such as galaxy clusters– happen to be directly aligned between us and a bright object, the light rays emitted by that said object are deflected and magnified (see Figure 2.5). The light from the source will then look distorted, and multiple images of the same object can even be observed in certain configurations.

The effect of gravitational lensing was first observed in May 1919 by Arthur Eddington and his team. By taking advantage of a total solar eclipse, they observed stars that were almost aligned with the Sun. As the light from these stars was getting very close to the Sun, stars were observed slightly out of position. This indicated that their light had been bent by the Sun on its way to Earth. The first extragalactic gravitationally lensed object was only discovered $\sim$ 60 years later, in 1979, by a team led by Dennis Walsh. Indeed, they observed two very similar quasars, very close to each other, that proved to be very close in redshifts, and to have very similar spectral properties. After numerous observations by different teams, it is now clear that these are indeed two images of the same quasar, located at $z \sim 1.41$, and that the two images have a time delay to reach Earth of about 14 months.

Gravitational lensing is typically split in two categories:

- Strong lensing: when the lensing effect is so strong that multiple images of the light source can be observed (or peculiar features such as Einstein rings) see

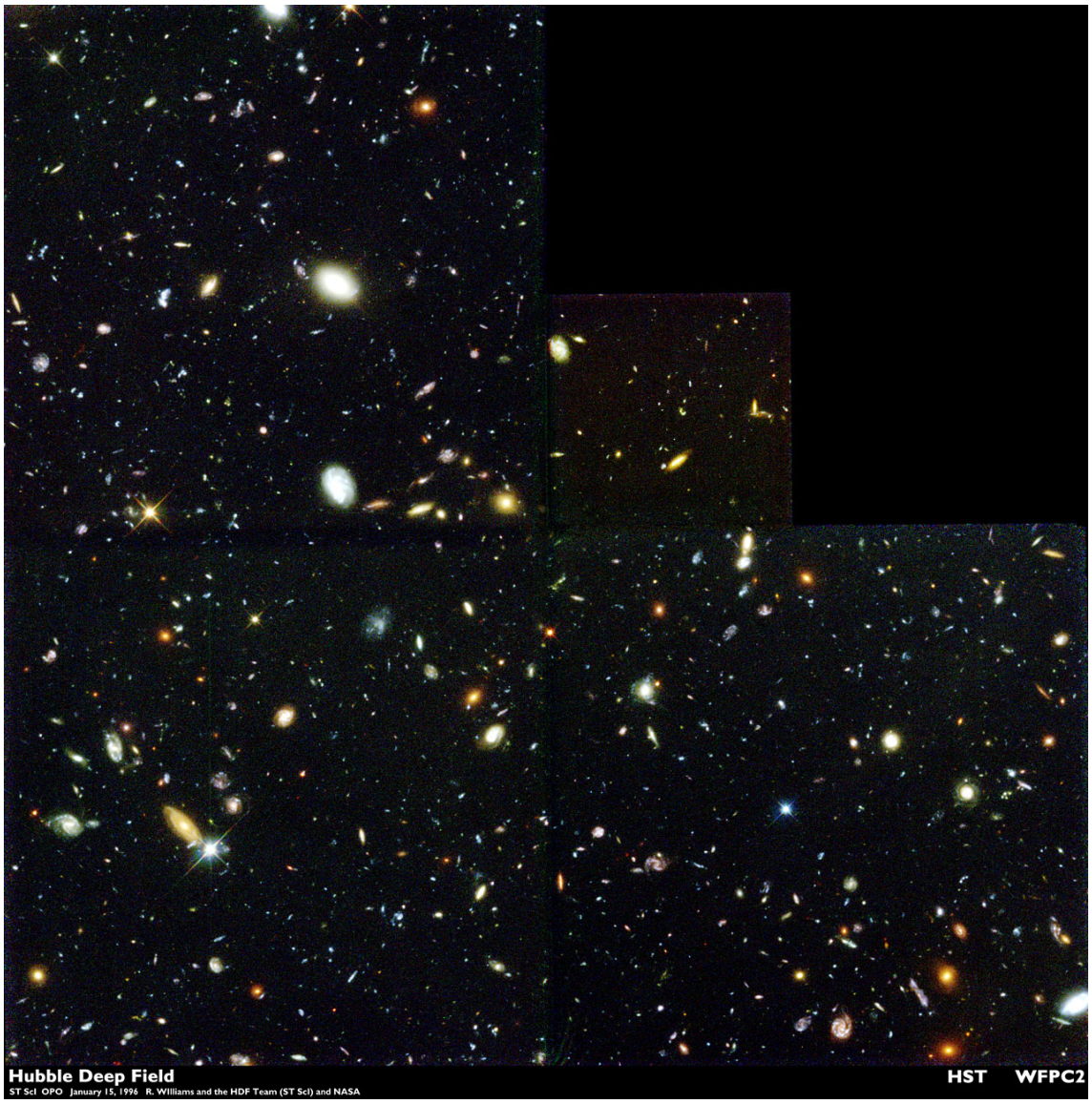

Figure 2.4: The Hubble Deep Field. Picture taken over a period of observation of ten days, in December 1995. ©NASA.

Image 2.6.

- Weak lensing: when the lensing effect is much weaker, resulting in only small distortions, typically elongation of the weakly lensed galaxies. Because they are much more subtle, weak lensing effects are typically detected through statistical analyses of many galaxies.

The magnification effect provided by gravitational lensing boosts the signal from distant galaxies, effectively allowing us to observe much fainter objects much further than otherwise possible. In rare cases (e.g. Khullar et al., 2021; Whitaker et al., 2021; Witstok et al., 2021) magnifications of up to a few dozens allow for much more detailed observations, as it amplifies both the brightness and the size of the lensed object. Consequently the volume probed behind the lens is smaller; as the lensing magnification varies across the field, it is not trivial to calcu-

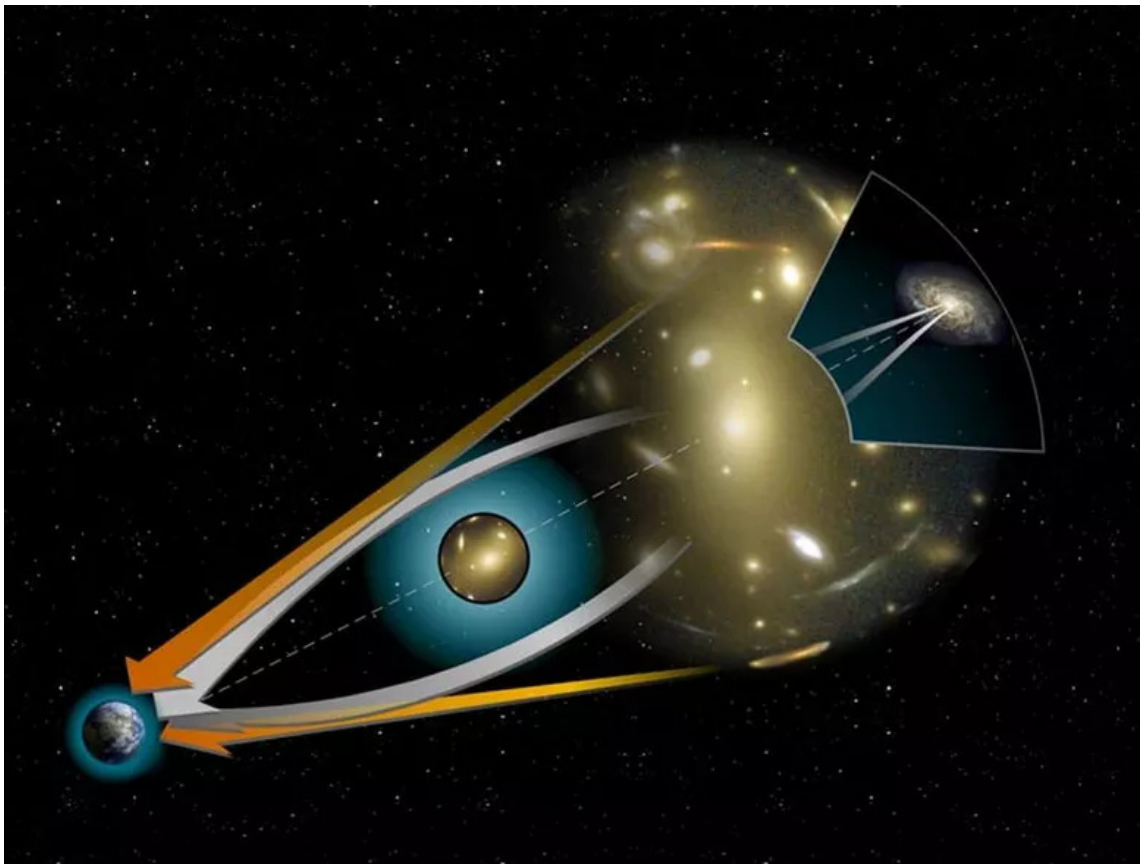

Figure 2.5: Figure representing the gravitational lensing functioning principle. The light from the background source is bent on its way to Earth as it comes near the massive object in its path. The orange arrows represent the apparent position of the source, while the white arrow represents the actual light path. ©NASA.

late the corresponding volume. In Paper III and Paper IV, we used the gravitational lensing effect by galaxy clusters as a magnifying glass to study faint galaxies at high and intermediate redshifts (see Sections 5.3 and 5.4).

Aside from their magnification potential, gravitational lensing effects can also be used to probe the very matter creating the lens. Because the lensing effect is directly tied to the overall matter distribution, by having a good understanding of the shear effect applied to the images of background galaxies by the lens, one can learn more about the masses causing the distortion of the light. These methods have been employed for example to learn more about the dark matter in clusters, and its distribution. Indeed, as most of the mass in galaxies and hence, by extension, in galaxy clusters, is in the form of dark matter, the majority of the matter responsible of the gravitational lens is actually dark matter (see Figure 2.7).

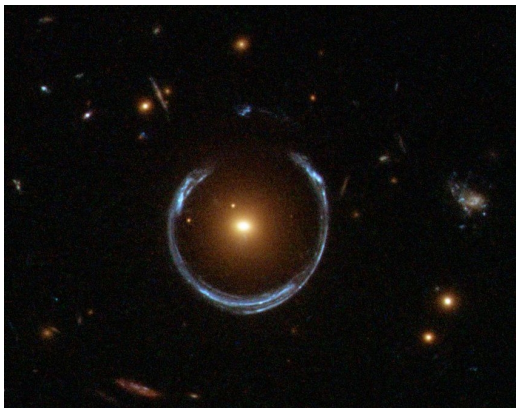

(a) An example of Einstein ring: *The Cosmic Horseshoe*. The central galaxy (LRG 3-757) is extremely massive, and right in our line of sight to a more distant galaxy, giving rise to strong lensing effect. Picture by the *Hubble Space Telescope*.

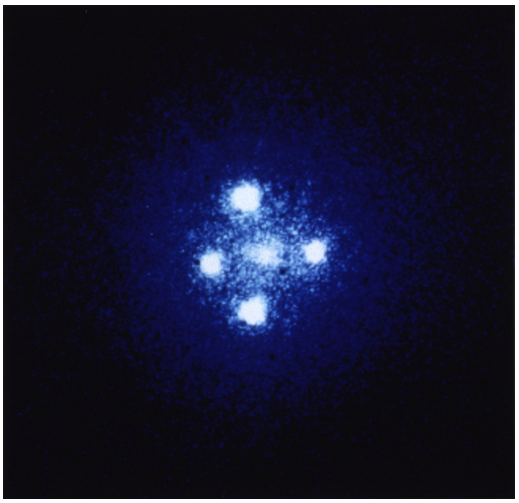

(b) *The Einstein Cross* consists of four multiple images of a single quasar, lensed by the foreground galaxy (in the center). While strong lensing effect will most often lead to the creation of Einistein Rings, the peculiar configuration of both the lensed quasar and its lensing galaxy lead to this peculiar cross-shaped image. Picture by the *Hubble Space Telescope*.

Figure 2.6: Two examples of strong lensing.

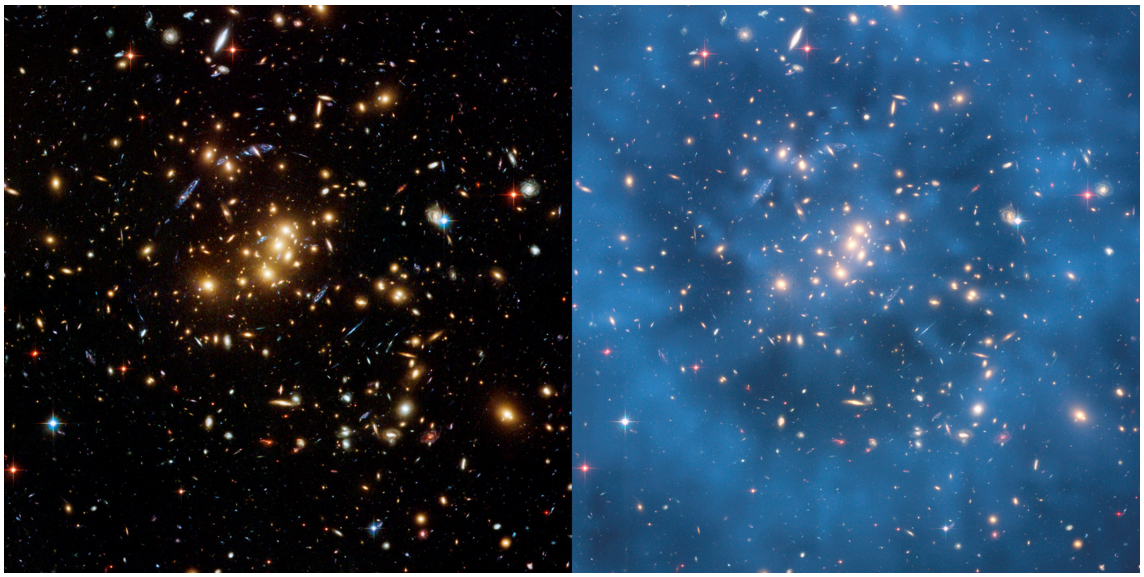

Figure 2.7: On the left panel one can see an image of the galaxy cluster Cl0024+17 taken by *the Hubble Space Telescope*. On the right panel the image is overlaid with the overall matter distribution inferred from lensing shear measurements. The ring structure, invisible on the image on the left, is a striking evidence of the existence of dark matter. Credit: NASA, ESA, M. J. Jee and H. Ford (Johns Hopkins University) and HubbleSite.

2.4 Observational probes of the gas content in distant galaxies

One key aspect of understanding galaxy evolution is the study of the evolution of the gas content through time. The interstellar medium (ISM) of star-forming galaxies contains the gas that fuels the star formation, as well as processed gas that comes from stellar evolution. There are two different gas phases in the ISM: neutral and ionized. Both often have a wide range of temperature and density profiles. The neutral phase is dominated by the neutral atomic and molecular gas, as well as by the dust content. This phase is found both as diffuse gas and in molecular clouds that can be the sites of star formation. The ionized phase is typically dominated by the ionized atomic gas with a very low content of molecules and dust. This gas can be found near young OB stars or in the diffuse medium.

Thorough studies can reveal the chemical composition of galaxies (e.g Costagliola et al., 2015; Henkel et al., 2018), and being able to map the evolution of galaxy composition through cosmic time would be a huge step in our understanding of galaxy formation, and specifically the evolution of our own Milky Way. By studying different atomic and molecular emission lines, it is possible to investigate the physical and chemical properties of the gas. The most common emission lines are (note: this is a non-exhaustive list, focused on the radio/mm/far-infrared):

- The atomic hydrogen HI 21 cm line. This line probes the large gas reservoirs in galaxies. It is mostly optically thin, allowing easier total mass calculation (e.g. Walter et al., 2008) and hence gas/stellar mass fraction estimate (e.g. Zwaan

et al., 2013). It can also possibly trace the gas streams growing galaxies – cold mode accretion, see Section 2.1.1 (e.g. Morganti et al., 2006). Unfortunately, HI observations at high redshift are very challenging because they require a high sensitivity.

- Atomic fine-structure lines in far-infrared probe different parts of the ISM. As examples, the [C II] 1900 GHz line is known to be one of the strongest cooling lines in the ISM, and one of the brightest emission lines from star-forming galaxies (e.g. Smith et al., 2017; Lagache et al., 2018, see Section 2.4.1). The neutral carbon line [C I] traces the physical and chemical conditions of the dense ISM (e.g. Stutzki et al., 1997). It has also been shown to trace molecular gas, acting as an alternative to CO (Clark et al., 2018). Ionized oxygen, [O III] at 88 μm, is a known tracer of activity in galatic nuclei (e.g. Kauffmann et al., 2003), as well as a good tracer of metal in galaxies (e.g. Pettini and Pagel, 2004).
- A large number of molecules, including the following: H_2, molecular hydrogen, is the most abundant molecule by far, with only around 1% of a given galaxy's gas in other molecules. However, H_2 has no permanent dipole moment and is therefore difficult to observe (e.g. Tielens, 2005). CO is the second most abundant molecule and is very easy to observe because its lowest excited level occurs at excitation temperatures of approximately 5.5 K and is thus very easy to excite, making the rotational transitions of CO the most common emission lines observed in high-redshift galaxy studies. CO is also used as a tracer of H_2 (e.g. review by Carilli and Walter, 2013; Lagos et al., 2014). CO primarily traces moderate density gas and has been shown to trace the star formation rate of a galaxy (e.g. Omont, 2007). There are, however, many more molecules of interest in galaxy evolution studies, e.g., the high density gas tracers HCN and HCO^+, and the water lines that have, so far, only been studied in a few sources.
- Dust is observed through absorption of the blue optical wavelengths to UV radiation from stars, which is then re-emitted and observed at far-infrared and millimeter wavelengths. ISM properties can be deduced from dust observations (see Scoville et al., 2014), and dust has been observed in galaxies at redshifts higher than seven (see Section 2.4.2).

All these can typically be detected through emission/absorption lines observations. Such investigation are much harder than continuum observations. When looking for lines, observations require good sensitivity on many spectral channels. Continuum allows to sum these channels together, hence recovering a higher SNR for the same observation.

2.4.1 The case of ionized carbon

Carbon is the fourth most abundant molecule in the solar system. It is typically produced by the triple nuclear fusion of Helium: $3\times{}^4\text{He} \rightarrow {}^{12}\text{C}$ (Ehrenfreund et al., 2002). It has an ionization potential of 11.3 eV (less than the 13.6 eV of hydrogen). The far-infrared fine-structure line [C II] is emitted from the ${}^2P_{3/2} \rightarrow {}^2P_{1/2}$ transition at 157.74 μm (1900.537 GHz Cooksy et al., 1986), and has an excitation tempera-

ture of 91.2 K. [C II] emission lines originate mostly from photo-dissociation regions (PDRs, see Stacey et al., 1991, 2010). In these regions the cold neutral medium is heated by stellar UV radiation, and cooled through the emission of [C II]. This line can therefore be used to probe the stellar radiation field, and its effect on the surrounding gas. [C II] is one of the strongest cooling line in the cold phase of the ISM (see Carilli and Walter, 2013; Dalgarno and McCray, 1972). However, because of its low ionization potential, single-ionized carbon is found both in the cold neutral and ionized gas phase, which can make the identification of the source complicated.

With a rest-frame frequency near 1.9 THz, the [C II] line is almost impossible to observe at low redshift with ground-based facilities. The first studies to detect the ionised carbon line used the Kuiper Airborne Observatory (KAO, Crawford et al., 1985). Early results from these studies found a detection of [C II] in about two dozen galaxies. They showed that the line was very bright, $\sim$0.1-1% of the total far-infrared continuum (see also Stacey et al., 1991; Wright et al., 1991; Brauher et al., 2008). Since then, [C II] has been studied extensively in local galaxies (e.g. Poglitsch et al., 1995; Madden et al., 1997, 2020; Hunter et al., 2001; Cormier et al., 2010; Israel and Maloney, 2011). In the $4.5 \lesssim z \lesssim 8.5$ redshift range, observing the [C II] line with ground-based telescopes becomes possible, as the line is redshifted into the submm and mm wavelengths bands. [C II] is now routinely observed in bright $z \sim 6-7$ quasars and starbursts galaxies (e.g. Riechers et al., 2013; Knudsen et al., 2016; Venemans et al., 2016; Decarli et al., 2017; Stanley et al., 2019; Le Fèvre et al., 2020a; Venemans et al., 2020). Its excitation temperature makes it less sensitive to the CMB, which is warmer at high-z and can hence be a limiting or compromising factor when studying, for example, CO lines.

In addition to tracing various phases of the ISM, [C II] has been proposed as a tracer of SFR in the local and more distant Universe (e.g. Stacey et al., 1991, 2010; Boselli et al., 2002; De Looze et al., 2011, 2014; Sargsyan et al., 2012; Herrera-Camus et al., 2015; Schaerer et al., 2020) as well as a tracer of gas mass (e.g. Hughes et al., 2017; Zanella et al., 2018; Madden et al., 2020; Dessauges-Zavadsky et al., 2020). The line has been detected in galaxies with a large range of SFRs (e.g. Capak et al., 2015; Willott et al., 2015; Knudsen et al., 2016; Pentericci et al., 2016; Bradač et al., 2017; Decarli et al., 2017; Matthee et al., 2017; Carniani et al., 2018; Smit et al., 2018; Hashimoto et al., 2019; Bakx et al., 2020; Béthermin et al., 2020; Harikane et al., 2020; Le Fèvre et al., 2020b; Fujimoto et al., 2021; Laporte et al., 2021) but non-detections have also been reported (e.g. Ouchi et al., 2013; González-López et al., 2014; Ota et al., 2014; Maiolino et al., 2015; Schaerer et al., 2015; Knudsen et al., 2016).

[C II] can prove difficult to interpret has it can probe different regions of the ISM, and observations at high-redshift have been selected either based on the presence of AGN (e.g. Maiolino et al., 2005; Stacey et al., 2010; Wang et al., 2013; Stanley et al., 2019), or starbursts galaxies (e.g. Ivison et al., 2010; Hailey-Dunsheath et al., 2010; Stacey et al., 2010; Cox et al., 2011; Swinbank et al., 2012; Walter et al., 2012; Riechers et al., 2013; Brisbin et al., 2015; Gullberg et al., 2015) leading to an irregular selection sample.

Finally, while the [C II] line luminosity is thought to be proportional to far-infrared (FIR) luminosity, deviation from this relation has been observed at

$L_{\mathrm{FIR}} > 10^{11} - 10^{11.5}\,\mathrm{L}_{\odot}$, where the [C II] to FIR luminosity ratio drops by an order of magnitude (e.g. Malhotra et al., 1997, 2001; Luhman et al., 1998, 2003; Negishi et al., 2001; Maiolino et al., 2009; Stacey et al., 2010; Graciá-Carpio et al., 2011; Sargsyan et al., 2012; Gullberg et al., 2015). Multiple explanations have been proposed to explain this effect (see Maiolino et al., 2009; Gullberg et al., 2015) including: (i) an increased ionization parameter leading to a higher fraction of UV photons being absorbed by dust and hence proportionally less photons available to ionize and heat the gas (Malhotra et al., 2001; Abel et al., 2009; Graciá-Carpio et al., 2011); (ii) opacity effects weakening the [C II] emission line in infrared luminous galaxies (Luhman et al., 1998; Gerin and Phillips, 2000); (iii) collisional de-excitation of [C II] (Appleton et al., 2013); (iv) contributions to the FIR luminosity from other sources than PDRs (Luhman et al., 2003), possibly from AGN (Malhotra et al., 2001; Sargsyan et al., 2012); (v) a saturation effect of [C II] emission in highly luminous compact regions while FIR emission remains unsaturated (Stacey et al., 2010; Gullberg et al., 2015), i.e. the [C II] emission becomes nearly optically thick and its brightness reaches a maximum, while cooling through the FIR continuum continues. More observations are needed to finally clarify the reason for the existence of the [C II] to FIR luminosity deficit, and to properly quantify it to infer the [C II] line luminosity from galaxies with high FIR luminosity (and the opposite).

Overall, the [C II] line is very useful and easily observable due to its overall brightness and correlation with multiple physical parameters. Its rest frequency makes it easily detectable at high redshifts ($z > 4.5$) with ground-based facilities and, in particular, for the epoch of reionization. Its brightness also makes it a good alternative candidate for confirming the redshifts of photometrically detected galaxies (e.g. Smit et al., 2018). Nonetheless, it has yet to be extensively studied in faint high-z objects, which is the main motivation behind Paper III (see Section 5.3).

2.4.2 Dust in galaxies: role and observation

The term "dust" is used to describe small grains of matter, usually a combination of C, O, M, Si, S and F, with sizes typically ranging from a few molecules to a few μm (Draine, 2011). Dust plays a critical role in galaxy assembly for several reasons. First, dust grains are thought to be one of the main facilitators of H_2 creation. Indeed, it has been shown that H_2 cannot be created efficiently enough in pure gas environments (see Wakelam et al., 2017), while catalytic reactions on the surface of the dust grains allow H_2 to be gathered much more efficiently. H_2 is is the most abundant molecule in the Universe and is thought to be the main component of the ISM (Hirashita et al., 2002). Since star formation primarily occurs within molecular gas clouds (in opposition to atomic gas clouds, see Scoville 2013), the presence of dust as well as its properties are crucial factors in the formation of stars.

Second, dust grains reprocess a significant portion of the light we can observe from the Earth today. It is believed that about half of the total UV/optical light we observe is reprocessed by dust (e.g. Dole et al., 2006). Light emitted from stars heats the surrounding dust by radiation absorption, which is then re-emitted, at much longer wavelengths (IR to mm) as thermal radiation. In total, one fourth

to one third of the total stellar radiation emitted from stars in local spiral galaxies is thought to be re-radiated by dust (Cox and Mezger, 1989; Calzetti, 2001). Due to the fact that dust re-transmits light originally emitted by stars, studying dust emission provides information not only on dust properties (e.g. dust mass, temperature and grain size), but also on the galactic properties (mainly SFR and gas mass) that gave rise to that radiation in the first place.

By absorbing and re-emitting UV and visible radiation, dusts also shields part of the information that would otherwise be directly visible. Recent work by Zavala et al. (2021) showed that dust-obscured star formation has been predominant from $z = 0$ to $z = 4$, and decreased to 25%–20% at $z = 6$–7 (see Figure 2.8). Hence, dust plays a major role in shielding star formation processes at all redshifts.

The dust SED can be split mostly into two parts: the Rayleigh-Jeans side, where $\lambda > \lambda_{peak}$ (where λ_{peak} is the wavelength at the peak of emission) and the Wien side, where $\lambda < \lambda_{peak}$ (see Figure 2.9). The Rayleigh-Jeans tail can be well fit with a single black-body component while fitting the Wien side, typically linked to warmer dust, is more complicated. Studies have shown that fitting both sides with a black-body function at a single temperature will generally fail (e.g. Casey, 2012). However, dusty galaxies observed at high redshift will most often only have a few photometric data-points, making multi-temperature fits very hazardous. In local galaxies it was shown that dust can be typically split into two components, a warmer component (at $20 < T < 60\,\mathrm{K}$) and a cold component (at $T < 30\,\mathrm{K}$). Orellana et al. (2017) showed that the cold component is actually responsible for the majority of the mass budget (>95%) in local galaxies. Scoville et al. (2014, 2016) suggest that this approximation should remain valid at higher redshifts, hence arguing in favor of fitting dust SEDs with a single modified black-body function, using only the temperature of the cold component. The underlying assumption behind this approximation is that the part of the SED used in the fitting process corresponds to the Rayleigh-Jeans tail and is sufficiently far from the peak of dust emission, where dust is optically thin. However, while the cold dust component temperature is thought to stay mostly constant with redshift (e.g. Liang et al., 2019; Sommovigo et al., 2020), the warmer dust component temperature has been shown to evolve significantly with redshift (e.g. Béthermin et al., 2020; Faisst et al., 2020).

With the advent of new IR, mm and radio telescopes such as the *Spitzer* Space Telescope (Fazio et al., 2004), the *Herschel* Space Observatory (Pilbratt et al., 2010), the South Pole Telescope (SPT Carlstrom et al., 2011) and the Atacama Large Millimeter/submillimeter Array (ALMA), it has now become possible to conduct deep studies of dust in the ISM. Specifically, ALMA and its extremely high angular resolution allow for dusty galaxies to now be detected even at $z > 7$ (e.g. Watson et al., 2015; Knudsen et al., 2016; Laporte et al., 2017; Tamura et al., 2019).

2.4.3 SED fitting and photometric redshifts

The spectral energy distribution (SED) of a galaxy encodes information about the multiple emission and absorption processes happening inside the galaxy across the whole electromagnetic spectrum. The different phenomenon giving rise to emission or absorption of radiation within the galaxy typically have different spectral

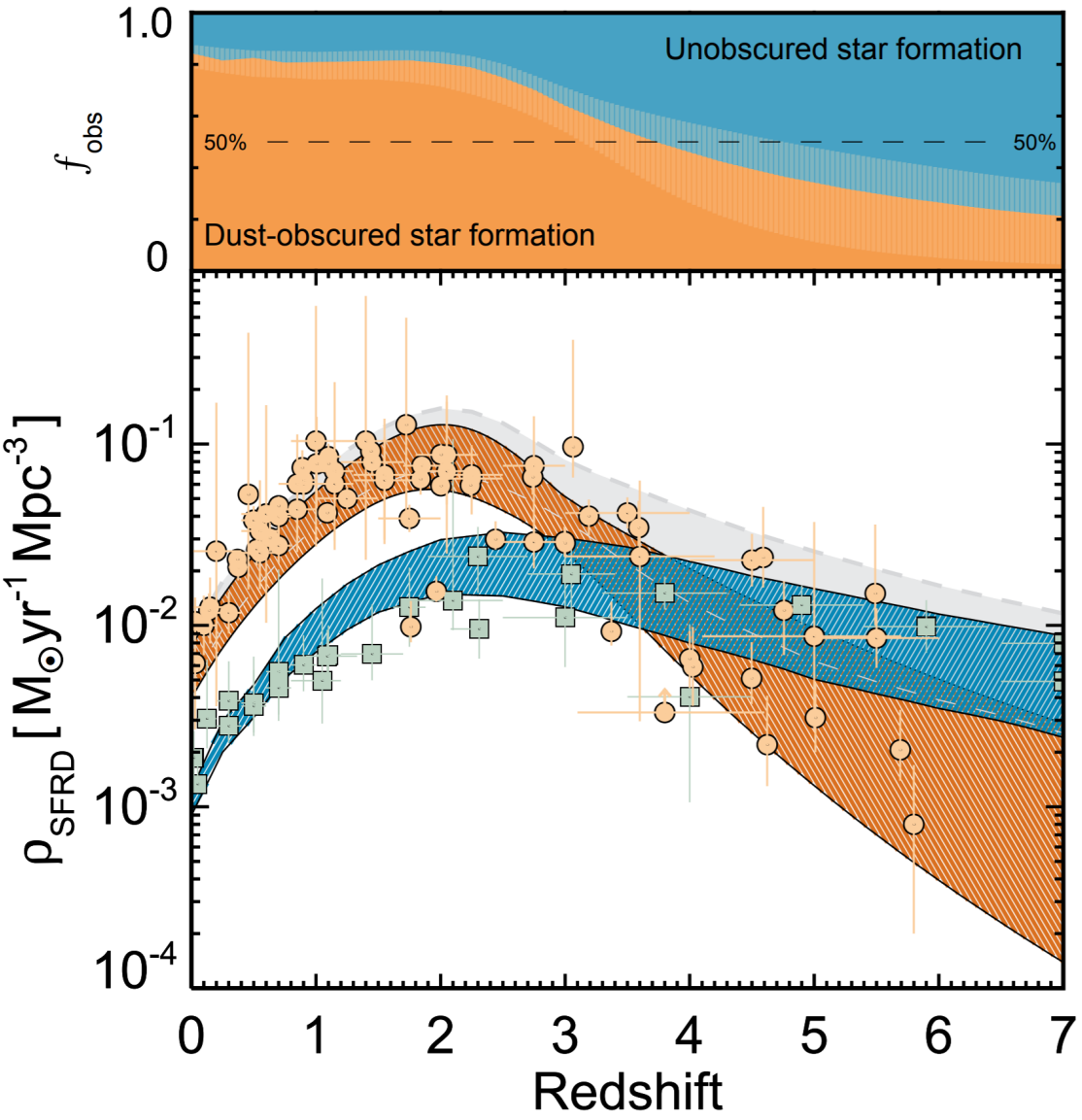

Figure 2.8: Dust obscured (respectively un-obscured) star formation history, represented by the orange shaded region (respectively blue). Independent measurements from the literature based on IR/sub-mm (UV) surveys are over-plotted, as orange (blue) dots for comparison (figure extracted from Zavala et al., 2021).

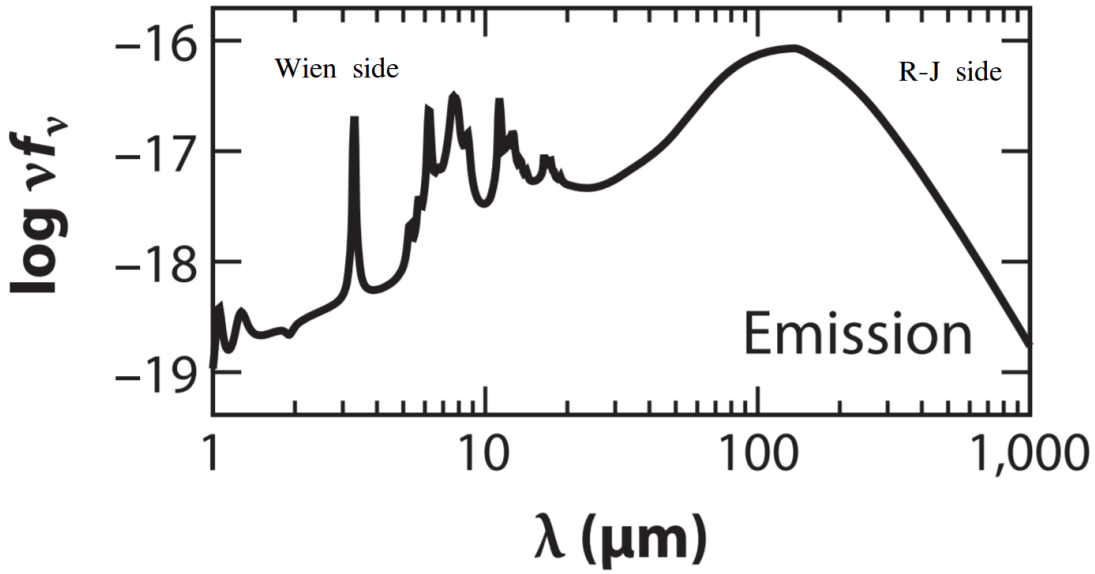

Figure 2.9: Illustrative example of dust SED. The Wien side lies on the lower wavelength side, while the Rayleigh-Jeans tail is located at wavelength higher than the peak of emission (figure extracted from Conroy, 2013).

signatures (see for example Figure 2.10). Certain physical characteristics of the sources are associated to specific spectral signatures, making it possible to extract information about galaxies from their SED.

The complete SED of a galaxy will be a complex mix of the spectrum emitted by each star, combined with the emission and absorption features of the other galactic components, such as dust, gas, and AGN. Each type of star has a distinct spectral emission signature. O-type stars for example, which are among the most massive stars, can have temperatures higher than 30 000 K, and are hence seen as blue. On the other hand, low-mass stars such as the M-type stars have temperatures reaching below 3 000 K, and show a red peak of emission. Atomic and molecular gas can be sources of emission or absorption lines that also modify the overall shape of the SED. Finally, the dust (as seen in Section 2.4.2), will be the dominant component in the far-infrared and (sub-)millimeter wavelength part of the spectrum, and will also play the important role of absorbing the light emitted by the stars. A complete description of a galaxy SED is very complex and difficult to model as it is a combination of these many different components. In addition, the overall stellar population, SFR and gas fraction, all evolve with the galaxy, making each galaxy's SED an object in constant evolution.

However, with the advent of advanced fitting techniques, it has become possible to extract characteristics of galaxies directly from their SED. In this work I will briefly present two different fitting codes that use a fairly different fitting procedure: MAGPHYS (da Cunha et al., 2008) and BAGPIPES (Carnall et al., 2018).

MAGPHYS has been used extensively since its first release. Unlike BAG-

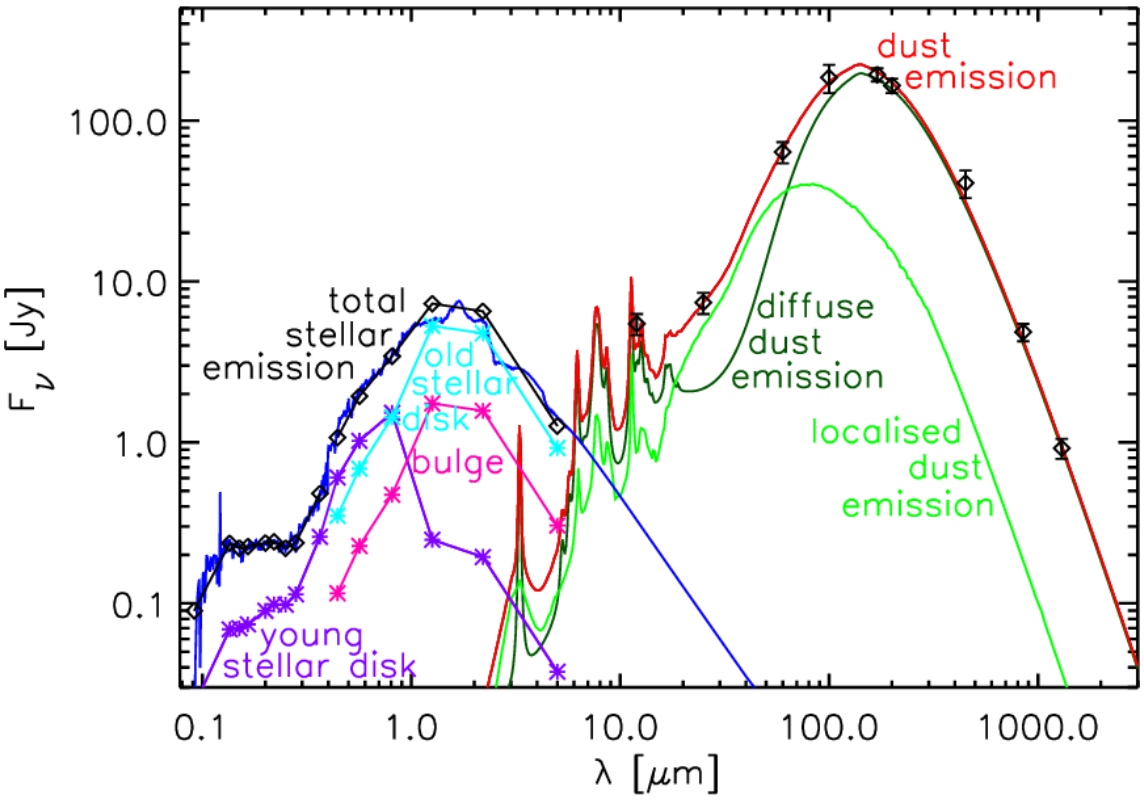

Figure 2.10: Example of SED from the different component of a galaxy (figure extracted from Popescu et al., 2011).

PIPES it functions with the use of a library of model SEDs. Its fitting routines are mostly done in two steps. First the library of model SEDs at the same redshift and in the same photometric bands as the studied galaxy are gathered. Second, through comparison between the observed SED and the library, the likelihood distribution of the free parameters is computed.

BAGPIPES, on the other hand, does not work with libraries but instead uses self generated, physically realistic, galaxy model spectra to asses the goodness of the fit. Depending on the desired complexity, a number of model components can be set as free parameters for the galaxy model creation. The luminosity function of the model galaxy spectrum is created as a sum of four components: a simple stellar population model, the star formation history, the transmission function of the ionized ISM, and the transmission function of the neutral ISM. Generated models are then fit to observed data within the framework of a Bayesian inference, using a nested sampling algorithm[2] (Skilling, 2006).

Aside from identifying the overall physical parameters of the studied galaxies, SED analysis techniques can also be used to recover the redshift of the source. Spectroscopy observations of galaxies provide valuable information about the physical properties, and importantly also allow for a spectroscopic redshift derivation. However, spectroscopic observations are expensive in terms of observing time. In-

[2]Nested sampling algorithms allow for an efficient exploration of multidimensional spaces with a high number of dimensions and highly degenerate parameter spaces.

deed, the overall SNR will go down as roughly the square root of the number of channels, meaning that if one needs high sensitivity in a high number of channels, the observation time should be very long. However, photometric observations allow for a higher SNR due to the nature of observations. Photometric analyses are hence very common, leading to the development of methods to infer redshifts from photometric observations i.e., photometric redshifts.

While photometric redshift derivation dates back to the 1960's (Baum, 1962) it was soon replaced by the usage of the much more precise spectroscopic redshifts. At the end of the 90's the development of large surveys, identifying dozens of galaxies, made for the come-back of photometric redshift derivations as an easy and cheap alternative. At first, the shift was directly observed by comparing the known redshift of galaxies in a given clusters, to a set of galaxies coming from an other cluster at unknown redshift Baum (1962). But this direct method was soon to be replaced by more indirect routines. For example, color-color diagrams were used as early as 1985 (Koo, 1985) and saw widespread usage and transformation in the late 90's (e.g. Madau et al., 1996; Pello et al., 1996; Steidel et al., 1996). Connolly et al. (1995) used a large training data-set of real galaxies with a large spread in color and confirmed spectroscopic redshifts, and with the use of simple linear regression techniques showed it was possible to derive impressively accurate redshifts. They found $\sigma_z \sim 0.05$ with their training set of 370 galaxies extending to a redshift of 0.5. An alternative is to use "template fitting" techniques; these methods involve building a complete library composed of the full SEDs of galaxies (both observed and/or modeled) at many different redshifts and comparing them to the observed one. While this method can prove very efficient, it suffers from potential mismatch between the models and the observations.

Due to the overall high uncertainties linked to the derivation of photometric redshifts, they are usually barely usable for spectral stacking analyses (see Section 5.1). However, their relatively easy derivation, even for large galaxy sample, makes them suitable for large continuum stacking analyses where their overall lack of accuracy washes out due to the high number of objects stacked (see Section 5.4).

2.5 AGN & outflows

Starting from the 1980's, numerous studies detected supermassive black holes in the center of galaxies (e.g. Sargent et al., 1978; Dressler and Richstone, 1988; Harms et al., 1994). It is now widely accepted that all massive galaxies contain a central supermassive black hole. In parallel, the presence of extreme optical/radio phenomenon in some galaxies was attributed to the mechanism of mass accretion onto a black hole (e.g. review by Rees, 1984; Lynden-Bell, 1969). These extreme sources are now known as active galactic nuclei (AGN).

By studying supermassive black holes, and their relation to their host galaxy, it was shown that there exists a proportionality between black hole mass and mass of the galactic bulge (e.g. Marconi and Hunt, 2003; Häring and Rix, 2004). Such a relation could be explained by a process known as AGN feedback. Both black hole growth and star formation require cold gas. However, while black holes only accrete gas on small scales ($< 1\,\mathrm{pc}$), star formation operates on galactic

scales. Thus, one can wonder how to expand the influence of AGN by a factor $\sim 10^5$, so short range AGN can impact the star formation on galactic scales? While still debated, many studies propose that the AGN would act on the galaxy's cold gas through violent outflows: either warming the gas or mainly expelling it out of the host galaxy, hence quenching star formation (e.g. reviews by Fabian, 2012; Alexander and Hickox, 2012). Furthermore, simulations of galaxy formation show that quenching processes from AGN feedback are required to properly reconstruct galaxy stellar mass functions, which would, without this feedback, be over-estimated (e.g. Di Matteo et al. (2005); Somerville et al. (2008); Schaye et al. (2015) and review by Naab and Ostriker (2017)).

While outflows have been observed in massive low redshift galaxies (e.g. Rupke and Veilleux, 2011; Maiolino et al., 2012; Cicone et al., 2014; Harrison et al., 2014) there have been but a few observations at higher redshifts (e.g. Cicone, 2015; Decarli et al., 2018), and mainly targeting sources with a high chances of being in an outflowing phase (Circosta et al., 2018). Furthermore, as shown in Harrison et al. (2018), deriving outflow properties (such as mass, extent, velocity etc.) is a hard process, and even more so to link them to AGN luminosity. Hence, using current observations, one cannot draw a definitive conclusion regarding the rate of outflows across redshift. Especially, on whether outflows are a common process or are limited to a certain galaxy-mass or redshift range, hence questioning the role of AGN feedback in the global picture of galaxy evolution. While studies like Circosta et al. (2018), which blindly searched for AGN-driven outflows in previously detected AGN at $z \sim 2$-3, are an important step toward generalizing outflow properties, studies like the one described in Paper II, allow for unbiased statistical analysis of high-redshift AGN (see Section 5.2).

2.6 Open questions

While both merging and accretion processes are mostly accepted as responsible for galaxy growth, many questions remain. For example, the respective distribution of both processes across redshifts remains unclear. Similarly, the relation between the supermassive black hole at the center of galaxies and the properties of the galaxy itself is still questioned, in particular the role of feedback processes from AGN in the early Universe and their consequences for star formation. In a broader view, the star formation evolution across ages, and the mechanism allowing star formation to be switched on or off, as well as its fueling, are still being investigated. Additionally, the content of galaxies, i.e., the nature and amount of gas and dust available at different stages of galaxy evolution, is not well described by current theories. Finally, the role of the environment on galaxy formation, as well as the galaxy population distribution as a function of the redshift are also still open questions. Current observations do not permit for a broad enough global view that would allow for a thorough description of galaxy evolution across the ages.

CHAPTER 3

RADIO INTERFEROMETRY

3.1 Introduction to interferometry

The main purpose of interferometry is to significantly improve the angular resolution of observations. A standard two-element interferometer functions by studying, not directly the signal received from the source but, the correlation between the outputs of two antenna systems. The outputs are superposed, creating interference that can be studied to retrieve information about the original signal, emitted by the source. In order to improve the limited performance of a two-element interferometer, "aperture synthesis" is done by using an array of antennas. For a single dish the resolution, R, is inversely proportional to the size of the dish, $R \propto \lambda/D$, where λ is the wavelength of observation and D the antenna dish diameter. In an interferometer, the resolution is $R \propto \lambda/L$ where L is the maximal distance between antennas in the array ($L >> D$, hence largely improving the resolution of interferometers compared to single dish observations). Aperture synthesis works by correlating the outputs of each antenna pair in the array. Every antenna measures the power of the incoming signal over time, and the visibilities are the measure of the coherence of the signal. The visibilities, $V_{j,k}(t)$, for antennas j and k at time t are linked to both the source brightness, I, and the distance between the antenna pair, $\vec{B}_{j,k}$:

$$V_{j,k}(t) \propto \int_{sky} I(\vec{\sigma}) e^{\frac{-2i\pi}{\lambda}\vec{B}_{j,k}\cdot\vec{\sigma}} d\Omega \tag{3.1}$$

Where $\vec{\sigma}$ is the vector describing the position on the sky. Visibilities are usually expressed in terms of (u, v), defined as:

$$\vec{B}_{j,k} \cdot \vec{\sigma} = \lambda(ul + vm) \tag{3.2}$$

where (l, m) is the coordinate system used to describe $\vec{\sigma}$. Allowing us to rewrite 3.1 as a 2D Fourier transform:

$$V_{u,v} \propto \int_{sky} I(l, m) e^{2i\pi(ul+vm)} dldm \tag{3.3}$$

However, because the number of antennas is not infinite, there is a limited number of antenna pairs ($N \times (N-1)$ where N is the total number of antennas), and hence a limited number of $\vec{B}$, which leads to a discrete spanning of the visibility space.

The combination of all (u, v) points sampled by the array configuration is referred to as *uv*-coverage (see Figure 3.1). Since there cannot exist a null distance between antennas, the point $u = v = 0$ is not probed[1]. Furthermore, a whole area in the center of the *uv*-plane corresponding to distances smaller than the shortest baseline, remains un-sampled. This means that extended emission will, to some extent, be lost when using interferometers. Similarly, the largest baseline will determine the maximum achievable resolution by the interferometer. The rotation of the Earth means that the *uv*-coverage changes as time passes, hence longer observations allow for a more complete coverage of the *uv*-plane (see Figure 3.1). Due to undersampling, using proper (inverse) Fourier transforms is not a possibility to go from the *uv*-plane to the image-plane. The most popular method to image visibilities is the CLEAN algorithm first developed in Högbom (1974). However, it is important to note that visibilities are the actual data, images are model representations of this data, and, as such, they are model dependent. The algorithm used to image the visibilities could significantly affect the produced images. This is especially true for low SNR data, where artifacts (such as a dirty beam) will be hard to remove when imaging.

3.2 Radio interferometers

There is a growing number of radio and millimeter interferometric arrays. Below we describe the two most prolific arrays, namely the Atacama Large Millimeter/submillimeter Array (ALMA) and the Karl G. Jansky Very Large Array (VLA). There are many others, e.g. the Submillimeter Array (SMA), the Low-Frequency Array (LOFAR), the Australia Telescope Compact Array (ATCA), the IRAM NOrthern Extended Millimeter Array (NOEMA). Among the new generation are MeerKAT and ASKAP (Australian Square Kilometre Array Pathfinder), the pathfinders for the future Square Kilometer Array (SKA), which will be the largest radio interferometer and is expected to be operational in 2028. Furthermore, radio interferometry is done on many scales with for example, the use of VLBI (Very Long Baseline Interferometry) techniques, which allow for baselines able to mimic the size of the Earth. VLBI gained a lot of traction in the year 2019, when a global VLBI effort, under the name of "Event Horizon Telescope", used telescopes from all around the globe to take the first ever, picture of a black hole (see Figure 3.2).

3.2.1 Atacama Large Millimeter/submillimeter Array

ALMA is an astronomical interferometer composed of 66 antennas. It is located in the Atacama desert in Chile at an elevation of roughly 5000 meters. Its con-

[1]The central region in the *uv*-coverage can be filled in with a "zero-spacing" observation: by using a single dish telescope to recover large angular scale information.

struction began in 2004 and it is a joint ESO (European Southern Observatory), NRAO (National Radio Astronomy Observatory), NAOJ (National Astronomical Observatory of Japan), and Chilean project. The location was chosen because it is one of the highest and driest place on Earth, minimizing the effect water vapor has on observations. As its name indicates, observations are carried out in the millimeter/submillimeter range (from 0.32 mm to 3.6 mm). The antennas are separated into 2 arrays: the main array, consisting of fifty 12 meter diameter antennas, and the Atacama Compact Array (ACA) composed of four 12 meter and twelve 7 meter diameter antennas. One of the impressive technological feats is that antennas can be moved (on trucks), allowing the array to assume different configurations. This creates the possibility of altering distances between antennas from 150 m to 16 km, allowing for different *uv*-coverage. This is beneficial as some configurations are better suited for specific observations. For example, longer baseline configurations will lead to better spatial resolution, while shorter ones will be favored for large scale observations due to an improved field of view. ALMA's spatial resolution is up to 10 milliarcseconds, five times better than that of the Hubble Space Telescope. Its spectral resolution is up to $50\,\mathrm{m\,s^{-1}}$. ALMA has been operating since late 2011, lead to the publication of more than 1000 scientific papers (reaching 1000 in June 2018) in many different areas of astronomy from smaller scales with studies of the Sun to very distant observations investigating early galaxy formation.

3.2.2 Karl G. Jansky Very Large Array

VLA is an astronomical interferometer composed of 27 antennas. It is located in the United States of America, in the state of New Mexico at an elevation of roughly 2100 meters. Its first observation took place in 1980 but the array was upgraded in 2011, changing its name from the former "Very Large Array" to the current "Karl G. Jansky Very Large Array" and upgrading its overall capacities by a factor 8000. Each of the VLA's antennas have a diameter of 25 meters and are positioned to form a "Y" shape (see Figure 3.1). Antennas can be moved along rails, resulting in four different possible configurations (depending on the baseline's length). The most compact configuration (configuration D) shows a maximum baseline of 1.03 km and a minimum baseline of 35 m, corresponding to a resolution of 7.2 arcsec and a field of view of 145 arcsec. The most extended (configuration A) shows a maximum baseline of 36.4 km and a minimum baseline of 680 m, corresponding to a resolution of 0.2 arcsec and a field of view of 5.3 arcsec. The frequency coverage is 74 MHz to 50 GHz. Similar to ALMA, VLA is used in basically all subfields of astronomy.

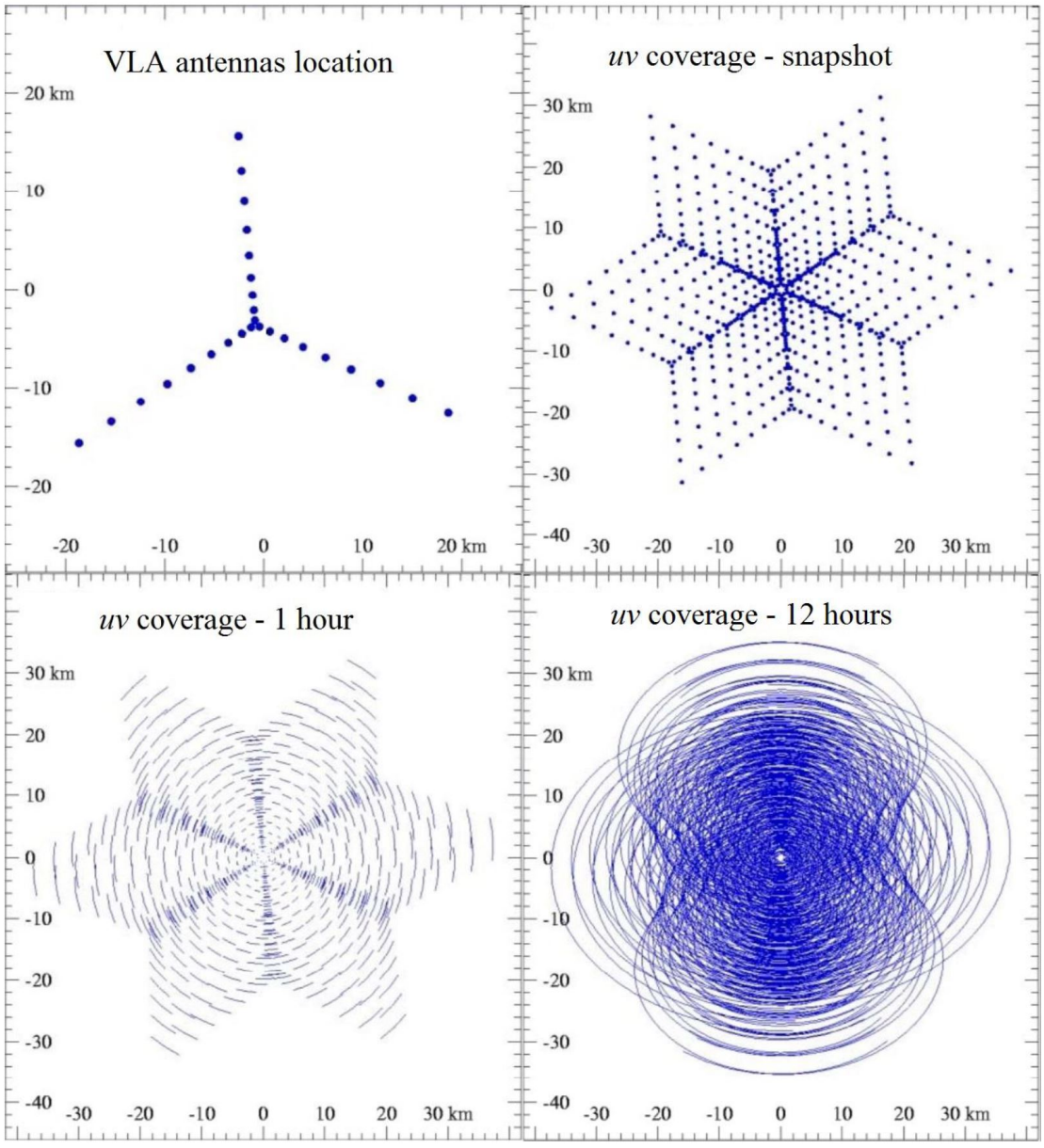

Figure 3.1: VLA antennas location and *uv* coverage as a snapshot after 1 hour and after 12 hours.

Figure 3.2: First ever picture of a black hole, the supermassive black hole of the galaxy M87 located 54 millions light-years away from Earth. This image was captured using the "Event Horizon Telescope", a VLBI network of 8 telescopes from (almost) all over the globe.

Figure 3.3: ALMA: aerial view of the antennas located in the Central Cluster, in their construction stage.

CHAPTER 4

LINESTACKER

Observing high-redshift galaxies is an extremely complex task, especially when trying to identify emission lines from low mass systems. About two days of ALMA integration time would be needed to detect a $z = 2.5$ CO(4-3) line of luminosity $L'_{\rm CO} = 10^9\,{\rm K\,km\,s^{-1}\,pc^2}$, which corresponds to a galaxy with gas mass about few times $10^9\,{\rm M_\odot}$. In contrast, a galaxy 10 times more massive would only require 37 minutes on source observation time. Similarly, to detect a [C II] line, with a width of $200\,{\rm km\,s^{-1}}$, coming from a galaxy at $z = 6$, with a star formation rate of $\sim 10\,{\rm M_\odot\,year^{-1}}$, would require an ALMA integration time of ~ 6 hours, simply to observe one single source. Many similar observations would be needed to draw a statistically significant conclusion about a specific galaxy population, this is especially relevant for our understanding of galaxy evolution. With that in mind, techniques such as stacking are used to allow retrieval of statistical observations while drastically reducing the need for observing time.

Stacking is a method first developed for optical data (Cady and Bates, 1980) that allows a statistical improvement of the SNR through averaging together many individual measurements from a previously known similar population. If the noise is Gaussian, and it should be to first-order approximation, averaging N stamps of pixels together improves the SNR by a factor $\sqrt{N}$, and leads to reveal patterns that were invisible before (see Figure 4.1 for an example of spectral stacking). Because stacking works through averaging, only patterns common to all (or at least most) sources will be properly enhanced, while peculiar individual properties will end up being smeared out by the averaging process. This is the reason why a good à priori knowledge of the stacked sample is needed to be sure that stacked sources share common properties.

For the above listed reasons, the usage of statistical tools to probe both the initial populations (if possible) and the properties of the resulting stack are essential. As an example of this method, let us imagine that we want to measure the average size of the adult population of a town. If we simply average the size of every citizen together we will obtain a biased result as children will also also be included in our sample, therefore driving down the average size. Alternatively, by randomly resampling the original sample into smaller sample sizes a high number of

times, we would eventually realize that the entire population is not homogeneous. Instead, it is composed of two distinct populations of different average sizes: those of the children and those of the adults. In this chapter I will discuss the details of the stacking algorithm I developed, as well as the data analysis/statistical tools included in the code.

4.1 Main algorithm

The stacking tool I developed, called LineStacker, is based on Stacker (Lindroos et al., 2015, 2016). It is an ensemble of CASA tasks, and enables stacking of interferometric data. Unlike Stacker, it allows stacking of spectral cubes *and* continuum data. The goal when developing the code was to create a means to stack together emission (or absorption) lines from a wide variety of sources. To do so, the algorithm requires the redshifts of the targets, the rest frequency of the line to stack, and the spatial position of the targets. A 3D stamp of user defined size centered on each source, both in space and spectral dimensions (using the redshift), is extracted from the data and buffered to facilitate access. Each stamp is then averaged together, pixel to pixel and spectral channel to spectral channel.

3D pixel averaging can be performed using mean, median, or weighted mean schemes. Some weighting methods are embedded in LineStacker, although weights can also be specified by the user. The weighting schemes included are:

- $w_i = \frac{1}{\sigma_i^2}$ where w_i is the weight of source i and σ_i the standard deviation of the stamp associated with source i. This is the most commonly used weighting method. It weights sources as inversely proportionally to the square of the noise around the source, implying that the weights will be the same for all spectral channels (see Paper II).
- $w_{i,j} = \frac{1}{\sigma_{i,j}^2}$ where $w_{i,j}$ is the weight of target source i at spectral channel j, and $\sigma_{i,j}$ is the standard deviation of the stamp associated with source i at spectral channel j. This method, similar to Fruchter and Hook (2002); Bischetti et al. (2018), allows the user to define individual weights for each spectral channel. This method can be especially useful when stacking data with large bandwidths where noise characteristics may be very different on different ends of the bandwidth.
- $w_i = \frac{1}{A_i}$ where A_i is the amplitude of the line associated with source i. This method can only be used if the line is visible pre-stacking, and it allows for a homogenization of the stack (see Paper II).

A particular issue arising from stacking spectral lines rather than continuum emission is the difficulty of trying to stack spectral bins outside of the observed spectral window. This can happen if the user requested large spectral stamps and/or if the observations are not centered on the line targeted for stacking. The algorithm was designed so that for such a case it would not include these sources when stacking such channels. Due to this, fewer sources will be stacked in the outer channels, resulting in a higher noise level at greater distances from the spectral center. Another method used, for example in Murray et al. (2014), is to fill the empty channels with zeros and add them to the stack. Although this method is technically simpler, it is

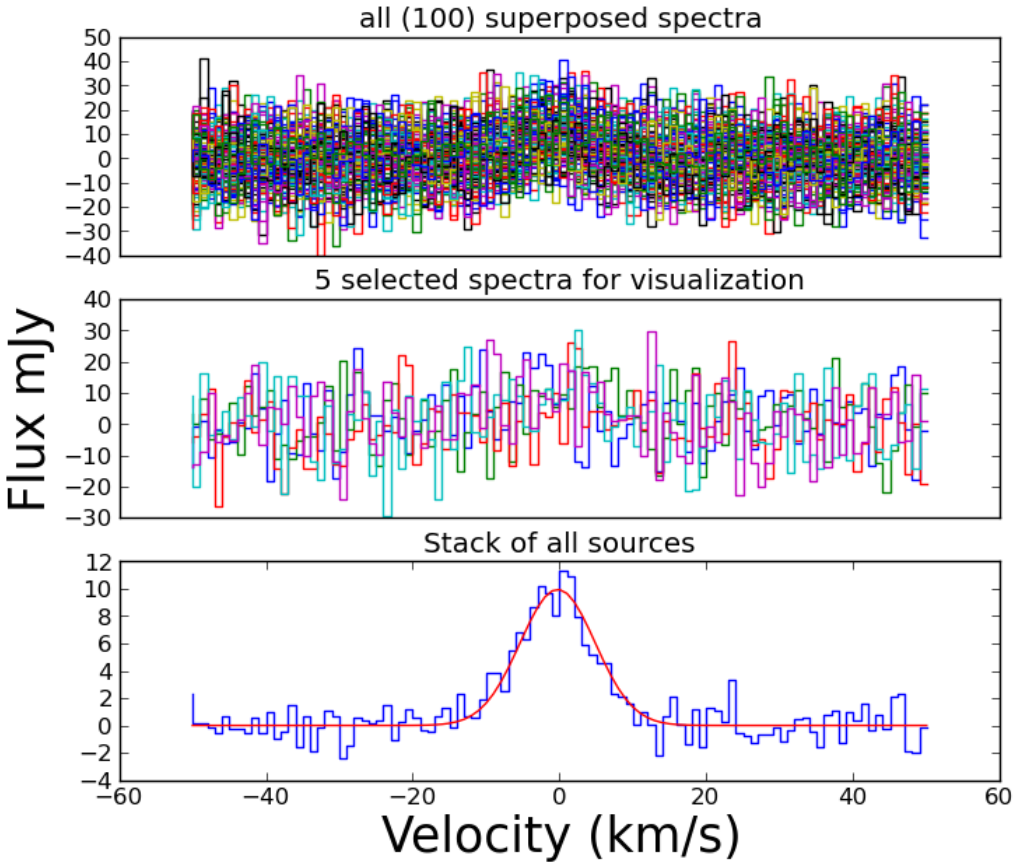

Figure 4.1: 1D stacking example of 100 spectra.

biased as zeros will be added to the stack, thus artificially reducing the stack values in these channels. To allow the user to have the best possible interpretation of their stack, the algorithm returns the number of sources stacked in each spectral channel. The stack output is a stacked cube, leaving the user free to extract spectra in any desired fashion.

For completion, a 1D version of LineStacker is also included. This 1D-Stacker functions similar to LineStacker but stacks the spectra directly instead of the cubes (see Figure 4.1). Thus this version does not require spatial positions of the sources to run. The 1D-Stacker can be used on all kinds of spectral data extracted beforehand. It features the same tools as 3D LineStacker and is useful when users wish to extract spectra from cubes before stacking. This can happen if sources have been observed with different telescopes or in different configuration which can lead to different primary beams for different sources. Similarly, if the sources are known to be extended or to differ in sizes it may be relevant to have a customized spectral extraction for each source (i.e. from different regions) before stacking.

4.2 Embedded tools

A series of computing tools are embedded in the program that can be used to increase the usefulness and capacity of LineStacker. These tools can be used either pre-stacking (to improve knowledge of the studied data) or post-stacking (to get a better handle of the statistics and to better understand the product of stacking). One should bear in mind that since stacking is a statistical method, its product is not fully straightforward to analyze. These tools aim at providing the user with ways to perform and analyze stacking in a controlled and meaningful way.

4.2.1 Evaluating relevance of stack

Stack products should always be compared, not to the general noise in sources pre-stacking, but to a "noise-stack". A "noise-stack" refers to a comparison stack where the stacking positions are chosen completely randomly as "empty" (i.e. noise only) positions. To generate this "noise-stack" a set of positions on the images are randomly chosen and then stacked (as many random positions as there are original target sources). This process is coupled to Monte Carlo methods to statistically avoid peculiar noise regions. Each time, stacking positions are chosen at random anywhere on the map, far enough from the original target sources to avoid contamination. These stacks of random, source free, positions are then compared to the original stack. This allows the user to see whether the stacking result could be reproduced by solely stacking random noise.

4.2.2 Bootstraping and subsampling

Bootstrapping and subsampling are statistical methods aimed at studying the distribution of the target sources' parameters through randomly resampling the original set of sources. Coupled to Monte Carlo methods, these processes are repeated a high number of times to explore a representative portion of the total number of possible resamples.

Bootstrapping acts through randomly resampling with replacement, leading to a resampled population the same size as the original sample. When used through LineStacker, all subsequent resamples are stacked and the corresponding stack result is saved. The distribution of stack results is then analyzed and compared to the original stack. The distribution should be close to Gaussian, centered on the original stack result – however, a larger negative tail is expected since noise reduction is not optimal when a given source is present more than once in the stack. An inhomogeneous original sample distribution (for example, one that includes some outliers among the input population) would lead to a possible strong deviation from Gaussianity and would hence be diagnosed as such by a bootstrapping analysis.

Subsampling acts through the creation of a new, smaller sample that is randomly selected from the original sources. The number of elements N_{sub} in the new subsample can be fixed or randomized for each iteration of the Monte Carlo process, with $N_{min} < N_{sub} < N_{max}$ where $N_{min} > 0$ and $N_{max} < N$, where N is the number of sources in the original sample. N_{min} and N_{max} are specified by the user.

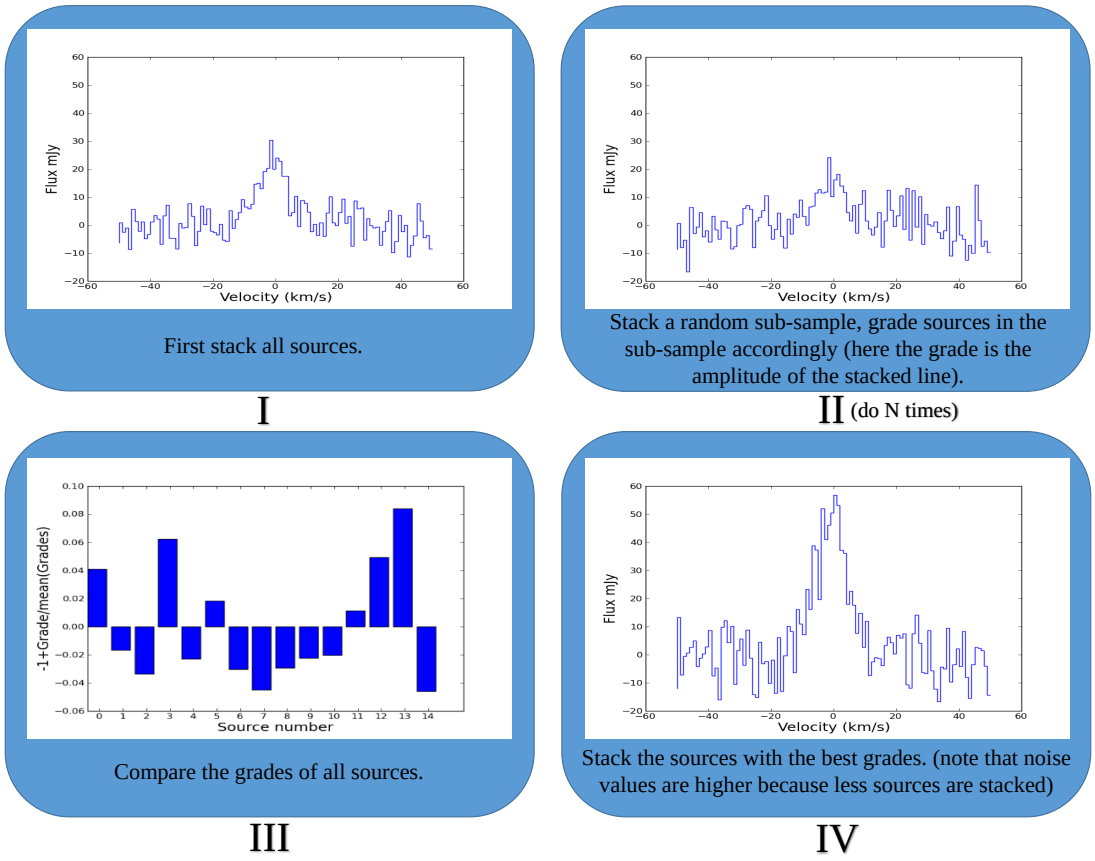

Figure 4.2: A block diagram example of the sub-sampling process.

It should be noted that if N_{sub} is small, the noise reduction effect of stacking will be drastically reduced (because of the low number of sources in the stack); additionally, spanning all possible configurations will be a lengthy process as there are

$$\binom{N}{N_{sub}} = \frac{N!}{N_{sub}!\,(N - N_{sub})!}$$

possible subsamples of size N_{sub}.

Subsampling can be used if one expects that some sources should not be included in the stack due to physical considerations (such as angular orientation in the case of a QSO, see Paper II). To identify such sources subsampling should be paired with a grading function, attributing a common grade to sources in the tested subsample (see Figure 4.2). The exact grading function has to be user input because it is dependent on the tested property. For example, in Paper II, the grading function utilized would grade a subsample proportionally to the presence of a spectral outflow signature. A pre-existing grading function is already embedded in LineStacker that grades the subsample proportionally to the corresponding stack's amplitude. Such methods can allow for the identification of the sources that are responsible for most of the stacked emission or that have a high probability to exhibit no emission –or much lower than average.

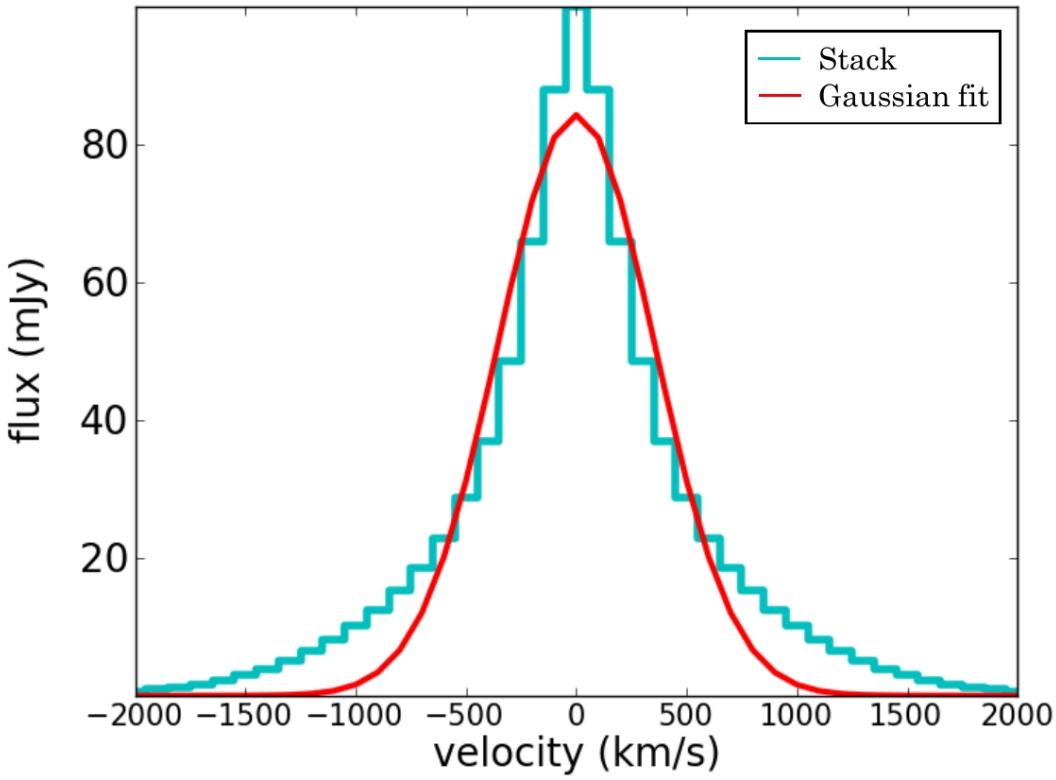

Figure 4.3: Example stack of 50 Gaussian lines with a large range of width, showing an artificial broad wing component. This showcases the necessity for spectral rebinning when studying line profiles.

4.2.3 Spectral rebinning

When trying to recover information about the line profile through stacking one should be aware that stacking lines of different sizes or shapes leads to a biased result. Since spectral stacking is performed from spectral bin to spectral bin, stacking Gaussian shaped lines with different widths (in bins) will result in a non-Gaussian stacked profile with wings (i.e. some additional flux in the outer channels, see Figure 4.3 and Paper I). More generally, even if all sources exhibit lines with the same arbitrary shape (Gaussian, Lorentzian, double peak Gaussian etc.), if they do not span the same amount of spectral bins, the spectral shape information will be lost, or at least diluted, in the resulting stack. A simple solution exists to prevent this as long as the lines are visible before stacking. This solution consists of rebinning all spectra such that all lines span the same number of bins. It should be noted that bin size information is lost through rebinning. Before rebinning all spectral bins should have a well defined physical size (i.e. in $\mathrm{km\,s^{-1}}$ or Hz) but once rebinned all spectra will show a different bin size. As such, deriving the size of the spectral channels in the stack of rebinned spectra is not straightforward.

Finally, it is important to keep in mind that since there is no reason to expect all lines to have the same width naturally, it would be basically impossible to confidently retrieve spectral shapes from sources that were invisible before stacking.

CHAPTER 5

RESULTS OF PAPERS

5.1 Paper I

5.1.1 Description of Paper I

Paper I aims at fully describing and testing LineStacker. To do so I simulated a number of data sets – data cubes as well as 1D data – to assess the tool's performances in different situations. Most simulations were performed using CASA's task SIMALMA which preforms full ALMA observation simulations using a custom sky input by the user as the observable. SIMALMA delivers a simulated set of visibilities as an output. These visibilities were transformed into an image using the CLEAN algorithm (first developed in Högbom, 1974). All the stacks consisted of 30 sources, yielding a noise reduction of $\sim \sqrt{30} \sim 5.5$. Each source consisted of an emission line and some noise. The different simulated datasets were built to be increasingly realistic. The first sets were very simple and built slowly into more specific test cases that could be expected from real observations. The effect of bright foreground sources, extended target sources, or using a different interferometer (e.g. VLA) were tested, among other expected different scenarios. To complete our study, four one-dimensional data sets were simulated to test the performances of the 1D-Stacker, and also to study cases with more complex spectral configuration. Special attention was given to the study of redshift uncertainties.

5.1.2 Results of Paper I

For a summary of the results, see Table 3, 4, 5 and 6 in Paper I. Reconstruction rates of the line amplitude were very satisfying. They were above, or close to, 90% for every set with even the most complicated ones properly reconstructed. Reconstruction kept similar values when the amplitude of the line was set to noise level, showing the efficiency in increasing the SNR by making use of stacking. Reconstruction of the linewidth[1], as well as the integrated flux showed similar results. As mentioned

[1]I will be referring to the Full Width Half Maximum (FWHM) of the line when referring to the width, or linewidth

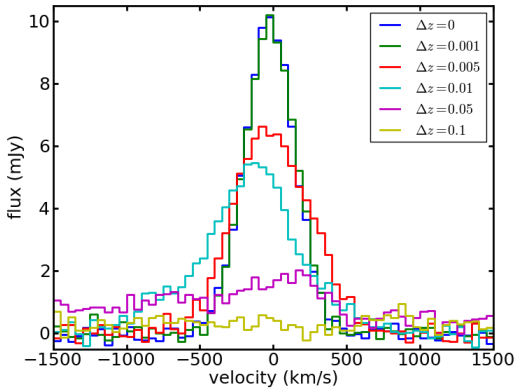

Figure 5.1: Stack spectrum of 30 sources of width 400 km s^{-1} for different redshift uncertainties. $\Delta z = 0.01$ shows a $\sim$ 50% drop in reconstruction accuracy, and the accuracy drops rapidly above this.

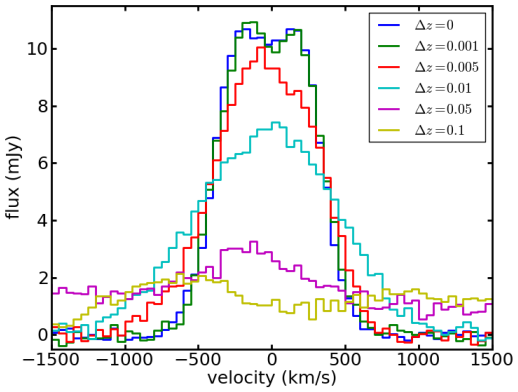

Figure 5.2: Stack spectrum of 30 sources of with double peaked profile for different redshift uncertainties (both peaks are Gaussian with a width of 400 km s^{-1} and a distance of 400 km s^{-1} between the two peaks). Uncertainties higher than 0.001 dilute the two peaks, showing that similar profiles will be extremely hard to reconstruct through stacking.

previously, when all lines have different widths the resulting stacked line will lose its Gaussian shape and hence the amplitude will be slightly underestimated by Gaussian fitting. This does not have a huge impact on the results but is important to keep in mind as it is inherent to spectral stacking.

Through stacking 1D simulated data sets, I quantified the effect of redshift uncertainties on spectral stacking. I showed that line reconstructions would be very inefficient when redshift uncertainties rose above 0.01. Furthermore, trying to reconstruct line profiles is virtually impossible if the redshift precision is not very accurate. See Figures 5.1 and 5.2.

5.2 Paper II

5.2.1 Description of Paper II

Paper II is our first application of LineStacker to real data. In this project we stacked a sample of 25 quasars at redshift $z \sim 6$ detected in [C II] to search for high velocity outflow components. Outflows can be characterized by a second, broader and fainter, component under the main line (see for example Sulentic et al., 2014; Decarli et al., 2018). As the main line of the host galaxy is clearly detected, and the redshift uncertainty is very low ($\Delta z < 0.01$), stacking can be performed accurately with all the lines properly centered. Furthermore the good identification of individual line widths allowed for spectral rebinning of the individual spectra, avoiding issues that would arise from stacking lines with different widths. Indeed, we

showed that stacking lines with different widths introduced artificial wing signatures into the stack making the analysis of the spectral profile biased toward finding outflows if the data were not rebinned before stacking. As stated in Section 2.5 outflow observation at high-redshift are needed to complete our understanding of the impact of AGN feedback on galaxy evolution.

It is expected that, even if all sources hosted outflows, they would not all be visible due to orientation effects. Thus, we used a subsampling method to identify sources that presented clearer outflow components when stacked. We performed two stacking techniques:

- First, spectra were extracted individually from each source from the regions in moment-0 maps with flux higher than two-sigma levels. All spectra were stacked together using 1D stacking. While this method is simpler and allows for a meaningful way to extract spectra, it is also biased. Since the spectra were extracted before stacking, the potential outflow components were not individually detected, and it was not clear that they would span the same region as the main line. By restricting the extracting region to regions with flux higher than two-sigma levels, we may miss the regions where the outflow is, especially if the emission is extended. On the contrary, if the outflow emission is very compact, taking a region that is too large would lower the outflow signal through summing pixels with no outflow component signatures with pixels that do contain some.
- Second, by stacking the cubes and extracting a spectrum afterward from the stacked cube. This allowed us to examine the spatial extent and characteristics of the stacked line, but also had certain caveats. Sources are stacked pixel to pixel, which means that if the emission was more extended in some sources than in others, stacking could dilute the outflow signal. Furthermore, finding the best region from which to extract the spectra was not straightforward.

However, both methods showed similar results. Additionally, three weighting schemes were used. The first was simply to use no weighting at all. Since that we do not know if there is a relation between the main component and the outflow component, it may be arbitrary to choose a peculiar weighting scheme based on the characteristics of the main component. However, if one thinks that the outflow amplitude is proportional to the main line amplitude, then using a weighting scheme that is inversely proportional to the amplitude of the line would allow all outflows to carry the same weight and correct for their brightness. The last set of weights used was inversely proportional to the noise in the associated cube which allowed for higher weights to be given to sources that presented lower noise values.

5.2.2 Results of Paper II

Through subsampling we identified a subsample of 11 sources that were the major contributors to the broad component emission. We named this subsample "max subsample". Similarly, we formed a subsample with the sources not included in the max subsample. We termed this subsample the "min subsample". The stack of the max subsample showed a tentative detection of a broad component, with FWHM $= 1110 \pm 203\,\mathrm{km\,s^{-1}}$ and $S_{\mathrm{peak}} = 2.03 \pm 0.61\,\mathrm{mJy}$, which is indicative of a

[CII] outflow. Furthermore, when stacking the min subsample we found no deviation from simple Gaussianity, indicating coherence in our subsampling scheme.

To ensure that the obtained results were neither purely random nor driven by a single bright source, we performed mock sample tests and additional analyses of our sample. To verify that one source was not responsible for most of the outflow emission, we restacked the subsample after removing one of its sources. We repeated this process for each source in the subsample. The resulting stacks did not show strong deviation from the original max subsample stack. Hence, we concluded that the max subsample was rather homogeneous, at least in terms of wing emission. Additionally, we performed tests to make sure that our signal could not be reproduced by stacking random noise. Finally, to prove the efficiency of our methods, we created mock data-sets containing outflows to determine their recovery rate. The outflows were generated with a width of three times the main components', and an amplitude five times weaker than the main components'. By stacking, we attained a recovery rate of the second component of 98.52% at $3\,\sigma$ and 31.72% at $5\,\sigma$, thus showing that our method should be able to recover outflows with similar properties to a least $3\,\sigma$ level.

Our results are consistent with the derived width and amplitude of the detected broad components of molecular outflows at low and high redshifts (e.g. Harrison et al., 2014; Cicone, 2015). Although deeper individual observations would be needed to improve our understanding of outflows at $z \sim 6$, our study is a first step in quantifying the ability to detect high-redshift outflows, and will also be useful when planning future observations of individual sources. In addition, we have demonstrated the efficiency of subsampling, which is a tool that could be combined with large surveys to identify sources more likely to present an outflow component.

My contribution to Paper II is that I developed the stacking tool (as described in Paper I), carried out the stacking analysis (including the subsampling), and performed the mock sample tests mentioned above. Additionally, I participated in the data reduction.

5.3 Paper III

5.3.1 Description of Paper III

In Paper III we once again focused on [C II] in $z \sim 6$ galaxies. In contrast to Paper II, which focused on luminous sources, we here targeted a large sample of faint sources. Indeed, we focused solely on sources not individually detected in our 1.2 mm data by making use of data from the ALMA Lensing Cluster Survey (ALCS). The ALCS is a large ALMA program in cycle 6 (PI: K. Kohno) designed to target 33 lensing cluster and totalling 110 arcsec^2 in band 6 ($\sim$ 1.2 mm). The observed frequency windows of the program (one from 250.0 to 257.5 GHz and one from 265.0 to 272.5 GHz) translates to a possible range of observable redshifts: $5.97 \lesssim z \lesssim 6.17$ and $6.38 \lesssim z \lesssim 6.60$ for [C II] observation. As we are dealing with line stacking, it is necessary to know the redshift accurately as shown in Paper I. This is why we selected only sources with either spectroscopic redshifts or photometric redshifts with a very good precision (σ_z<0.02). After selection, the final full sample consisted

of 52 sources. All these sources physical coordinates and redshifts were found and extracted from a variety of different catalogs, from which we also extracted SFR and magnification when available. Alternatively, for those sources without SFR measurements available in online catalogs, we used the SED fitting tool BAGPIPES (Carnall et al., 2018) to retrieve SFRs when possible (i.e. when photometry for these objects could be found online).

The 52 sources were located behind nine different galaxy clusters out of the 33 available in ALCS. To improve our selection method we built three additional subsamples from our 52 sources. The first was termed the "good-z subsample" and consisted of only sources with the highest redshift precision, meaning this sample was comprised of only sources with high precision spectroscopic redshifts. If the source had a photometric redshift or poor spectroscopic redshift flags, it was not included in the subsample. In total this subsample contained 36 sources. The second was termed the "high-SFR subsample" and consisted of only the sources with a SFR higher than the median SFR of the full sample (SFR $>$ 10 $M_\odot$ per year). This subsample was composed of 17 sources. The third subsample was termed the "sfr-z subsample" and was composed of the 11 sources that were included in both the good-z and high-SFR subsamples.

All the different subsamples were stacked with LineStacker using both weighted-average stacking (where the weight of each source is the inverse of the square of the local RMS) and median stacking. In addition, we performed continuum stacking on the same samples.

As explained in Chapter 2.4.2, [C II] is a known tracer of a galaxy's SFR and the correlation between the [C II] line luminosity and a galaxy's SFR has been studied in-depth at low redshift. However, only a few studies at $z \sim 6$ have detected [C II] , and mostly from bright objects. The goal of our analysis was to shed light on the [C II] - SFR relationship at high-z, more specifically in the low-SFR domain.

5.3.2 Results of Paper III

After stacking we found no detections in [C II] nor in continuum emission in both the weighted-average and median stacks. From this absence of emission we derived 3σ upper limits for both the [C II] line luminosity and the 1.2 mm flux (see Béthermin et al., 2020). Using the measured [C II] luminosity upper limits we inferred an upper limit on the [C II] - SFR relationship. These results, shown on Figure 5.3, were separated into two sets of data points; one for the mean-stacking results and one for the median-stacking results. The [C II] luminosity was corrected for the mean or median magnification of the sources depending on the type of stacking that was performed. Although both analyses (weighted-average and median) actually produced similar results when looking at the direct flux extracted from the stacking analyses, the substantial difference between the mean and median results shown in Figure 5.3 came from two factors: (i) the difference between mean and median SFR (induced by a few objects with higher SFR) which moved data points on the x-axis, and (ii), the difference between mean and median magnification which moved data points along the y-axis. Overall, the results derived from the weighted-average stacking analysis indicated a deviation from the local relationship, while median-

stacking results showed a marginal agreement with it. Finally, our results seem to indicate that high-redshift sources show lower [C II] luminosity than local galaxies at the same SFR.

In Paper III I produced most of the analysis. The only parts I did not produce are: (i) the SED fitting analysis (nor did I write the section associated to it) and (ii) the dust mass computations from the continuum stacking results (however, I did produce the continuum stack maps). All the observations and input data were made available through the ALCS collaboration.

5.4 Paper IV

5.4.1 Description of Paper IV

Paper IV is fairly different, from a technical perspective, to other work in this thesis, as it focused on continuum stacking rather than spectral stacking. Indeed, the goal of our analysis was to study the evolution of dust mass and comoving dust mass density (CDMD) with lookback-time in the ALCS data. To obtain the dust mass we used continuum observations from the ALCS paired with a catalog provided by team members (see Kokorev et al. in prep.) selected from *HST*/*Spitzer* IRAC observations and photometry. From the catalog we extracted 3903 sources located within the ALCS clusters. With the photometry extracted from the catalog, we used BAGPIPES (Carnall et al., 2018) with four different star formation histories (SFHs) to perform SED fitting. The SED fits provided redshifts and physical properties of the sources, most notably SFRs and stellar masses. Individual magnifications were computed at each source position using magnification maps produced using the GLAFIC model and scaled to the redshift of the source.

To study how dust mass evolves with redshift we binned the sources in five different redshift bins: $1 < z \lesssim 2$, $2 < z \lesssim 3$, $3 < z \lesssim 4$ and $z > 5$. We note that all sources with redshifts below one ($z < 1$) were not studied in this work; however, an analysis of their properties, coupled with clusters sources analyses, will be presented in a separate paper (Guerrero et al. in prep). In addition, we grouped sources with similar physical properties into two different decoupled bins corresponding to SFR and stellar masses.

Since ALCS observations are performed at millimeter wavelength, the optically thin and single cold dust temperature approximations (described in this work in Section 2.4.2 and in (among others) Scoville et al. (2014, 2016); Magnelli et al. (2020)) are expected to be valid. We use the median stacked ALMA 1.2 mm fluxes to compute dust masses, similar to Kovács et al. (2010); Magnelli et al. (2020).

To compute the CDMD, we multiply the median dust mass computed in each bin by the total number of sources in that bin, and divide by the total area covered by the survey (corrected for harmonic-mean magnification).

5.4.2 Results of Paper IV

From the stack stamps in each bin (see Figure 5.4 for an example) we extracted the flux in the central circular region of radius 1.6 arcsec (corresponding to the average

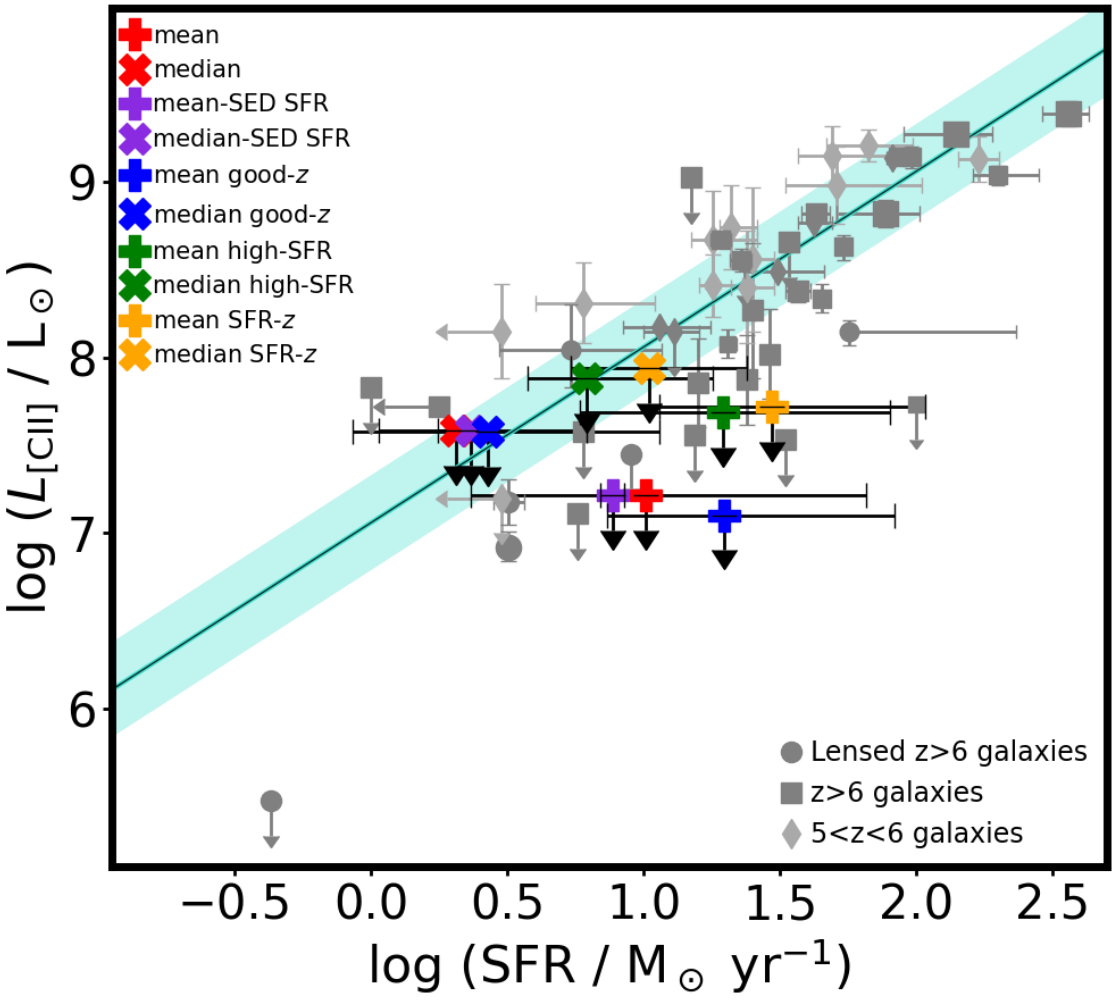

Figure 5.3: Stacking results, upper limit $L_{[CII]}$ vs. SFR. The error bars of the data obtained in this study are the standard deviation in the case of the mean stacking analyses, and the median absolute deviation for the median stacking analyses (for the SFR obtained from mean and median SED the errors are extracted from SED fitting). Other data points are extracted from the following studies: Ouchi et al. (2013); Ota et al. (2014); González-López et al. (2014); Capak et al. (2015); Maiolino et al. (2015); Schaerer et al. (2015); Willott et al. (2015); Knudsen et al. (2016); Pentericci et al. (2016); Bradač et al. (2017); Decarli et al. (2017); Matthee et al. (2017); Carniani et al. (2018); Smit et al. (2018); Hashimoto et al. (2019); Béthermin et al. (2020); Bakx et al. (2020); Harikane et al. (2020); Fujimoto et al. (2021). The cyan line is the relation extracted for low-z starburst galaxies from the De Looze et al. (2014) study including its 1σ dispersion.

source size when above 3σ). The noise was computed as the standard deviation across the rest of the map. When the central flux was lower than 3σ we used 3σ upper limits (see for example Béthermin et al., 2020; Schaerer et al., 2020).

We detected much less dust mass than expected at the studied redshifts, SFRs, and stellar masses, especially considering the very good sensitivity in the resulting stacked maps. More specifically, at $z > 2$, we find nominal detections, while the global RMS of the stacked maps remains low (of order 0.01 mJy). When looking specifically at the evolution of dust mass with stellar mass and SFR, we similarly observe a lower dust content compared to modeling (e.g. Popping et al., 2017), at least in the higher stellar mass bins. Computing the CDMD as a function of redshift, we again find a significant difference compared to previous observations/models. Our results being systematically lower by almost one dex.

The reason for such a low detections could be due to selection biases. Indeed, since we used *HST* and *Spitzer* data to select the galaxies, we may be targeting objects with intrinsically lower dust masses. Furthermore, and considering we decided to include all sources regardless of their luminosity, we may be stacking the fainter end of the population as well. Our median stacking analysis may hence be lead by the dust-poor bulk of the population; it should be noted however, that weighted-average stacking analyses produced similar results.

In paper IV I carried out the entire analysis. The SED fitting analysis was supervised by N. Laporte who shared the BAGPIPES templates that I used in the study. All the observations and input data were made available through the ALCS collaboration.

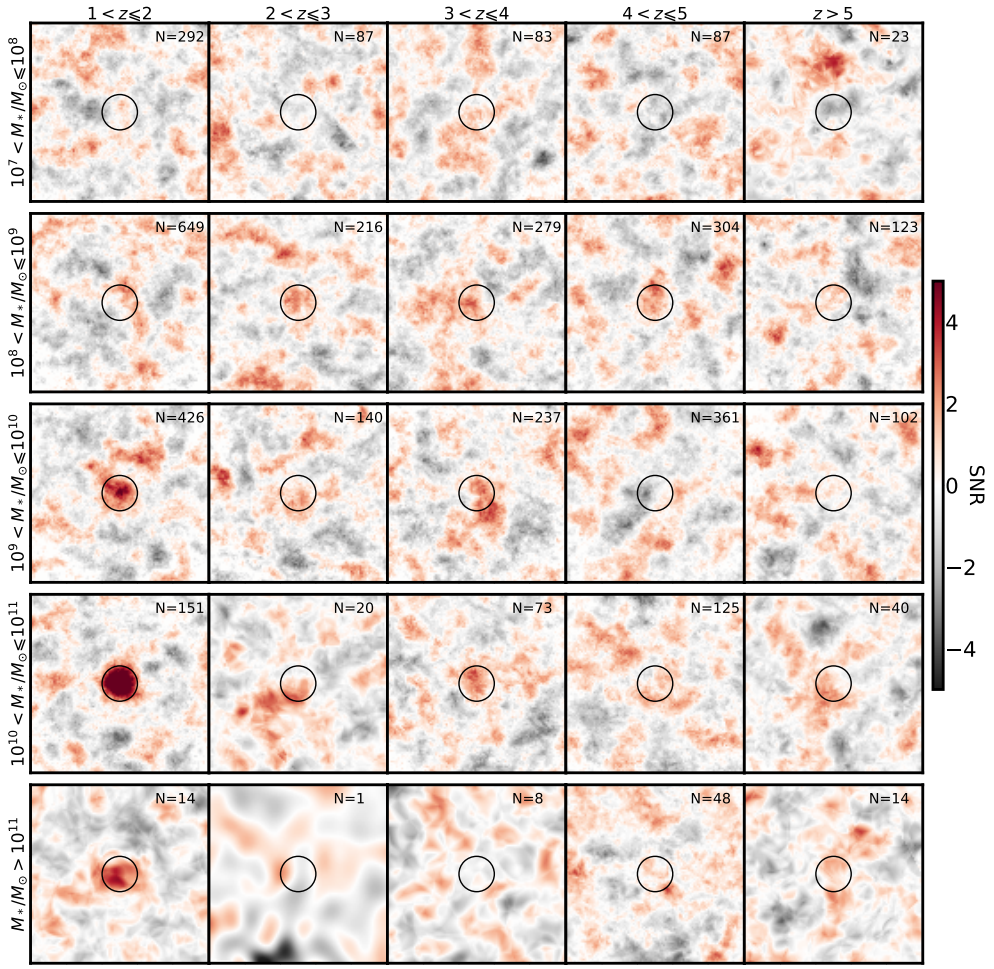

Figure 5.4: 16.16 × 16.16 arcsec^2 (101 × 101 pixels) median Stacking stamps, split in bins of stellar mass and redshift. Each map is normalised by the overall standard deviation computed across the stamp, outside of the central circular region of radius 1.6 arcsec. The number of sources stacked (N) is indicated in each bin. The black circle in the center indicates the region from which the flux is extracted.

CHAPTER 6

CONCLUSION & OUTLOOK

In this thesis I provided the reader with the motivation and background required to understand our analyses in the field of galaxy evolution. The studies we carried out allowed us to investigate the gas and dust content of both high-mass and low-mass galaxies. I also presented the different tools that I built throughout my PhD, to help and improve analyses of galaxy studies.

I showed the reliability and power of (spectral-) stacking analyses, showcasing the importance for statistical, large scale studies. Stacking is unique in its ability to bring to light even the faintest objects, and to get past one of the main bias in astronomy: looking only at the tip of the iceberg. With stacking analyses in mind, one can rethink future observation projects: by targeting larger volume. Even with lower integration time, one could still reach very deep through stacking.

LineStacker is now fully operational and publicly available as an open source tool. It has been used in several projects, as described in the Papers appended in this thesis. LineStacker and its embedded tools have proved useful when targeting:

- Bright lines covering a second fainter component.
- Presumed emission lines hidden under the noise.
- Continuum emission coming from a high number of sources.

Indeed, aside from the paper presenting and testing the tool, we carried out analyses of outflows under bright [C II] lines near the end of the epoch of reionization; we searched for [C II] in faint galaxies at similar redshifts; and we studied the evolution of dust –both its mass and its overall comoving density– from $z \sim 1 - 6$. In all cases we showed the importance of including even the faintest objects, and the usefulness of stacking for such analyses.

However, spectral stacking, and LineStacker more specifically, can be used for many other analyses. Spectral stacking could for example be used to study local galaxies, where redshift uncertainties are much smaller, or using extremely large samples of high-redshift galaxies to study their average properties using subsampling techniques.

In addition to the main stacking algorithm, the statistical tools included in LineStacker allow to properly diagnose the stack detections to gain further insights on the studied population. One of the additional tools that could be added, is an algorithm that could potentially help with redshift precision when performing line stacking. The idea, which is also briefly mentioned in Guerrero et al. (in prep), is the following: by randomly shifting the stack centers of each spectrum as a Monte-Carlo process, one could in theory optimize the stacking by eventually aligning all the peaks perfectly. This could prove useful in cases where lines are observed after stacking but where the redshift precision was not high. Shifting the line to the proper redshift of each source would allow not solely to maximize the stacking results but also to improve the knowledge of the redshift of each source individually. Of course the possibility for LineStacker to perform spectral stacking directly in the *uv*-plane, like Stacker, is still under consideration for future development.

A new generation of telescopes/interferometers is going to come online in the coming years (such as the SKA or the LSST), and with them a huge amount of data. In this context I expect that stacking analyses, and LineStacker, will become unavoidable tools to extract the most from their observations.

BIBLIOGRAPHY

Abel, N. P., Dudley, C., Fischer, J., Satyapal, S., and van Hoof, P. A. M. (2009). Dust-Bounded Ultraluminous Infrared Galaxies: Model Predictions for Infrared Spectroscopic Surveys. *ApJ*, 701(2):1147–1160.

Alexander, D. M. and Hickox, R. C. (2012). What drives the growth of black holes? *New Astronomy Reviews*, 56:93–121.

Alvarez, M. A., Bromm, V., and Shapiro, P. R. (2006). The H II Region of the First Star. *ApJ*, 639(2):621–632.

Appleton, P. N., Guillard, P., Boulanger, F., Cluver, M. E., Ogle, P., Falgarone, E., Pineau des Forêts, G., O'Sullivan, E., Duc, P. A., Gallagher, S., Gao, Y., Jarrett, T., Konstantopoulos, I., Lisenfeld, U., Lord, S., Lu, N., Peterson, B. W., Struck, C., Sturm, E., Tuffs, R., Valchanov, I., van der Werf, P., and Xu, K. C. (2013). Shock-enhanced C^+ Emission and the Detection of H_2O from the Stephan's Quintet Group-wide Shock Using Herschel. *ApJ*, 777(1):66.

Bakx, T. J. L. C., Tamura, Y., Hashimoto, T., Inoue, A. K., Lee, M. M., Mawatari, K., Ota, K., Umehata, H., Zackrisson, E., Hatsukade, B., Kohno, K., Matsuda, Y., Matsuo, H., Okamoto, T., Shibuya, T., Shimizu, I., Taniguchi, Y., and Yoshida, N. (2020). ALMA uncovers the [C II] emission and warm dust continuum in a z = 8.31 Lyman break galaxy. *MNRAS*, 493(3):4294–4307.

Baldry, I. K. (2008). Hubble's galaxy nomenclature. *Astronomy & Geophysics*, 49(5):5–25.

Barnes, J. E. and Hernquist, L. (1996). Transformations of Galaxies. II. Gasdynamics in Merging Disk Galaxies. *ApJ*, 471:115.

Baum, W. A. (1962). Photoelectric Magnitudes and Red-Shifts. In McVittie, G. C., editor, *Problems of Extra-Galactic Research*, volume 15, page 390.

Bertone, S. and Conselice, C. J. (2009). A comparison of galaxy merger history observations and predictions from semi-analytic models. *MNRAS*, 396:2345–2358.

Béthermin, M., Fudamoto, Y., Ginolfi, M., Loiacono, F., Khusanova, Y., Capak,

P. L., Cassata, P., Faisst, A., Le Fèvre, O., Schaerer, D., Silverman, J. D., Yan, L., Amorin, R., Bardelli, S., Boquien, M., Cimatti, A., Davidzon, I., Dessauges-Zavadsky, M., Fujimoto, S., Gruppioni, C., Hathi, N. P., Ibar, E., Jones, G. C., Koekemoer, A. M., Lagache, G., Lemaux, B. C., Moreau, C., Oesch, P. A., Pozzi, F., Riechers, D. A., Talia, M., Toft, S., Vallini, L., Vergani, D., Zamorani, G., and Zucca, E. (2020). The ALPINE-ALMA [CII] survey: Data processing, catalogs, and statistical source properties. *A&A*, 643:A2.

Bischetti, M., Maiolino, R., Fiore, S. C. F., Piconcelli, E., and Fluetsch, A. (2018). Widespread QSO-driven outflows in the early Universe. *ArXiv e-prints*.

Boselli, A., Gavazzi, G., Lequeux, J., and Pierini, D. (2002). [CII] at 158 mu m as a star formation tracer in late-type galaxies. *A&A*, 385:454–463.

Bouwens, R. J., Illingworth, G. D., Oesch, P. A., Trenti, M., Labbé, I., Franx, M., Stiavelli, M., Carollo, C. M., van Dokkum, P., and Magee, D. (2012). Lower-luminosity Galaxies Could Reionize the Universe: Very Steep Faint-end Slopes to the UV Luminosity Functions at z >= 5-8 from the HUDF09 WFC3/IR Observations. *ApJ*, 752(1):L5.

Bowman, J. D., Cairns, I., Kaplan, D. L., Murphy, T., Oberoi, D., Staveley-Smith, L., Arcus, W., Barnes, D. G., Bernardi, G., Briggs, F. H., Brown, S., Bunton, J. D., Burgasser, A. J., Cappallo, R. J., Chatterjee, S., Corey, B. E., Coster, A., Deshpande, A., deSouza, L., Emrich, D., Erickson, P., Goeke, R. F., Gaensler, B. M., Greenhill, L. J., Harvey-Smith, L., Hazelton, B. J., Herne, D., Hewitt, J. N., Johnston-Hollitt, M., Kasper, J. C., Kincaid, B. B., Koenig, R., Kratzenberg, E., Lonsdale, C. J., Lynch, M. J., Matthews, L. D., McWhirter, S. R., Mitchell, D. A., Morales, M. F., Morgan, E. H., Ord, S. M., Pathikulangara, J., Prabu, T., Remillard, R. A., Robishaw, T., Rogers, A. E. E., Roshi, A. A., Salah, J. E., Sault, R. J., Shankar, N. U., Srivani, K. S., Stevens, J. B., Subrahmanyan, R., Tingay, S. J., Wayth, R. B., Waterson, M., Webster, R. L., Whitney, A. R., Williams, A. J., Williams, C. L., and Wyithe, J. S. B. (2013). Science with the Murchison Widefield Array. *PASA*, 30:e031.

Bowman, J. D., Rogers, A. E. E., Monsalve, R. A., Mozdzen, T. J., and Mahesh, N. (2018). An absorption profile centred at 78 megahertz in the sky-averaged spectrum. *Nature*, 555(7694):67–70.

Bradač, M., Garcia-Appadoo, D., Huang, K.-H., Vallini, L., Quinn Finney, E., Hoag, A., Lemaux, B. C., Borello Schmidt, K., Treu, T., Carilli, C., Dijkstra, M., Ferrara, A., Fontana, A., Jones, T., Ryan, R., Wagg, J., and Gonzalez, A. H. (2017). ALMA [C II] 158 μm Detection of a Redshift 7 Lensed Galaxy behind RXJ1347.1-1145. *ApJ*, 836(1):L2.

Brauher, J. R., Dale, D. A., and Helou, G. (2008). A Compendium of Far-Infrared Line and Continuum Emission for 227 Galaxies Observed by the Infrared Space Observatory. *ApJS*, 178(2):280–301.

Brisbin, D., Ferkinhoff, C., Nikola, T., Parshley, S., Stacey, G. J., Spoon, H., Hailey-Dunsheath, S., and Verma, A. (2015). Strong C^+ Emission in Galaxies at z $\sim$1-2:

Evidence for Cold Flow Accretion Powered Star Formation in the Early Universe. *ApJ*, 799(1):13.

Cady, F. M. and Bates, R. H. T. (1980). Speckle processing gives diffraction-limited true images from severely aberrated instruments. *Optics Letters*, 5:438–440.

Calzetti, D. (2001). The Dust Opacity of Star-forming Galaxies. *PASP*, 113(790):1449–1485.

Capak, P. L., Carilli, C., Jones, G., Casey, C. M., Riechers, D., Sheth, K., Carollo, C. M., Ilbert, O., Karim, A., Lefevre, O., Lilly, S., Scoville, N., Smolcic, V., and Yan, L. (2015). Galaxies at redshifts 5 to 6 with systematically low dust content and high [C II] emission. *Nature*, 522(7557):455–458.

Carilli, C. L. and Walter, F. (2013). Cool Gas in High-Redshift Galaxies. *Annual Review of Astronomy and Astrophysics*, 51:105–161.

Carlstrom, J. E., Ade, P. A. R., Aird, K. A., Benson, B. A., Bleem, L. E., Busetti, S., Chang, C. L., Chauvin, E., Cho, H.-M., Crawford, T. M., Crites, A. T., Dobbs, M. A., Halverson, N. W., Heimsath, S., Holzapfel, W. L., Hrubes, J. D., Joy, M., Keisler, R., Lanting, T. M., Lee, A. T., Leitch, E. M., Leong, J., Lu, W., Lueker, M., Luong-Van, D., McMahon, J. J., Mehl, J., Meyer, S. S., Mohr, J. J., Montroy, T. E., Padin, S., Plagge, T., Pryke, C., Ruhl, J. E., Schaffer, K. K., Schwan, D., Shirokoff, E., Spieler, H. G., Staniszewski, Z., Stark, A. A., Tucker, C., Vanderlinde, K., Vieira, J. D., and Williamson, R. (2011). The 10 meter south pole telescope. *Publications of the Astronomical Society of the Pacific*, 123(903):568–581.

Carnall, A. C., McLure, R. J., Dunlop, J. S., and Davé, R. (2018). Inferring the star formation histories of massive quiescent galaxies with BAGPIPES: evidence for multiple quenching mechanisms. *MNRAS*, 480(4):4379–4401.

Carniani, S., Maiolino, R., Smit, R., and Amorín, R. (2018). ALMA Detection of Extended [C II] Emission in Himiko at z = 6.6. *ApJ*, 854(1):L7.

Carrasco, E. R., Gomez, P. L., Verdugo, T., Lee, H., Diaz, R., Bergmann, M., Turner, J. E. H., Miller, B. W., and West, M. J. (2010). Strong Gravitational Lensing by the Super-massive cD Galaxy in Abell 3827. *ApJ*, 715:L160–L164.

Casey, C. M. (2012). Far-infrared spectral energy distribution fitting for galaxies near and far. *Monthly Notices of the Royal Astronomical Society*, 425(4):3094–3103.

Cicone, C. (2015). Powerful quasar feedback in local and very distant galaxies. In *IAU General Assembly*, volume 29, page 2245440.

Cicone, C., Maiolino, R., Sturm, E., Graciá-Carpio, J., Feruglio, C., Neri, R., Aalto, S., Davies, R., Fiore, F., Fischer, J., García-Burillo, S., González-Alfonso, E., Hailey-Dunsheath, S., Piconcelli, E., and Veilleux, S. (2014). Massive molecular outflows and evidence for AGN feedback from CO observations. *A&A*, 562:A21.

Circosta, C., Mainieri, V., Padovani, P., Lanzuisi, G., Salvato, M., Harrison, C. M.,

Kakkad, D., Puglisi, A., Vietri, G., Zamorani, G., Cicone, C., Husemann, B., Vignali, C., Balmaverde, B., Bischetti, M., Bongiorno, A., Brusa, M., Carniani, S., Civano, F., Comastri, A., Cresci, G., Feruglio, C., Fiore, F., Fotopoulou, S., Karim, A., Lamastra, A., Magnelli, B., Mannucci, F., Marconi, A., Merloni, A., Netzer, H., Perna, M., Piconcelli, E., Rodighiero, G., Schinnerer, E., Schramm, M., Schulze, A., Silverman, J., and Zappacosta, L. (2018). SUPER. I. Toward an unbiased study of ionized outflows in z $\sim$ 2 active galactic nuclei: survey overview and sample characterization. *A&A*, 620:A82.

Clark, P. C., Glover, S. C. O., Ragan, S. E., and Duarte-Cabral, A. (2018). Tracing the formation of molecular clouds via [CII], [CI] and CO emission. *arXiv e-prints*, page arXiv:1809.00489.

Coc, A. and Vangioni, E. (2017). Primordial nucleosynthesis. *International Journal of Modern Physics E*, 26:1741002.

Connolly, A. J., Csabai, I., Szalay, A. S., Koo, D. C., Kron, R. G., and Munn, J. A. (1995). Slicing through multicolor space: Galaxy redshifts from broadband photometry. *The Astronomical Journal*, 110:2655.

Conroy, C. (2013). Modeling the Panchromatic Spectral Energy Distributions of Galaxies. *ARA&A*, 51(1):393–455.

Cooksy, A. L., Blake, G. A., and Saykally, R. J. (1986). Direct Measurement of the Fine-Structure Interval and G J Factors of Singly Ionized Atomic Carbon by Laser Magnetic Resonance. *ApJ*, 305:L89.

Cormier, D., Madden, S. C., Hony, S., Contursi, A., Poglitsch, A., Galliano, F., Sturm, E., Doublier, V., Feuchtgruber, H., Galametz, M., Geis, N., de Jong, J., Okumura, K., Panuzzo, P., and Sauvage, M. (2010). The effects of star formation on the low-metallicity ISM: NGC 4214 mapped with Herschel/PACS spectroscopy. *A&A*, 518:L57.

Costagliola, F., Sakamoto, K., Muller, S., Martín, S., Aalto, S., Harada, N., van der Werf, P., Viti, S., Garcia-Burillo, S., and Spaans, M. (2015). Exploring the molecular chemistry and excitation in obscured luminous infrared galaxies. An ALMA mm-wave spectral scan of NGC 4418. *A&A*, 582:A91.

Cox, P., Krips, M., Neri, R., Omont, A., Güsten, R., Menten, K. M., Wyrowski, F., Weiß, A., Beelen, A., Gurwell, M. A., Dannerbauer, H., Ivison, R. J., Negrello, M., Aretxaga, I., Hughes, D. H., Auld, R., Baes, M., Blundell, R., Buttiglione, S., Cava, A., Cooray, A., Dariush, A., Dunne, L., Dye, S., Eales, S. A., Frayer, D., Fritz, J., Gavazzi, R., Hopwood, R., Ibar, E., Jarvis, M., Maddox, S., Michałowski, M., Pascale, E., Pohlen, M., Rigby, E., Smith, D. J. B., Swinbank, A. M., Temi, P., Valtchanov, I., van der Werf, P., and de Zotti, G. (2011). Gas and Dust in a Submillimeter Galaxy at z = 4.24 from the Herschel Atlas. *ApJ*, 740(2):63.

Cox, P. and Mezger, P. G. (1989). The galactic infrared/submillimeter dust radiation. *A&A Rev.*, 1(1):49–83.

Crawford, M. K., Genzel, R., Townes, C. H., and Watson, D. M. (1985). Far-

infrared spectroscopy of galaxies : the 158 micron C+ line and the energy balance of molecular clouds. *ApJ*, 291:755–771.

da Cunha, E., Charlot, S., and Elbaz, D. (2008). A simple model to interpret the ultraviolet, optical and infrared emission from galaxies. *MNRAS*, 388(4):1595–1617.

Daddi, E., Cimatti, A., and Renzini, A. (2000). Eros and the formation epoch of field ellipticals. *arXiv preprint astro-ph/0010093*.

Daddi, E., Cimatti, A., Renzini, A., Fontana, A., Mignoli, M., Pozzetti, L., Tozzi, P., and Zamorani, G. (2004). A new photometric technique for the joint selection of star-forming and passive galaxies at 1.4<z<2.5. *The Astrophysical Journal*, 617(2):746.

Dalgarno, A. and McCray, R. A. (1972). Heating and Ionization of HI Regions. *ARA&A*, 10:375.

De Looze, I., Baes, M., Bendo, G. J., Cortese, L., and Fritz, J. (2011). The reliability of [C II] as an indicator of the star formation rate. *MNRAS*, 416(4):2712–2724.

De Looze, I., Cormier, D., Lebouteiller, V., Madden, S., Baes, M., Bendo, G. J., Boquien, M., Boselli, A., Clements, D. L., Cortese, L., Cooray, A., Galametz, M., Galliano, F., Graciá-Carpio, J., Isaak, K., Karczewski, O. Ł., Parkin, T. J., Pellegrini, E. W., Rémy-Ruyer, A., Spinoglio, L., Smith, M. W. L., and Sturm, E. (2014). The applicability of far-infrared fine-structure lines as star formation rate tracers over wide ranges of metallicities and galaxy types. *A&A*, 568:A62.

Decarli, R., Walter, F., Venemans, B. P., Bañados, E., Bertoldi, F., Carilli, C., Fan, X., Farina, E. P., Mazzucchelli, C., Riechers, D., Rix, H. W., Strauss, M. A., Wang, R., and Yang, Y. (2017). Rapidly star-forming galaxies adjacent to quasars at redshifts exceeding 6. *Nature*, 545(7655):457–461.

Decarli, R., Walter, F., Venemans, B. P., Bañados, E., Bertoldi, F., Carilli, C., Fan, X., Farina, E. P., Mazzucchelli, C., Riechers, D., Rix, H.-W., Strauss, M. A., Wang, R., and Yang, Y. (2018). An ALMA [C II] Survey of 27 Quasars at z > 5.94. *ApJ*, 854:97.

Dekel, A., Birnboim, Y., Engel, G., Freundlich, J., Goerdt, T., Mumcuoglu, M., Neistein, E., Pichon, C., Teyssier, R., and Zinger, E. (2009). Cold streams in early massive hot haloes as the main mode of galaxy formation. *Nature*, 457(7228):451.

Dessauges-Zavadsky, M., Ginolfi, M., Pozzi, F., Béthermin, M., Le Fèvre, O., Fujimoto, S., Silverman, J. D., Jones, G. C., Vallini, L., Schaerer, D., Faisst, A. L., Khusanova, Y., Fudamoto, Y., Cassata, P., Loiacono, F., Capak, P. L., Yan, L., Amorin, R., Bardelli, S., Boquien, M., Cimatti, A., Gruppioni, C., Hathi, N. P., Ibar, E., Koekemoer, A. M., Lemaux, B. C., Narayanan, D., Oesch, P. A., Rodighiero, G., Romano, M., Talia, M., Toft, S., Vergani, D., Zamorani, G., and Zucca, E. (2020). The ALPINE-ALMA [C II] survey. Molecular gas budget in the early Universe as traced by [C II]. *A&A*, 643:A5.

Dewdney, P. E., Hall, P. J., Schilizzi, R. T., and Lazio, T. J. L. W. (2009). The square kilometre array. *Proceedings of the IEEE*, 97(8):1482–1496.

Dey, A., Soifer, B., Desai, V., Brand, K., Le Floc'h, E., Brown, M. J., Jannuzi, B. T., Armus, L., Bussmann, S., Brodwin, M., et al. (2008). A significant population of very luminous dust-obscured galaxies at redshift z˜ 2. *The Astrophysical Journal*, 677(2):943.

Di Matteo, T., Springel, V., and Hernquist, L. (2005). Energy input from quasars regulates the growth and activity of black holes and their host galaxies. *Nature*, 433:604–607.

Dijkstra, M. (2014). Lyα Emitting Galaxies as a Probe of Reionisation. *PASA*, 31:e040.

Dole, H., Lagache, G., Puget, J. L., Caputi, K. I., Fernández-Conde, N., Le Floc'h, E., Papovich, C., Pérez-González, P. G., Rieke, G. H., and Blaylock, M. (2006). The cosmic infrared background resolved by Spitzer. Contributions of mid-infrared galaxies to the far-infrared background. *A&A*, 451(2):417–429.

Draine, B. T. (2011). *Physics of the Interstellar and Intergalactic Medium*.

Dressler, A. and Richstone, D. O. (1988). Stellar Dynamics in the Nuclei of M31 and M32: Evidence for Massive Black Holes. *ApJ*, 324:701.

Ehrenfreund, P., Irvine, W., Becker, L., Blank, J., Brucato, J., Colangeli, L., Derenne, S., Despois, D., Dutrey, A., Fraaije, H., Lazcano, A., Owen, T., Robert, F., and ISSI-Team, a. (2002). Astrophysical and astrochemical insights into the origin of life. *Reports on Progress in Physics*, 65:1427.

Fabian, A. C. (2012). Observational Evidence of Active Galactic Nuclei Feedback. *Annual Review of Astronomy and Astrophysics*, 50:455–489.

Faisst, A. L., Fudamoto, Y., Oesch, P. A., Scoville, N., Riechers, D. A., Pavesi, R., and Capak, P. (2020). ALMA characterizes the dust temperature of z $\sim$ 5.5 star-forming galaxies. *MNRAS*, 498(3):4192–4204.

Fan, X., Strauss, M. A., Becker, R. H., White, R. L., Gunn, J. E., Knapp, G. R., Richards, G. T., Schneider, D. P., Brinkmann, J., and Fukugita, M. (2006). Constraining the Evolution of the Ionizing Background and the Epoch of Reionization with z$\sim$6 Quasars. II. A Sample of 19 Quasars. *AJ*, 132(1):117–136.

Fazio, G. G., Hora, J. L., Allen, L. E., Ashby, M. L. N., Barmby, P., Deutsch, L. K., Huang, J. S., Kleiner, S., Marengo, M., Megeath, S. T., Melnick, G. J., Pahre, M. A., Patten, B. M., Polizotti, J., Smith, H. A., Taylor, R. S., Wang, Z., Willner, S. P., Hoffmann, W. F., Pipher, J. L., Forrest, W. J., McMurty, C. W., McCreight, C. R., McKelvey, M. E., McMurray, R. E., Koch, D. G., Moseley, S. H., Arendt, R. G., Mentzell, J. E., Marx, C. T., Losch, P., Mayman, P., Eichhorn, W., Krebs, D., Jhabvala, M., Gezari, D. Y., Fixsen, D. J., Flores, J., Shakoorzadeh, K., Jungo, R., Hakun, C., Workman, L., Karpati, G., Kichak, R., Whitley, R., Mann, S., Tollestrup, E. V., Eisenhardt, P., Stern, D., Gorjian, V., Bhattacharya, B., Carey, S., Nelson, B. O., Glaccum, W. J., Lacy, M., Lowrance, P. J., Laine, S.,

Reach, W. T., Stauffer, J. A., Surace, J. A., Wilson, G., Wright, E. L., Hoffman, A., Domingo, G., and Cohen, M. (2004). The Infrared Array Camera (IRAC) for the Spitzer Space Telescope. *ApJS*, 154(1):10–17.

Franx, M., Labbe, I., Rudnick, G., van Dokkum, P. G., Daddi, E., Schreiber, N. M. F., Moorwood, A., Rix, H.-W., Röttgering, H., van de Wel, A., et al. (2003). A significant population of red, near-infrared-selected high-redshift galaxies. *The Astrophysical Journal Letters*, 587(2):L79.

Fruchter, A. S. and Hook, R. N. (2002). Drizzle: A Method for the Linear Reconstruction of Undersampled Images. *Publications of the Astronomical Society of the Pacific*, 114:144–152.

Fujimoto, S., Oguri, M., Brammer, G., Yoshimura, Y., Laporte, N., González-López, J., Caminha, G. B., Kohno, K., Zitrin, A., Richard, J., Ouchi, M., Bauer, F. E., Smail, I., Hatsukade, B., Ono, Y., Kokorev, V., Umehata, H., Schaerer, D., Knudsen, K., Sun, F., Magdis, G., Valentino, F., Ao, Y., Toft, S., Dessauges-Zavadsky, M., Shimasaku, K., Caputi, K., Kusakabe, H., Morokuma-Matsui, K., Shotaro, K., Egami, E., Lee, M. M., Rawle, T., and Espada, D. (2021). ALMA Lensing Cluster Survey: Bright [CII] 158 μm Lines from a Multiply Imaged Sub-$L^\star$ Galaxy at $z = 6.0719$. *arXiv e-prints*, page arXiv:2101.01937.

Gerin, M. and Phillips, T. G. (2000). Atomic Carbon in Galaxies. *ApJ*, 537(2):644–653.

Gnedin, N. Y. and Ostriker, J. P. (1997). Reionization of the Universe and the Early Production of Metals. *ApJ*, 486(2):581–598.

González-López, J., Riechers, D. A., Decarli, R., Walter, F., Vallini, L., Neri, R., Bertoldi, F., Bolatto, A. D., Carilli, C. L., Cox, P., da Cunha, E., Ferrara, A., Gallerani, S., and Infante, L. (2014). Search for [C II] Emission in z = 6.5-11 Star-forming Galaxies. *ApJ*, 784(2):99.

Graciá-Carpio, J., Sturm, E., Hailey-Dunsheath, S., Fischer, J., Contursi, A., Poglitsch, A., Genzel, R., González-Alfonso, E., Sternberg, A., Verma, A., Christopher, N., Davies, R., Feuchtgruber, H., de Jong, J. A., Lutz, D., and Tacconi, L. J. (2011). Far-infrared Line Deficits in Galaxies with Extreme L_{FIR}/M_{H_{2}} Ratios. *ApJ*, 728(1):L7.

Gullberg, B., De Breuck, C., Vieira, J. D., Weiß, A., Aguirre, J. E., Aravena, M., Béthermin, M., Bradford, C. M., Bothwell, M. S., Carlstrom, J. E., Chapman, S. C., Fassnacht, C. D., Gonzalez, A. H., Greve, T. R., Hezaveh, Y., Holzapfel, W. L., Husband, K., Ma, J., Malkan, M., Marrone, D. P., Menten, K., Murphy, E. J., Reichardt, C. L., Spilker, J. S., Stark, A. A., Strandet, M., and Welikala, N. (2015). The nature of the [C II] emission in dusty star-forming galaxies from the SPT survey. *MNRAS*, 449(3):2883–2900.

Gunn, J. E. and Peterson, B. A. (1965). On the Density of Neutral Hydrogen in Intergalactic Space. *ApJ*, 142:1633–1636.

Hailey-Dunsheath, S., Nikola, T., Stacey, G. J., Oberst, T. E., Parshley, S. C.,

Benford, D. J., Staguhn, J. G., and Tucker, C. E. (2010). Detection of the 158 μm [C II] Transition at z = 1.3: Evidence for a Galaxy-wide Starburst. *ApJ*, 714(1):L162–L166.

Harikane, Y., Ouchi, M., Inoue, A. K., Matsuoka, Y., Tamura, Y., Bakx, T., Fujimoto, S., Moriwaki, K., Ono, Y., Nagao, T., Tadaki, K.-i., Kojima, T., Shibuya, T., Egami, E., Ferrara, A., Gallerani, S., Hashimoto, T., Kohno, K., Matsuda, Y., Matsuo, H., Pallottini, A., Sugahara, Y., and Vallini, L. (2020). Large Population of ALMA Galaxies at z > 6 with Very High [O III] 88 μm to [C II] 158 μm Flux Ratios: Evidence of Extremely High Ionization Parameter or PDR Deficit? *ApJ*, 896(2):93.

Häring, N. and Rix, H.-W. (2004). On the Black Hole Mass-Bulge Mass Relation. *ApJ*, 604:L89–L92.

Harms, R. J., Ford, H. C., Tsvetanov, Z. I., Hartig, G. F., Dressel, L. L., Kriss, G. A., Bohlin, R., Davidsen, A. F., Margon, B., and Kochhar, A. K. (1994). HST FOS Spectroscopy of M87: Evidence for a Disk of Ionized Gas around a Massive Black Hole. *ApJ*, 435:L35.

Harrison, C. M., Alexander, D. M., Mullaney, J. R., and Swinbank, A. M. (2014). Kiloparsec-scale outflows are prevalent among luminous AGN: outflows and feedback in the context of the overall AGN population. *MNRAS*, 441:3306–3347.

Harrison, C. M., Costa, T., Tadhunter, C. N., Flütsch, A., Kakkad, D., Perna, M., and Vietri, G. (2018). AGN outflows and feedback twenty years on. *Nature Astronomy*, 2:198–205.

Hashimoto, T., Inoue, A. K., Mawatari, K., Tamura, Y., Matsuo, H., Furusawa, H., Harikane, Y., Shibuya, T., Knudsen, K. K., Kohno, K., Ono, Y., Zackrisson, E., Okamoto, T., Kashikawa, N., Oesch, P. A., Ouchi, M., Ota, K., Shimizu, I., Taniguchi, Y., Umehata, H., and Watson, D. (2019). Big Three Dragons: A z = 7.15 Lyman-break galaxy detected in [O III] 88 μm, [C II] 158 μm, and dust continuum with ALMA. *PASJ*, 71(4):71.

Henkel, C., Mühle, S., Bendo, G., Józsa, G. I. G., Gong, Y., Viti, S., Aalto, S., Combes, F., García-Burillo, S., Hunt, L. K., Mangum, J., Martín, S., Muller, S., Ott, J., van der Werf, P., Malawi, A. A., Ismail, H., Alkhuja, E., Asiri, H. M., Aladro, R., Alves, F., Ao, Y., Baan, W. A., Costagliola, F., Fuller, G., Greene, J., Impellizzeri, C. M. V., Kamali, F., Klessen, R. S., Mauersberger, R., Tang, X. D., Tristram, K., Wang, M., and Zhang, J. S. (2018). Molecular line emission in NGC 4945, imaged with ALMA. *A&A*, 615:A155.

Herrera-Camus, R., Bolatto, A. D., Wolfire, M. G., Smith, J. D., Croxall, K. V., Kennicutt, R. C., Calzetti, D., Helou, G., Walter, F., Leroy, A. K., Draine, B., Brandl, B. R., Armus, L., Sandstrom, K. M., Dale, D. A., Aniano, G., Meidt, S. E., Boquien, M., Hunt, L. K., Galametz, M., Tabatabaei, F. S., Murphy, E. J., Appleton, P., Roussel, H., Engelbracht, C., and Beirao, P. (2015). [C II] 158 μm Emission as a Star Formation Tracer. *ApJ*, 800(1):1.

Hirashita, H., Hunt, L. K., and Ferrara, A. (2002). Dust and hydrogen molecules in the extremely metal-poor dwarf galaxy SBS 0335-052. *MNRAS*, 330(1):L19–L23.

Högbom, J. A. (1974). Aperture Synthesis with a Non-Regular Distribution of Interferometer Baselines. *A&AS*, 15:417.

Hopkins, P. F., Cox, T. J., Kereš, D., and Hernquist, L. (2007). Preprint typeset using latex style emulateapj v. 10/09/06 a cosmological framework for the co-evolution of quasars, supermassive black holes, and elliptical galaxies: Ii. formation of red ellipticals.

Hopkins, P. F., Hernquist, L., Cox, T. J., Di Matteo, T., Robertson, B., and Springel, V. (2006). A unified, merger-driven model of the origin of starbursts, quasars, the cosmic x-ray background, supermassive black holes, and galaxy spheroids. *The Astrophysical Journal Supplement Series*, 163(1):1.

Hughes, T. M., Ibar, E., Villanueva, V., Aravena, M., Baes, M., Bourne, N., Cooray, A., Dunne, L., Dye, S., Eales, S., Furlanetto, C., Herrera-Camus, R., Ivison, R. J., van Kampen, E., Lara-López, M. A., Maddox, S. J., Michałowski, M. J., Smith, M. W. L., Valiante, E., van der Werf, P., and Xue, Y. Q. (2017). VALES. II. The physical conditions of interstellar gas in normal star-forming galaxies up to z = 0.2 revealed by ALMA. *A&A*, 602:A49.

Hunter, D. A., Kaufman, M., Hollenbach, D. J., Rubin, R. H., Malhotra, S., Dale, D. A., Brauher, J. R., Silbermann, N. A., Helou, G., Contursi, A., and Lord, S. D. (2001). The Interstellar Medium of Star-forming Irregular Galaxies: The View with ISO. *ApJ*, 553(1):121–145.

Israel, F. P. and Maloney, P. R. (2011). C^+ emission from the Magellanic Clouds. II. [C II] maps of star-forming regions LMC-N 11, SMC-N 66, and several others. *A&A*, 531:A19.

Ivison, R. J., Swinbank, A. M., Swinyard, B., Smail, I., Pearson, C. P., Rigopoulou, D., Polehampton, E., Baluteau, J. P., Barlow, M. J., Blain, A. W., Bock, J., Clements, D. L., Coppin, K., Cooray, A., Danielson, A., Dwek, E., Edge, A. C., Franceschini, A., Fulton, T., Glenn, J., Griffin, M., Isaak, K., Leeks, S., Lim, T., Naylor, D., Oliver, S. J., Page, M. J., Pérez Fournon, I., Rowan-Robinson, M., Savini, G., Scott, D., Spencer, L., Valtchanov, I., Vigroux, L., and Wright, G. S. (2010). Herschel and SCUBA-2 imaging and spectroscopy of a bright, lensed submillimetre galaxy at z = 2.3. *A&A*, 518:L35.

Katz, N., Keres, D., Dave, R., and Weinberg, D. H. (2003). How Do Galaxies Get Their Gas? In Rosenberg, J. L. and Putman, M. E., editors, *The IGM/Galaxy Connection. The Distribution of Baryons at z=0*, volume 281 of *Astrophysics and Space Science Library*, page 185.

Kauffmann, G., Heckman, T. M., Tremonti, C., Brinchmann, J., Charlot, S., White, S. D. M., Ridgway, S. E., Brinkmann, J., Fukugita, M., Hall, P. B., Ivezić, Ž., Richards, G. T., and Schneider, D. P. (2003). The host galaxies of active galactic nuclei. *MNRAS*, 346:1055–1077.

Kaurov, A. A., Venumadhav, T., Dai, L., and Zaldarriaga, M. (2018). Implication of the Shape of the EDGES Signal for the 21 cm Power Spectrum. *ApJ*, 864(1):L15.

Kereš, D., Katz, N., Weinberg, D. H., and Davé, R. (2005). How do galaxies get their gas? *MNRAS*, 363:2–28.

Khullar, G., Gozman, K., Lin, J. J., Martinez, M. N., Matthews Acuña, O. S., Medina, E., Merz, K., Sanchez, J. A., Sisco, E. E., Kavin Stein, D. J., Sukay, E. O., Tavangar, K., Bayliss, M. B., Bleem, L. E., Brownsberger, S., Dahle, H., Florian, M. K., Gladders, M. D., Mahler, G., Rigby, J. R., Sharon, K., and Stark, A. A. (2021). COOL-LAMPS. I. An Extraordinarily Bright Lensed Galaxy at Redshift 5.04. *ApJ*, 906(2):107.

Kirby, E. N., Boylan-Kolchin, M., Cohen, J. G., Geha, M., Bullock, J. S., and Kaplinghat, M. (2013). Segue 2: The Least Massive Galaxy. *ApJ*, 770:16.

Knudsen, K. K., Richard, J., Kneib, J.-P., Jauzac, M., Clément, B., Drouart, G., Egami, E., and Lindroos, L. (2016). [C II] emission in z $\sim$ 6 strongly lensed, star-forming galaxies. *MNRAS*, 462(1):L6–L10.

Koo, D. C. (1985). Optical multicolors : a poor person's Z machine for galaxies. *AJ*, 90:418–440.

Kovács, A., Omont, A., Beelen, A., Lonsdale, C., Polletta, M., Fiolet, N., Greve, T. R., Borys, C., Cox, P., De Breuck, C., Dole, H., Dowell, C. D., Farrah, D., Lagache, G., Menten, K. M., Bell, T. A., and Owen, F. (2010). Far-infrared Properties of Spitzer-selected Luminous Starbursts. *ApJ*, 717(1):29–39.

Lagache, G., Cousin, M., and Chatzikos, M. (2018). The [CII] 158 μm line emission in high-redshift galaxies. *A&A*, 609:A130.

Lagos, C. D. P., Baugh, C. M., Zwaan, M. A., Lacey, C. G., Gonzalez-Perez, V., Power, C., Swinbank, A. M., and van Kampen, E. (2014). Which galaxies dominate the neutral gas content of the Universe? *MNRAS*, 440:920–941.

Laporte, N., Ellis, R. S., Boone, F., Bauer, F. E., Quénard, D., Roberts-Borsani, G. W., Pelló, R., Pérez-Fournon, I., and Streblyanska, A. (2017). Dust in the Reionization Era: ALMA Observations of a z = 8.38 Gravitationally Lensed Galaxy. *ApJ*, 837(2):L21.

Laporte, N., Zitrin, A., Ellis, R. S., Fujimoto, S., Brammer, G., Richard, J., Oguri, M., Caminha, G. B., Kohno, K., Yoshimura, Y., Ao, Y., Bauer, F. E., Caputi, K., Egami, E., Espada, D., González-López, J., Hatsukade, B., Knudsen, K. K., Lee, M. M., Magdis, G., Ouchi, M., Valentino, F., and Wang, T. (2021). ALMA Lensing Cluster Survey: a strongly lensed multiply imaged dusty system at z $\geq$ 6. *MNRAS*, 505(4):4838–4846.

Lauer, T. R., Postman, M., Weaver, H. A., Spencer, J. R., Stern, S. A., Buie, M. W., Durda, D. D., Lisse, C. M., Poppe, A. R., Binzel, R. P., Britt, D. T., Buratti, B. J., Cheng, A. F., Grundy, W. M., Horányi, M., Kavelaars, J. J., Linscott, I. R., McKinnon, W. B., Moore, J. M., Núñez, J. I., Olkin, C. B., Parker, J. W., Porter, S. B., Reuter, D. C., Robbins, S. J., Schenk, P., Showalter, M. R., Singer,

K. N., Verbiscer, A. J., and Young, L. A. (2021). New Horizons Observations of the Cosmic Optical Background. *ApJ*, 906(2):77.

Le Fèvre, O., Béthermin, M., Faisst, A., Jones, G. C., Capak, P., Cassata, P., Silverman, J. D., Schaerer, D., Yan, L., Amorin, R., Bardelli, S., Boquien, M., Cimatti, A., Dessauges-Zavadsky, M., Giavalisco, M., Hathi, N. P., Fudamoto, Y., Fujimoto, S., Ginolfi, M., Gruppioni, C., Hemmati, S., Ibar, E., Koekemoer, A., Khusanova, Y., Lagache, G., Lemaux, B. C., Loiacono, F., Maiolino, R., Mancini, C., Narayanan, D., Morselli, L., Méndez-Hernàndez, H., Oesch, P. A., Pozzi, F., Romano, M., Riechers, D., Scoville, N., Talia, M., Tasca, L. A. M., Thomas, R., Toft, S., Vallini, L., Vergani, D., Walter, F., Zamorani, G., and Zucca, E. (2020a). The ALPINE-ALMA [CII] survey. Survey strategy, observations, and sample properties of 118 star-forming galaxies at $4 < z < 6$. *A&A*, 643:A1.

Le Fèvre, O., Béthermin, M., Faisst, A., Jones, G. C., Capak, P., Cassata, P., Silverman, J. D., Schaerer, D., Yan, L., Amorin, R., Bardelli, S., Boquien, M., Cimatti, A., Dessauges-Zavadsky, M., Giavalisco, M., Hathi, N. P., Fudamoto, Y., Fujimoto, S., Ginolfi, M., Gruppioni, C., Hemmati, S., Ibar, E., Koekemoer, A., Khusanova, Y., Lagache, G., Lemaux, B. C., Loiacono, F., Maiolino, R., Mancini, C., Narayanan, D., Morselli, L., Méndez-Hernàndez, H., Oesch, P. A., Pozzi, F., Romano, M., Riechers, D., Scoville, N., Talia, M., Tasca, L. A. M., Thomas, R., Toft, S., Vallini, L., Vergani, D., Walter, F., Zamorani, G., and Zucca, E. (2020b). The ALPINE-ALMA [CII] survey. Survey strategy, observations, and sample properties of 118 star-forming galaxies at $4 < z < 6$. *A&A*, 643:A1.

Le Fèvre, O., Sanjuan, C., Tasca, L., Vvds Team, Massiv Team, and Vuds Team (2013). The Galaxy Merger Rate History (GMRH) since $z \sim 3$. In Sun, W. H., Xu, C. K., Scoville, N. Z., and Sanders, D. B., editors, *Galaxy Mergers in an Evolving Universe*, volume 477 of *Astronomical Society of the Pacific Conference Series*, page 133.

Liang, L., Feldmann, R., Kereš, D., Scoville, N. Z., Hayward, C. C., Faucher-Giguère, C.-A., Schreiber, C., Ma, X., Hopkins, P. F., and Quataert, E. (2019). On the dust temperatures of high-redshift galaxies. *MNRAS*, 489(1):1397–1422.

Lin, L., Patton, D. R., Koo, D. C., Casteels, K., Conselice, C. J., Faber, S., Lotz, J., Willmer, C. N., Hsieh, B., Chiueh, T., et al. (2008). The redshift evolution of wet, dry, and mixed galaxy mergers from close galaxy pairs in the deep2 galaxy redshift survey. *The Astrophysical Journal*, 681(1):232.

Lindroos, L., Knudsen, K. K., Fan, L., Conway, J., Coppin, K., Decarli, R., Drouart, G., Hodge, J. A., Karim, A., Simpson, J. M., and Wardlow, J. (2016). Estimating sizes of faint, distant galaxies in the submillimetre regime. *MNRAS*, 462:1192–1202.

Lindroos, L., Knudsen, K. K., Vlemmings, W., Conway, J., and Martí-Vidal, I. (2015). Stacking of large interferometric data sets in the image- and uv-domain - a comparative study. *MNRAS*, 446:3502–3515.

Lu, L., Sargent, W. L. W., Barlow, T. A., and Rauch, M. (1998). The Metal

Contents of Very Low Column Density Lyman-alpha Clouds: Implications for the Origin of Heavy Elements in the Intergalactic Medium. *arXiv e-prints*, pages astro–ph/9802189.

Luhman, M. L., Satyapal, S., Fischer, J., Wolfire, M. G., Cox, P., Lord, S. D., Smith, H. A., Stacey, G. J., and Unger, S. J. (1998). Infrared Space Observatory Measurements of a [C II] 158 Micron Line Deficit in Ultraluminous Infrared Galaxies. *ApJ*, 504(1):L11–L15.

Luhman, M. L., Satyapal, S., Fischer, J., Wolfire, M. G., Sturm, E., Dudley, C. C., Lutz, D., and Genzel, R. (2003). The [C II] 158 Micron Line Deficit in Ultraluminous Infrared Galaxies Revisited. *ApJ*, 594(2):758–775.

Lynden-Bell, D. (1969). Galactic Nuclei as Collapsed Old Quasars. *Nature*, 223:690–694.

Madau, P., Ferguson, H. C., Dickinson, M. E., Giavalisco, M., Steidel, C. C., and Fruchter, A. (1996). High-redshift galaxies in the Hubble Deep Field: colour selection and star formation history to z∼4. *MNRAS*, 283(4):1388–1404.

Madden, S. C., Cormier, D., Hony, S., Lebouteiller, V., Abel, N., Galametz, M., De Looze, I., Chevance, M., Polles, F. L., Lee, M. Y., Galliano, F., Lambert-Huyghe, A., Hu, D., and Ramambason, L. (2020). Tracing the total molecular gas in galaxies: [CII] and the CO-dark gas. *A&A*, 643:A141.

Madden, S. C., Poglitsch, A., Geis, N., Stacey, G. J., and Townes, C. H. (1997). [C II] 158 Micron Observations of IC 10: Evidence for Hidden Molecular Hydrogen in Irregular Galaxies. *ApJ*, 483(1):200–209.

Magnelli, B., Boogaard, L., Decarli, R., Gónzalez-López, J., Novak, M., Popping, G., Smail, I., Walter, F., Aravena, M., Assef, R. J., Bauer, F. E., Bertoldi, F., Carilli, C., Cortes, P. C., Cunha, E. d., Daddi, E., Díaz-Santos, T., Inami, H., Ivison, R. J., Fèvre, O. L., Oesch, P., Riechers, D., Rix, H.-W., Sargent, M. T., Werf, P. v. d., Wagg, J., and Weiss, A. (2020). The ALMA Spectroscopic Survey in the HUDF: The Cosmic Dust and Gas Mass Densities in Galaxies up to z $\sim$ 3. *ApJ*, 892(1):66.

Maiolino, R., Carniani, S., Fontana, A., Vallini, L., Pentericci, L., Ferrara, A., Vanzella, E., Grazian, A., Gallerani, S., Castellano, M., Cristiani, S., Brammer, G., Santini, P., Wagg, J., and Williams, R. (2015). The assembly of 'normal' galaxies at z $\sim$ 7 probed by ALMA. *MNRAS*, 452(1):54–68.

Maiolino, R., Caselli, P., Nagao, T., Walmsley, M., De Breuck, C., and Meneghetti, M. (2009). Strong [CII] emission at high redshift. *A&A*, 500(2):L1–L4.

Maiolino, R., Cox, P., Caselli, P., Beelen, A., Bertoldi, F., Carilli, C. L., Kaufman, M. J., Menten, K. M., Nagao, T., Omont, A., Weiß, A., Walmsley, C. M., and Walter, F. (2005). First detection of [CII]158 μm at high redshift: vigorous star formation in the early universe. *A&A*, 440(2):L51–L54.

Maiolino, R., Gallerani, S., Neri, R., Cicone, C., Ferrara, A., Genzel, R., Lutz, D., Sturm, E., Tacconi, L. J., Walter, F., Feruglio, C., Fiore, F., and Piconcelli,

E. (2012). Evidence of strong quasar feedback in the early Universe. *MNRAS*, 425:L66–L70.

Malhotra, S., Helou, G., Stacey, G., Hollenbach, D., Lord, S., Beichman, C. A., Dinerstein, H., Hunter, D. A., Lo, K. Y., Lu, N. Y., Rubin, R. H., Silbermann, N., Thronson, H. A., J., and Werner, M. W. (1997). Infrared Space Observatory Measurements of [C II] Line Variations in Galaxies. *ApJ*, 491(1):L27–L30.

Malhotra, S., Kaufman, M. J., Hollenbach, D., Helou, G., Rubin, R. H., Brauher, J., Dale, D., Lu, N. Y., Lord, S., Stacey, G., Contursi, A., Hunter, D. A., and Dinerstein, H. (2001). Far-Infrared Spectroscopy of Normal Galaxies: Physical Conditions in the Interstellar Medium. *ApJ*, 561(2):766–786.

Marconi, A. and Hunt, L. K. (2003). The Relation between Black Hole Mass, Bulge Mass, and Near-Infrared Luminosity. *ApJ*, 589:L21–L24.

Martin, N. F., Ibata, R. A., Bellazzini, M., Irwin, M. J., Lewis, G. F., and Dehnen, W. (2004). A dwarf galaxy remnant in Canis Major: the fossil of an in-plane accretion on to the Milky Way. *MNRAS*, 348:12–23.

Matthee, J., Sobral, D., Darvish, B., Santos, S., Mobasher, B., Paulino-Afonso, A., Röttgering, H., and Alegre, L. (2017). Spectroscopic properties of luminous Ly α emitters at z $\approx$ 6-7 and comparison to the Lyman-break population. *MNRAS*, 472(1):772–787.

Morganti, R., de Zeeuw, P. T., Oosterloo, T. A., McDermid, R. M., Krajnović, D., Cappellari, M., Kenn, F., Weijmans, A., and Sarzi, M. (2006). Neutral hydrogen in nearby elliptical and lenticular galaxies: the continuing formation of early-type galaxies. *MNRAS*, 371:157–169.

Murray, C. E., Lindner, R. R., Stanimirović, S., Goss, W. M., Heiles, C., Dickey, J., Pingel, N. M., Lawrence, A., Jencson, J., Babler, B. L., and Hennebelle, P. (2014). Excitation Temperature of the Warm Neutral Medium as a New Probe of the Lyα Radiation Field. *ApJ*, 781:L41.

Naab, T., Johansson, P. H., and Ostriker, J. P. (2009). Minor Mergers and the Size Evolution of Elliptical Galaxies. *ApJ*, 699:L178–L182.

Naab, T. and Ostriker, J. P. (2017). Theoretical Challenges in Galaxy Formation. *Annual Review of Astronomy and Astrophysics*, 55:59–109.

Neben, A. R., Bradley, R. F., Hewitt, J. N., DeBoer, D. R., Parsons, A. R., Aguirre, J. E., Ali, Z. S., Cheng, C., Ewall-Wice, A., Patra, N., Thyagarajan, N., Bowman, J., Dickenson, R., Dillon, J. S., Doolittle, P., Egan, D., Hedrick, M., Jacobs, D. C., Kohn, S. A., Klima, P. J., Moodley, K., Saliwanchik, B. R. B., Schaffner, P., Shelton, J., Taylor, H. A., Taylor, R., Tegmark, M., Wirt, B., and Zheng, H. (2016). The Hydrogen Epoch of Reionization Array Dish. I. Beam Pattern Measurements and Science Implications. *ApJ*, 826(2):199.

Negishi, T., Onaka, T., Chan, K. W., and Roellig, T. L. (2001). Global physical conditions of the interstellar medium in nearby galaxies. *A&A*, 375:566–578.

Okumura, T., Matsubara, T., Eisenstein, D. J., Kayo, I., Hikage, C., Szalay, A. S., and Schneider, D. P. (2008). Large-Scale Anisotropic Correlation Function of SDSS Luminous Red Galaxies. *ApJ*, 676:889–898.

Omont, A. (2007). Molecules in galaxies. *Reports on Progress in Physics*, 70:1099–1176.

Orellana, G., Nagar, N. M., Elbaz, D., Calderón-Castillo, P., Leiton, R., Ibar, E., Magnelli, B., Daddi, E., Messias, H., Cerulo, P., and Slater, R. (2017). Molecular gas, dust, and star formation in galaxies. I. Dust properties and scalings in 1600 nearby galaxies. *A&A*, 602:A68.

Ota, K., Walter, F., Ohta, K., Hatsukade, B., Carilli, C. L., da Cunha, E., González-López, J., Decarli, R., Hodge, J. A., Nagai, H., Egami, E., Jiang, L., Iye, M., Kashikawa, N., Riechers, D. A., Bertoldi, F., Cox, P., Neri, R., and Weiss, A. (2014). ALMA Observation of 158 μm [C II] Line and Dust Continuum of a z = 7 Normally Star-forming Galaxy in the Epoch of Reionization. *ApJ*, 792(1):34.

Ouchi, M., Ellis, R., Ono, Y., Nakanishi, K., Kohno, K., Momose, R., Kurono, Y., Ashby, M. L. N., Shimasaku, K., Willner, S. P., Fazio, G. G., Tamura, Y., and Iono, D. (2013). An Intensely Star-forming Galaxy at z $\sim$7 with Low Dust and Metal Content Revealed by Deep ALMA and HST Observations. *ApJ*, 778(2):102.

Parsons, A. R., Backer, D. C., Foster, G. S., Wright, M. C. H., Bradley, R. F., Gugliucci, N. E., Parashare, C. R., Benoit, E. E., Aguirre, J. E., Jacobs, D. C., Carilli, C. L., Herne, D., Lynch, M. J., Manley, J. R., and Werthimer, D. J. (2010). The Precision Array for Probing the Epoch of Re-ionization: Eight Station Results. *AJ*, 139(4):1468–1480.

Pello, R., Miralles, J. M., Le Borgne, J. F., Picat, J. P., Soucail, G., and Bruzual, G. (1996). Identification of a high redshift cluster. in the field of Q2345+007 through deep BRIJK' photometry. *A&A*, 314:73–86.

Pentericci, L., Carniani, S., Castellano, M., Fontana, A., Maiolino, R., Guaita, L., Vanzella, E., Grazian, A., Santini, P., Yan, H., Cristiani, S., Conselice, C., Giavalisco, M., Hathi, N., and Koekemoer, A. (2016). Tracing the Reionization Epoch with ALMA: [C II] Emission in z $\sim$ 7 Galaxies. *ApJ*, 829(1):L11.

Persic, M. and Salucci, P. (1992). The baryon content of the universe. *MNRAS*, 258:14P–18P.

Pettini, M. and Pagel, B. E. J. (2004). [OIII]/[NII] as an abundance indicator at high redshift. *MNRAS*, 348:L59–L63.

Pilbratt, G. L., Riedinger, J. R., Passvogel, T., Crone, G., Doyle, D., Gageur, U., Heras, A. M., Jewell, C., Metcalfe, L., Ott, S., and Schmidt, M. (2010). Herschel Space Observatory. An ESA facility for far-infrared and submillimetre astronomy. *A&A*, 518:L1.

Planck Collaboration (2016). Planck 2015 results. I. Overview of products and scientific results. *A&A*, 594:A1.

Planck Collaboration, Aghanim, N., Akrami, Y., Ashdown, M., Aumont, J., Baccigalupi, C., Ballardini, M., Banday, A. J., Barreiro, R. B., Bartolo, N., Basak, S., Battye, R., Benabed, K., Bernard, J. P., Bersanelli, M., Bielewicz, P., Bock, J. J., Bond, J. R., Borrill, J., Bouchet, F. R., Boulanger, F., Bucher, M., Burigana, C., Butler, R. C., Calabrese, E., Cardoso, J. F., Carron, J., Challinor, A., Chiang, H. C., Chluba, J., Colombo, L. P. L., Combet, C., Contreras, D., Crill, B. P., Cuttaia, F., de Bernardis, P., de Zotti, G., Delabrouille, J., Delouis, J. M., Di Valentino, E., Diego, J. M., Doré, O., Douspis, M., Ducout, A., Dupac, X., Dusini, S., Efstathiou, G., Elsner, F., Enßlin, T. A., Eriksen, H. K., Fantaye, Y., Farhang, M., Fergusson, J., Fernandez-Cobos, R., Finelli, F., Forastieri, F., Frailis, M., Fraisse, A. A., Franceschi, E., Frolov, A., Galeotta, S., Galli, S., Ganga, K., Génova-Santos, R. T., Gerbino, M., Ghosh, T., González-Nuevo, J., Górski, K. M., Gratton, S., Gruppuso, A., Gudmundsson, J. E., Hamann, J., Handley, W., Hansen, F. K., Herranz, D., Hildebrandt, S. R., Hivon, E., Huang, Z., Jaffe, A. H., Jones, W. C., Karakci, A., Keihänen, E., Keskitalo, R., Kiiveri, K., Kim, J., Kisner, T. S., Knox, L., Krachmalnicoff, N., Kunz, M., Kurki-Suonio, H., Lagache, G., Lamarre, J. M., Lasenby, A., Lattanzi, M., Lawrence, C. R., Le Jeune, M., Lemos, P., Lesgourgues, J., Levrier, F., Lewis, A., Liguori, M., Lilje, P. B., Lilley, M., Lindholm, V., López-Caniego, M., Lubin, P. M., Ma, Y. Z., Macías-Pérez, J. F., Maggio, G., Maino, D., Mandolesi, N., Mangilli, A., Marcos-Caballero, A., Maris, M., Martin, P. G., Martinelli, M., Martínez-González, E., Matarrese, S., Mauri, N., McEwen, J. D., Meinhold, P. R., Melchiorri, A., Mennella, A., Migliaccio, M., Millea, M., Mitra, S., Miville-Deschênes, M. A., Molinari, D., Montier, L., Morgante, G., Moss, A., Natoli, P., Nørgaard-Nielsen, H. U., Pagano, L., Paoletti, D., Partridge, B., Patanchon, G., Peiris, H. V., Perrotta, F., Pettorino, V., Piacentini, F., Polastri, L., Polenta, G., Puget, J. L., Rachen, J. P., Reinecke, M., Remazeilles, M., Renzi, A., Rocha, G., Rosset, C., Roudier, G., Rubiño-Martín, J. A., Ruiz-Granados, B., Salvati, L., Sandri, M., Savelainen, M., Scott, D., Shellard, E. P. S., Sirignano, C., Sirri, G., Spencer, L. D., Sunyaev, R., Suur-Uski, A. S., Tauber, J. A., Tavagnacco, D., Tenti, M., Toffolatti, L., Tomasi, M., Trombetti, T., Valenziano, L., Valiviita, J., Van Tent, B., Vibert, L., Vielva, P., Villa, F., Vittorio, N., Wandelt, B. D., Wehus, I. K., White, M., White, S. D. M., Zacchei, A., and Zonca, A. (2020). Planck 2018 results. VI. Cosmological parameters. *A&A*, 641:A6.

Poglitsch, A., Krabbe, A., Madden, S. C., Nikola, T., Geis, N., Johansson, L. E. B., Stacey, G. J., and Sternberg, A. (1995). A Multiwavelength Study of 30 Doradus: The Interstellar Medium in a Low-Metallicity Galaxy. *ApJ*, 454:293.

Popescu, C. C., Tuffs, R. J., Dopita, M. A., Fischera, J., Kylafis, N. D., and Madore, B. F. (2011). Modelling the spectral energy distribution of galaxies. V. The dust and PAH emission SEDs of disk galaxies. *A&A*, 527:A109.

Popping, G., Somerville, R. S., and Galametz, M. (2017). The dust content of galaxies from z = 0 to z = 9. *MNRAS*, 471(3):3152–3185.

Rees, M. J. (1984). Black Hole Models for Active Galactic Nuclei. *Annual Review of Astronomy and Astrophysics*, 22:471–506.

Riechers, D. A., Bradford, C. M., Clements, D. L., Dowell, C. D., Pérez-Fournon, I., Ivison, R. J., Bridge, C., Conley, A., Fu, H., Vieira, J. D., Wardlow, J., Calanog, J., Cooray, A., Hurley, P., Neri, R., Kamenetzky, J., Aguirre, J. E., Altieri, B., Arumugam, V., Benford, D. J., Béthermin, M., Bock, J., Burgarella, D., Cabrera-Lavers, A., Chapman, S. C., Cox, P., Dunlop, J. S., Earle, L., Farrah, D., Ferrero, P., Franceschini, A., Gavazzi, R., Glenn, J., Solares, E. A. G., Gurwell, M. A., Halpern, M., Hatziminaoglou, E., Hyde, A., Ibar, E., Kovács, A., Krips, M., Lupu, R. E., Maloney, P. R., Martinez-Navajas, P., Matsuhara, H., Murphy, E. J., Naylor, B. J., Nguyen, H. T., Oliver, S. J., Omont, A., Page, M. J., Petitpas, G., Rangwala, N., Roseboom, I. G., Scott, D., Smith, A. J., Staguhn, J. G., Streblyanska, A., Thomson, A. P., Valtchanov, I., Viero, M., Wang, L., Zemcov, M., and Zmuidzinas, J. (2013). A dust-obscured massive maximum-starburst galaxy at a redshift of 6.34. *Nature*, 496(7445):329–333.

Rodriguez-Gomez, V., Genel, S., Vogelsberger, M., Sijacki, D., Pillepich, A., Sales, L. V., Torrey, P., Snyder, G., Nelson, D., Springel, V., Ma, C.-P., and Hernquist, L. (2015). The merger rate of galaxies in the Illustris simulation: a comparison with observations and semi-empirical models. *MNRAS*, 449:49–64.

Rupke, D. S. N. and Veilleux, S. (2011). Integral Field Spectroscopy of Massive, Kiloparsec-scale Outflows in the Infrared-luminous QSO Mrk 231. *ApJ*, 729:L27.

Sanders, D. B. and Mirabel, I. F. (1996). Luminous Infrared Galaxies. *Annual Review of Astronomy and Astrophysics*, 34:749.

Sargent, W. L. W., Young, P. J., Boksenberg, A., Shortridge, K., Lynds, C. R., and Hartwick, F. D. A. (1978). Dynamical evidence for a central mass concentration in the galaxy M87. *ApJ*, 221:731–744.

Sargsyan, L., Lebouteiller, V., Weedman, D., Spoon, H., Bernard-Salas, J., Engels, D., Stacey, G., Houck, J., Barry, D., Miles, J., and Samsonyan, A. (2012). [C II] 158 μm Luminosities and Star Formation Rate in Dusty Starbursts and Active Galactic Nuclei. *ApJ*, 755(2):171.

Schaerer, D., Boone, F., Zamojski, M., Staguhn, J., Dessauges-Zavadsky, M., Finkelstein, S., and Combes, F. (2015). New constraints on dust emission and UV attenuation of z = 6.5-7.5 galaxies from millimeter observations. *A&A*, 574:A19.

Schaerer, D., Ginolfi, M., Béthermin, M., Fudamoto, Y., Oesch, P. A., Le Fèvre, O., Faisst, A., Capak, P., Cassata, P., Silverman, J. D., Yan, L., Jones, G. C., Amorin, R., Bardelli, S., Boquien, M., Cimatti, A., Dessauges-Zavadsky, M., Giavalisco, M., Hathi, N. P., Fujimoto, S., Ibar, E., Koekemoer, A., Lagache, G., Lemaux, B. C., Loiacono, F., Maiolino, R., Narayanan, D., Morselli, L., Méndez-Hernàndez, H., Pozzi, F., Riechers, D., Talia, M., Toft, S., Vallini, L., Vergani, D., Zamorani, G., and Zucca, E. (2020). The ALPINE-ALMA [C II] survey. Little to no evolution in the [C II]-SFR relation over the last 13 Gyr. *A&A*, 643:A3.

Schaye, J., Crain, R. A., Bower, R. G., Furlong, M., Schaller, M., Theuns, T., Dalla Vecchia, C., Frenk, C. S., McCarthy, I. G., Helly, J. C., Jenkins, A., Rosas-Guevara, Y. M., White, S. D. M., Baes, M., Booth, C. M., Camps, P., Navarro,

J. F., Qu, Y., Rahmati, A., Sawala, T., Thomas, P. A., and Trayford, J. (2015). The EAGLE project: simulating the evolution and assembly of galaxies and their environments. *MNRAS*, 446:521–554.

Scoville, N., Aussel, H., Sheth, K., Scott, K. S., Sanders, D., Ivison, R., Pope, A., Capak, P., Vanden Bout, P., Manohar, S., Kartaltepe, J., Robertson, B., and Lilly, S. (2014). The Evolution of Interstellar Medium Mass Probed by Dust Emission: ALMA Observations at z = 0.3-2. *ApJ*, 783:84.

Scoville, N., Sheth, K., Aussel, H., Vanden Bout, P., Capak, P., Bongiorno, A., Casey, C. M., Murchikova, L., Koda, J., Álvarez-Márquez, J., Lee, N., Laigle, C., McCracken, H. J., Ilbert, O., Pope, A., Sanders, D., Chu, J., Toft, S., Ivison, R. J., and Manohar, S. (2016). ISM Masses and the Star formation Law at Z = 1 to 6: ALMA Observations of Dust Continuum in 145 Galaxies in the COSMOS Survey Field. *ApJ*, 820:83.

Scoville, N. Z. (2013). *Evolution of star formation and gas*, page 491.

Skilling, J. (2006). Skilling, j.: Nested sampling for general bayesian computation. bayesian anal. 1(4), 833-860. *Bayesian Analysis*, 1:833–860.

Smit, R., Bouwens, R. J., Carniani, S., Oesch, P. A., Labbé, I., Illingworth, G. D., van der Werf, P., Bradley, L. D., Gonzalez, V., Hodge, J. A., Holwerda, B. W., Maiolino, R., and Zheng, W. (2018). Rotation in [C II]-emitting gas in two galaxies at a redshift of 6.8. *Nature*, 553(7687):178–181.

Smith, J. D. T., Croxall, K., Draine, B., De Looze, I., Sandstrom, K., Armus, L., Beirão, P., Bolatto, A., Boquien, M., Brandl, B., Crocker, A., Dale, D. A., Galametz, M., Groves, B., Helou, G., Herrera-Camus, R., Hunt, L., Kennicutt, R., Walter, F., and Wolfire, M. (2017). The Spatially Resolved [CII] Cooling Line Deficit in Galaxies. *ApJ*, 834:5.

Somerville, R. S., Hopkins, P. F., Cox, T. J., Robertson, B. E., and Hernquist, L. (2008). A semi-analytic model for the co-evolution of galaxies, black holes and active galactic nuclei. *MNRAS*, 391:481–506.

Sommovigo, L., Ferrara, A., Pallottini, A., Carniani, S., Gallerani, S., and Decataldo, D. (2020). Warm dust in high-z galaxies: origin and implications. *MNRAS*, 497(1):956–968.

Springel, V., White, S. D., Jenkins, A., Frenk, C. S., Yoshida, N., Gao, L., Navarro, J., Thacker, R., Croton, D., Helly, J., et al. (2005). Simulations of the formation, evolution and clustering of galaxies and quasars. *nature*, 435(7042):629.

Stacey, G. J., Geis, N., Genzel, R., Lugten, J. B., Poglitsch, A., Sternberg, A., and Townes, C. H. (1991). The 158 Micron [C ii] Line: A Measure of Global Star Formation Activity in Galaxies. *ApJ*, 373:423.

Stacey, G. J., Hailey-Dunsheath, S., Ferkinhoff, C., Nikola, T., Parshley, S. C., Benford, D. J., Staguhn, J. G., and Fiolet, N. (2010). A 158 μm [C II] Line Survey of Galaxies at z $\sim$1-2: An Indicator of Star Formation in the Early Universe. *ApJ*, 724(2):957–974.

Stanley, F., Jolly, J. B., König, S., and Knudsen, K. K. (2019). A spectral stacking analysis to search for faint outflow signatures in z $\sim$ 6 quasars. *A&A*, 631:A78.

Steidel, C. C., Giavalisco, M., Dickinson, M., and Adelberger, K. L. (1996). Spectroscopy of Lyman Break Galaxies in the Hubble Deep Field. *AJ*, 112:352.

Steidel, C. C., Giavalisco, M., Pettini, M., Dickinson, M., and Adelberger, K. L. (1996). Spectroscopic confirmation of a population of normal star-forming galaxies at redshifts z> 3. *The Astrophysical Journal Letters*, 462(1):L17.

Stutzki, J., Graf, U. U., Haas, S., Honingh, C. E., Hottgenroth, D., Jacobs, K., Schieder, R., Simon, R., Staguhn, J., Winnewisser, G., Martin, R. N., Peters, W. L., and McMullin, J. P. (1997). Atomic Carbon in M82: Physical Conditions Derived from Simultaneous Observations of the [C I] Fine-Structure Submillimeter-Wave Transitions. *ApJ*, 477:L33–L36.

Sulentic, J., Marziani, P., Dultzin, D., D'Onofrio, M., and del Olmo, A. (2014). Fifty years of quasars: physical insights and potential for cosmology. In *Journal of Physics: Conference Series*, volume 565, page 012018. IOP Publishing.

Swinbank, A. M., Smail, I., Sobral, D., Theuns, T., Best, P. N., and Geach, J. E. (2012). The Properties of the Star-forming Interstellar Medium at z = 0.8-2.2 from HiZELS: Star Formation and Clump Scaling Laws in Gas-rich, Turbulent Disks. *ApJ*, 760(2):130.

Tamura, Y., Mawatari, K., Hashimoto, T., Inoue, A. K., Zackrisson, E., Christensen, L., Binggeli, C., Matsuda, Y., Matsuo, H., Takeuchi, T. T., Asano, R. S., Sunaga, K., Shimizu, I., Okamoto, T., Yoshida, N., Lee, M. M., Shibuya, T., Taniguchi, Y., Umehata, H., Hatsukade, B., Kohno, K., and Ota, K. (2019). Detection of the Far-infrared [O III] and Dust Emission in a Galaxy at Redshift 8.312: Early Metal Enrichment in the Heart of the Reionization Era. *ApJ*, 874(1):27.

Tanabashi, M. et al. (2018). Review of particle physics. *Phys. Rev. D*, 98:030001.

Tielens, A. G. (2005). *The physics and chemistry of the interstellar medium*. Cambridge University Press.

van der Marel, R. P., Besla, G., Cox, T. J., Sohn, S. T., and Anderson, J. (2012). The M31 Velocity Vector. III. Future Milky Way M31-M33 Orbital Evolution, Merging, and Fate of the Sun. *ApJ*, 753:9.

van Haarlem, M. P., Wise, M. W., Gunst, A. W., Heald, G., McKean, J. P., Hessels, J. W. T., de Bruyn, A. G., Nijboer, R., Swinbank, J., Fallows, R., Brentjens, M., Nelles, A., Beck, R., Falcke, H., Fender, R., Hörandel, J., Koopmans, L. V. E., Mann, G., Miley, G., Röttgering, H., Stappers, B. W., Wijers, R. A. M. J., Zaroubi, S., van den Akker, M., Alexov, A., Anderson, J., Anderson, K., van Ardenne, A., Arts, M., Asgekar, A., Avruch, I. M., Batejat, F., Bähren, L., Bell, M. E., Bell, M. R., van Bemmel, I., Bennema, P., Bentum, M. J., Bernardi, G., Best, P., Bîrzan, L., Bonafede, A., Boonstra, A. J., Braun, R., Bregman, J., Breitling, F., van de Brink, R. H., Broderick, J., Broekema, P. C., Brouw, W. N., Brüggen, M., Butcher, H. R., van Cappellen, W., Ciardi, B., Coenen, T.,

Conway, J., Coolen, A., Corstanje, A., Damstra, S., Davies, O., Deller, A. T., Dettmar, R. J., van Diepen, G., Dijkstra, K., Donker, P., Doorduin, A., Dromer, J., Drost, M., van Duin, A., Eislöffel, J., van Enst, J., Ferrari, C., Frieswijk, W., Gankema, H., Garrett, M. A., de Gasperin, F., Gerbers, M., de Geus, E., Grießmeier, J. M., Grit, T., Gruppen, P., Hamaker, J. P., Hassall, T., Hoeft, M., Holties, H. A., Horneffer, A., van der Horst, A., van Houwelingen, A., Huijgen, A., Iacobelli, M., Intema, H., Jackson, N., Jelic, V., de Jong, A., Juette, E., Kant, D., Karastergiou, A., Koers, A., Kollen, H., Kondratiev, V. I., Kooistra, E., Koopman, Y., Koster, A., Kuniyoshi, M., Kramer, M., Kuper, G., Lambropoulos, P., Law, C., van Leeuwen, J., Lemaitre, J., Loose, M., Maat, P., Macario, G., Markoff, S., Masters, J., McFadden, R. A., McKay-Bukowski, D., Meijering, H., Meulman, H., Mevius, M., Middelberg, E., Millenaar, R., Miller-Jones, J. C. A., Mohan, R. N., Mol, J. D., Morawietz, J., Morganti, R., Mulcahy, D. D., Mulder, E., Munk, H., Nieuwenhuis, L., van Nieuwpoort, R., Noordam, J. E., Norden, M., Noutsos, A., Offringa, A. R., Olofsson, H., Omar, A., Orrú, E., Overeem, R., Paas, H., Pandey-Pommier, M., Pandey, V. N., Pizzo, R., Polatidis, A., Rafferty, D., Rawlings, S., Reich, W., de Reijer, J. P., Reitsma, J., Renting, G. A., Riemers, P., Rol, E., Romein, J. W., Roosjen, J., Ruiter, M., Scaife, A., van der Schaaf, K., Scheers, B., Schellart, P., Schoenmakers, A., Schoonderbeek, G., Serylak, M., Shulevski, A., Sluman, J., Smirnov, O., Sobey, C., Spreeuw, H., Steinmetz, M., Sterks, C. G. M., Stiepel, H. J., Stuurwold, K., Tagger, M., Tang, Y., Tasse, C., Thomas, I., Thoudam, S., Toribio, M. C., van der Tol, B., Usov, O., van Veelen, M., van der Veen, A. J., ter Veen, S., Verbiest, J. P. W., Vermeulen, R., Vermaas, N., Vocks, C., Vogt, C., de Vos, M., van der Wal, E., van Weeren, R., Weggemans, H., Weltevrede, P., White, S., Wijnholds, S. J., Wilhelmsson, T., Wucknitz, O., Yatawatta, S., Zarka, P., Zensus, A., and van Zwieten, J. (2013). LOFAR: The LOw-Frequency ARray. *A&A*, 556:A2.

Venemans, B. P., Walter, F., Neeleman, M., Novak, M., Otter, J., Decarli, R., Bañados, E., Drake, A., Farina, E. P., Kaasinen, M., Mazzucchelli, C., Carilli, C., Fan, X., Rix, H.-W., and Wang, R. (2020). Kiloparsec-scale ALMA Imaging of [C II] and Dust Continuum Emission of 27 Quasar Host Galaxies at z $\sim$ 6. *ApJ*, 904(2):130.

Venemans, B. P., Walter, F., Zschaechner, L., Decarli, R., De Rosa, G., Findlay, J. R., McMahon, R. G., and Sutherland, W. J. (2016). Bright [C II] and Dust Emission in Three z $>$ 6.6 Quasar Host Galaxies Observed by ALMA. *ApJ*, 816(1):37.

Vogelsberger, M., Genel, S., Springel, V., Torrey, P., Sijacki, D., Xu, D., Snyder, G., Bird, S., Nelson, D., and Hernquist, L. (2014). Properties of galaxies reproduced by a hydrodynamic simulation. *Nature*, 509(7499):177.

Wakelam, V., Bron, E., Cazaux, S., Dulieu, F., Gry, C., Guillard, P., Habart, E., Hornekær, L., Morisset, S., Nyman, G., Pirronello, V., Price, S. D., Valdivia, V., Vidali, G., and Watanabe, N. (2017). H_2 formation on interstellar dust grains: The viewpoints of theory, experiments, models and observations. *Molecular Astrophysics*, 9:1–36.

Walter, F., Brinks, E., de Blok, W. J. G., Bigiel, F., Kennicutt, Robert C., J., Thornley, M. D., and Leroy, A. (2008). THINGS: The H I Nearby Galaxy Survey. *AJ*, 136:2563–2647.

Walter, F., Decarli, R., Carilli, C., Bertoldi, F., Cox, P., da Cunha, E., Daddi, E., Dickinson, M., Downes, D., Elbaz, D., Ellis, R., Hodge, J., Neri, R., Riechers, D. A., Weiss, A., Bell, E., Dannerbauer, H., Krips, M., Krumholz, M., Lentati, L., Maiolino, R., Menten, K., Rix, H.-W., Robertson, B., Spinrad, H., Stark, D. P., and Stern, D. (2012). The intense starburst HDF 850.1 in a galaxy overdensity at z$\approx$5.2 in the Hubble Deep Field. *Nature*, 486(7402):233–236.

Wang, R., Wagg, J., Carilli, C. L., Walter, F., Lentati, L., Fan, X., Riechers, D. A., Bertoldi, F., Narayanan, D., Strauss, M. A., Cox, P., Omont, A., Menten, K. M., Knudsen, K. K., Neri, R., and Jiang, L. (2013). Star Formation and Gas Kinematics of Quasar Host Galaxies at z $\sim$6: New Insights from ALMA. *ApJ*, 773(1):44.

Watson, D., Christensen, L., Knudsen, K. K., Richard, J., Gallazzi, A., and Michałowski, M. J. (2015). A dusty, normal galaxy in the epoch of reionization. *Nature*, 519(7543):327–330.

Whitaker, K. E., Williams, C. C., Mowla, L., Spilker, J. S., Toft, S., Narayanan, D., Pope, A., Magdis, G. E., van Dokkum, P. G., Akhshik, M., Bezanson, R., Brammer, G. B., Leja, J., Man, A., Nelson, E. J., Richard, J., Pacifici, C., Sharon, K., and Valentino, F. (2021). Quenching of star formation from a lack of inflowing gas to galaxies. *arXiv e-prints*, page arXiv:2109.10384.

White, S. D. M. and Rees, M. J. (1978). Core condensation in heavy halos - A two-stage theory for galaxy formation and clustering. *MNRAS*, 183:341–358.

Willott, C. J., Carilli, C. L., Wagg, J., and Wang, R. (2015). Star Formation and the Interstellar Medium in z $>$ 6 UV-luminous Lyman-break Galaxies. *ApJ*, 807(2):180.

Wise, J. H. (2019). An Introductory Review on Cosmic Reionization. *arXiv e-prints*, page arXiv:1907.06653.

Wise, J. H., Demchenko, V. G., Halicek, M. T., Norman, M. L., Turk, M. J., Abel, T., and Smith, B. D. (2014). The birth of a galaxy - III. Propelling reionization with the faintest galaxies. *MNRAS*, 442(3):2560–2579.

Wise, J. H., Turk, M. J., Norman, M. L., and Abel, T. (2012). The Birth of a Galaxy: Primordial Metal Enrichment and Stellar Populations. *ApJ*, 745(1):50.

Witstok, J., Smit, R., Maiolino, R., Curti, M., Laporte, N., Massey, R., Richard, J., and Swinbank, M. (2021). Assessing the sources of reionisation: a spectroscopic case study of a 30$\times$ lensed galaxy at z 5 with Lyα, C IV, Mg II, and [Ne III]. *MNRAS*.

Wright, E. L., Mather, J. C., Bennett, C. L., Cheng, E. S., Shafer, R. A., Fixsen, D. J., Eplee, R. E., J., Isaacman, R. B., Read, S. M., Boggess, N. W., Gulkis, S., Hauser, M. G., Janssen, M., Kelsall, T., Lubin, P. M., Meyer, S. S., Moseley, S. H., J., Murdock, T. L., Silverberg, R. F., Smoot, G. F., Weiss, R., and Wilkinson,

D. T. (1991). Preliminary Spectral Observations of the Galaxy with a 7 degrees Beam by the Cosmic Background Explorer (COBE). *ApJ*, 381:200.

Zanella, A., Daddi, E., Magdis, G., Diaz Santos, T., Cormier, D., Liu, D., Cibinel, A., Gobat, R., Dickinson, M., Sargent, M., Popping, G., Madden, S. C., Bethermin, M., Hughes, T. M., Valentino, F., Rujopakarn, W., Pannella, M., Bournaud, F., Walter, F., Wang, T., Elbaz, D., and Coogan, R. T. (2018). The [C II] emission as a molecular gas mass tracer in galaxies at low and high redshifts. *MNRAS*, 481(2):1976–1999.

Zaroubi, S. (2013). *The Epoch of Reionization*, volume 396, page 45.

Zavala, J. A., Casey, C. M., Manning, S. M., Aravena, M., Bethermin, M., Caputi, K. I., Clements, D. L., Cunha, E. d., Drew, P., Finkelstein, S. L., Fujimoto, S., Hayward, C., Hodge, J., Kartaltepe, J. S., Knudsen, K., Koekemoer, A. M., Long, A. S., Magdis, G. E., Man, A. W. S., Popping, G., Sanders, D., Scoville, N., Sheth, K., Staguhn, J., Toft, S., Treister, E., Vieira, J. D., and Yun, M. S. (2021). The Evolution of the IR Luminosity Function and Dust-obscured Star Formation over the Past 13 Billion Years. *ApJ*, 909(2):165.

Zwaan, M. A., Kuntschner, H., Pracy, M. B., and Couch, W. J. (2013). The cold gas content of post-starburst galaxies. *MNRAS*, 432:492–499.